

Topological Heavy Fermion Principle For Flat (Narrow) Bands With Concentrated Quantum Geometry

Jonah Herzog-Arbeitman,^{1,*} Jiabin Yu,^{1,*} Dumitru Călugăru*,^{1,*} Haoyu Hu,^{2,*} Nicolas Regnault,^{1,3} Chaoxing Liu,⁴ Oskar Vafek,^{5,6} Piers Coleman,^{7,8} Alexei Tsvelik,⁹ Zhi-da Song,^{10,11,12} and B. Andrei Bernevig^{1,2,13,†}

¹*Department of Physics, Princeton University, Princeton, New Jersey 08544, USA*

²*Donostia International Physics Center, P. Manuel de Lardizabal 4, 20018 Donostia-San Sebastian, Spain*

³*Laboratoire de Physique de l'Ecole normale supérieure,
ENS, Université Paris-PSL, CNRS, Sorbonne Université,*

Université Paris-Diderot, Sorbonne Paris Cité, 75005 Paris, France

⁴*Department of Physics, the Pennsylvania State University, University Park, Pennsylvania 16802, USA*

⁵*National High Magnetic Field Laboratory, Tallahassee, Florida, 32310, USA*

⁶*Department of Physics, Florida State University, Tallahassee, Florida 32306, USA*

⁷*Center for Materials Theory, Department of Physics and Astronomy, Rutgers University, Piscataway, NJ 08854 USA*

⁸*Department of Physics, Royal Holloway University of London, Egham, Surrey TW20 0EX, UK*

⁹*Division of Condensed Matter Physics and Materials Science,
Brookhaven National Laboratory, Upton, NY 11973-5000, USA*

¹⁰*International Center for Quantum Materials, School of Physics, Peking University, Beijing 100871, China*

¹¹*Hefei National Laboratory, Hefei 230088, China*

¹²*Collaborative Innovation Center of Quantum Matter, Beijing 100871, China*

¹³*IKERBASQUE, Basque Foundation for Science, Bilbao, Spain*

We propose a general principle for the low-energy theory of narrow bands with concentrated Berry curvature and Fubini-Study metric in the form of a map to Anderson-“+” models composed of heavy fermions hybridizing and interacting with semi-metallic modes. This map resolves the obstruction preventing topological bands from being realized in a local Hamiltonian acting on the low-energy degrees of freedom. The concentrated quantum geometry is reproduced through band inversion with a dispersive semi-metal, leaving a nearly flat, trivial band which becomes the heavy fermion. This representation is natural when the narrow band is not energetically isolated on the scale of the interaction and an enlarged Hilbert space is inescapable, but also provides analytical insight into the projected-interaction limit. First exemplified in twisted bilayer graphene (TBG), we extend it to (1) the twisted checkerboard, which we find has a chiral symmetric stable anomaly that forbids a lattice realization at all energies, and (2) the Lieb lattice with gapless flat bands, where we show the heavy fermions can be obtained by minimizing a Euclidean instanton action to saturate its BPS bound. The heavy fermion approach is widely applicable and physically transparent: heavy electrons carry the strong correlations and dispersive electrons carry the topology. This simple picture unifies the dichotomous phenomena observed in TBG and points to connections between moiré and stoichiometric materials.

I. INTRODUCTION

Flat or narrow bands resulting from quantum interference can appear in any dimension, in both stoichiometric and engineered (moiré) materials, and engender strongly correlated phases of matter [1–3]. In stoichiometric compounds, exactly flat bands arise in local tight binding models on bipartite lattices and their descendants[4–8], providing a principle for the existence of flat or narrow band materials [9–14]. Moreover, flat bands arising from strong hoppings are likely to be (fragile) topological if they are gapped from dispersive bands [5]. Topology, and more generally quantum geometry, is a crucial feature for flat bands to host exotic correlated states, since trivial flat bands can be formed from spatially decoupled atomic limits. In moiré systems, flat bands typically arise in continuum models away from the tight-binding limit

[15, 16], and exhibit emergent symmetries in the small twist angle limit which frequently render them topological. In these cases, no exponentially localized Wannier description which faithfully represents the symmetries of the flat bands is possible. Since continuum Hamiltonians are infinite, analytic expressions for the wavefunctions are difficult to find, a notable exception being the idealized “chiral” limit [17–21] of twisted bilayer graphene (TBG) which remains separated from experimentally relevant parameters.

A common characteristic of these flat bands (outside the chiral limit) is the presence of concentrated, generically non-abelian, quantum geometry in isolated regions of the Brillouin zone. The question then arises: what is the interacting physics particular to this type of flat band system? There are several limits, schematized in Fig. 1. If the interaction scale U is weaker than the narrow band bandwidth M , then a Fermi liquid (with its own instabilities at Van Hove singularities) is expected and weak coupling Hartree-Fock methods can be used, though analytic progress is dependent upon expressions

* These authors contributed equally.

† bernevig@princeton.edu

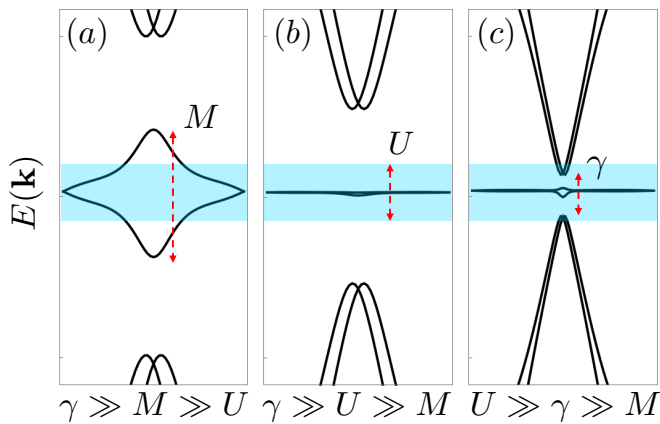


FIG. 1. Characteristic energy scales of a Fermi liquid (a), a projected/strong coupling ferromagnet (b), and a heavy fermion model (c).

for the eigenstates which may not be available. Second, if the interaction is much larger than the bandwidth M but smaller than the gap to dispersive bands γ , then one can project the interaction to the flat bands and solve a strong coupling interacting problem with exact Slater groundstates [22–26] in the repulsive case at integer filling, or exact eta-pairing groundstates in the attractive case [27–31] in the spin-0 sector. These exact results are also in agreement with Hartree-Fock, and analytical insight again requires knowledge of the flat eigenstates to obtain the form factors. Third, if the interaction U is larger than both the bandwidth M and the gap to the dispersive bands γ one cannot perform any meaningful restriction and the problem is both strongly coupled and not prone to projection. The \mathbf{k} -space formalism obfuscates any local description. Realistic models of TBG, as well as gapless flat bands including the Lieb lattice [4] and twisted trilayer graphene [32], and many stoichiometric materials fall under this latter category.

In twisted bilayer graphene, detailed microscopic calculations [33–37] have shown that the topological flat bands can be mapped into a set of trivial and highly localized heavy fermions (f -electrons) hybridized with untwisted bilayer graphene c -electrons of mass $\pm M \approx 4$ meV via a matrix element $\gamma \approx 25$ meV. Their band structure matches that of the Bistritzer-MacDonald (BM) model [15] almost perfectly within the range of the Coulomb interaction $U \approx 40 - 50$ meV, obtained assuming a dielectric constant $\epsilon = 6$. $2M$ becomes the bandwidth of the narrow (almost flat) bands and γ is the gap between the flat bands and a set of dispersive bands in the BM model. This is a faithful, symmetric, unitary transformation of the low-energy bands of the model, where strain, relaxation, and other effects can be included [38–43]. The immediate benefit of this transformation is that it identifies the heavy carriers of the interaction U — the f -electrons — and the itinerant carriers of the topology — the c -electrons. The interaction can be rewritten in this basis, and one obtains a gen-

eralized Anderson model consisting of a large Hubbard $U \approx 50$ meV on the f -electrons, as well as other interactions. This model is suitable for DMFT implementation [44–51], and can match in a natural way a large amount of the experimental features observed in a wide array of experiments. Furthermore, it provides for a Kondo mechanism [52, 53] for screening of the repulsive U as a potential pathway to understand superconductivity — the core mystery of TBG.

Twisted bilayer and trilayer graphene [54] are not the only systems whose flat bands can be mapped into a topological heavy fermion model. Recently, a quadratic touching model that is related to the twisted checkerboard model [55] has also been mapped to a heavy fermion problem [21]. Here we present a wider perspective, arguing that a broad class of narrow/flat band models with concentrated Berry curvature or quantum geometry admit such a heavy fermion description. This entails a single particle Hamiltonian that separates the bands into atomic f -electrons coupled to topological semi-metals, as well as periodic Anderson-“+” interacting terms. This broad class includes gapped and gapless bands in continuum or tight-binding models as we will exemplify.

We first review the emergence of heavy fermions in TBG, and give a simple two-band example on the lattice of a Chern band hybridizing with a metal. We then consider the twisted checkerboard lattice in the chiral limit [21], completing the heavy fermion theory by (i) showing the stable anomaly that obstructs a chiral-symmetric tight-binding model at all energies and (ii) specifying the forms of the Anderson-“+” interacting terms. We also consider a family of gapless flat bands on bipartite lattices whose most famous representative is the Lieb lattice. There we examine the heavy fermion Wannier state wavefunction, showing that it can be solved analytically by mapping the Wannier spread localization problem to a Euclidean instanton action.

Finally, we present arguments that heavy fermion physics arises in interacting narrow bands with concentrated (even divergent, in the gapless case) quantum geometry when the interaction strength is larger than the gap and the narrow band width. To this end, we provide simple estimates for when this regime is reached, and also characterize flat bands that cannot be mapped to heavy fermion models.

II. GAPPED TOPOLOGICAL BANDS

A. $C_{2z}T$ protected obstruction: Heavy Fermions in Twisted Bilayer Graphene

Twisted bilayer graphene (TBG) is formed by stacking together two layers of graphene with a slight twist [15] and exhibits unique electronic properties, such as correlated insulators [56] and superconducting phases [57]. Its non-interacting band structure, which can be described

by the Bistritzer-MacDonald (BM) model [15], exhibits eight flat bands with stable/fragile topology (in the presence/absence of eigenstate particle-hole symmetry) [58–60] around charge neutrality. Importantly, the non-abelian Berry curvature associated with these flat bands is predominantly localized near the Γ point [33], as shown in Fig. 2 (a). This observation enables one to model the TBG as a topological heavy fermion (THF) system, which consists of strongly correlated, localized f -orbitals and topological, dispersive c -electrons [33]. The concentrated Berry curvature allows over 95% of the states within the flat bands to be accurately described by the f orbitals as shown in Fig. 2 (b). The non-trivial topology of the flat bands arises from the hybridization between f and topological c electrons. Remarkably, this mapping also enables one to analytically obtain the wavefunctions of the active TBG flat bands in the zero-bandwidth limit. These flat bands exhibit a chiral symmetry which differs from the conventional chiral symmetry of the BM model in the unrealistic $w_0/w_1 = 0$ limit [61]. Hence the resulting wavefunctions (see Appendix. [B 1]) [33]

$$\hat{f}_{\mathbf{k},1,\eta,s}^\dagger - \frac{\left(\gamma e^{-\frac{|\mathbf{k}|^2 \lambda^2}{2}} / v_\star\right) \hat{c}_{\mathbf{k},3,\eta,s}^\dagger}{\eta k_x + i k_y}, \quad (1)$$

are a good approximation of the realistic TBG bands. Here $\hat{d}_{\mathbf{k},\zeta=+,\eta,s}^\dagger$ is the electron operator in the Chern band basis with Chern number $\zeta \cdot \eta$, valley $\eta \in \{+, -\}$, spin $s \in \{\uparrow, \downarrow\}$, while $\hat{f}_{\mathbf{k},\alpha,\eta,s}^\dagger$ and $\hat{c}_{\mathbf{k}+\mathbf{G},a,\eta,s}^\dagger$ are the corresponding electron operators of the f - and c -fermions, respectively. $\alpha \in \{1, 2\}$, $a \in \{1, 2, 3, 4\}$ denote the orbital indices of f - and c -fermions respectively. γ characterizes the f - c hybridization strength with a decay factor λ . v_\star is the Fermi velocity of non-interacting c electrons. $\hat{d}_{\mathbf{k},\zeta=+,\eta,s}^\dagger$ electron operators admit analytical expressions in the plane-wave BM basis [33, 35] using the form of the f -electron Wannier states and of the c -electron basis. This allows for computing form factors of the $\hat{d}_{\mathbf{k},+,\eta,s}^\dagger$ operators. Approximate analytic formulas can be obtained as shown in Appendix. [B 1 b] and were used in Ref. [62] to compute the electron-phonon interaction.

There are two interesting limits of this heavy fermion formalism. First, if the Hubbard interactions U_1 of f -fermions is larger than the f - c hybridization strength $|\gamma|$ (which is also the gap between flat active bands and remote bands), we should include both flat and dispersive bands and treat the system as an effective heavy fermion system with both f and c fermions. In the opposite limit, where $|\gamma| > U_1$, a flat-band-projected approach [23, 25] is more suitable for the problem. However, even in this limit, the THF model can still be employed to derive the analytical expressions of the flat-band wavefunction and to calculate the excitation spectrum as we discuss in Appendix. [B].

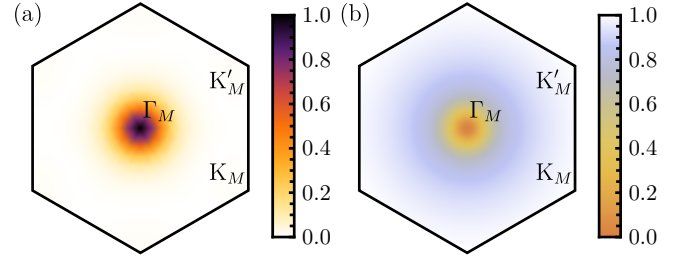


FIG. 2. (a) The non-abelian Berry curvature, expressed in arbitrary units, of the flat Chern band in TBG at the magic angle. (b) The f -electron orbital weight within the active TBG bands at the magic angle.

B. Chern bands with localized Berry curvature

A similar heavy fermion construction can also be obtained for gapped Chern bands with concentrated Berry curvature. To see this, we consider a simple model with s and p_z orbitals located at the $1a$ position of a square lattice (see Appendix. [C]) [63]. We use $\hat{f}_{\mathbf{k},\sigma}^\dagger$ and $\hat{c}_{\mathbf{k},\sigma}^\dagger$ to denote the creation operator for the s and p_z orbitals, respectively, with \mathbf{k} being the momentum and σ , the spin index. The p_z orbitals host a doubly-degenerate quadratic band near the Γ point with dispersion $\epsilon_{\mathbf{k},p_z} \approx -\Delta\epsilon + \frac{t_p |\mathbf{k}|^2}{2}$, where t_p denotes the nearest-neighbor hopping of the p_z orbitals, and $\Delta\epsilon$ controls the energy level of the p_z orbitals. The s orbitals have vanishing kinetic energy, but hybridize with the p_z orbitals.

The single-particle Hamiltonian can be written as

$$H_0 = \sum_{|\mathbf{k}| < \Lambda_c, \sigma} \left(\Delta\epsilon - \frac{t_p}{2} |\mathbf{k}|^2 \right) \hat{c}_{\mathbf{k},\sigma}^\dagger \hat{c}_{\mathbf{k},\sigma} + \frac{t_{sp}}{\sqrt{N}} \sum_{|\mathbf{k}| < \Lambda_c, \mathbf{R}, \sigma} \left[e^{-i\mathbf{k} \cdot \mathbf{R}} (\sigma k_y + i k_x) \hat{c}_{\mathbf{k},\sigma}^\dagger \hat{f}_{\mathbf{R},\sigma} + \text{h.c.} \right]. \quad (2)$$

where N is the number of unit cells, t_{sp} characterizes the f - c hybridization strength and Λ_c is the momentum cutoff of c electrons. We consider the limit where $|\Delta\epsilon|, |t_{sp}| \ll |t_p|$ and $\Delta\epsilon < 0$. Then the system consists of a two-fold degenerate narrow Chern band with bandwidth $\sim |\Delta\epsilon|$ and Chern numbers ± 1 , and dispersive bands that are mostly formed by the dispersive p_z orbitals. The non-trivial topology of the narrow band comes from the band inversion that happens near the Γ point, where we can observe that the Chern bands are mostly formed by p_z orbitals near Γ and s orbitals away from it. The Berry curvature is also concentrated near the Γ point (see Appendix. [C]). Therefore, our simple model indeed realizes a system with both narrow Chern bands and dispersive bands. We can already observe that, this system is equivalent to a heavy fermion system where the s orbitals correspond to the localized f electrons, while the p_z orbitals represent dispersive c electrons. The flatness of the bands comes from the local-

ized nature of s orbitals (f fermions) and the non-trivial topology emerges from the hybridization between s and p_z orbitals. After further introducing the on-site Hubbard interaction of the s orbital (U) and p orbital (V), along with the Coulomb repulsion between s and p orbitals (W), the full Hamiltonian adapts a formula similar to the THF Hamiltonian of the TBG (Appendix. [C]). Therefore, we have established the duality between a topological heavy fermion systems and a system that contains narrow Chern bands with concentrated Berry curvatures. This duality has also been demonstrated in a moiré system featuring Chern flat bands [64].

C. Chiral-Symmetry-Protected Wannier Obstruction: Heavy Fermions in the Twisted Checkerboard

The stable anomaly giving rise to the topology of the TBG narrow bands is protected by particle-hole symmetry for small twist angles [65]. We now discuss a stable anomaly protected by another symmetry, chiral symmetry, which is present in various models, including the twisted checkerboard model which we now discuss. Given a generic 2D single-particle matrix Hamiltonian $h(\mathbf{k})$ with chiral symmetry \mathcal{C} obeying $\{\mathcal{C}, h(\mathbf{k})\} = 0$ and $\mathcal{C}^2 = \mathcal{C}\mathcal{C}^\dagger = 1$, there may still be an obstruction to finding exponentially localized Wannier functions for an isolated set of bands, even if the set of bands have zero total Chern number. To see this is so, let us consider a generic isolated set of $2N$ chirally symmetric bands: their energies are symmetric with respect to the zero energy and their projection matrix $P(\mathbf{k})$ commutes with \mathcal{C} . An odd number of chirally symmetric bands would necessarily have an exactly-flat zero-energy band, and is not our focus here. At a fixed \mathbf{k} , we can separate the Hilbert space for $P(\mathbf{k})$ into the chiral-even and chiral-odd subspaces, each of which has the dimension N ; in other words, $P(\mathbf{k}) = P_+(\mathbf{k}) + P_-(\mathbf{k})$ with $\mathcal{C}P_\pm(\mathbf{k}) = \pm P_\pm(\mathbf{k})$. We then define the Berry curvature and Chern numbers for $P_\pm(\mathbf{k})$ as $F_\pm(\mathbf{k})$ and Ch_\pm , respectively, and the total Chern number of the entire isolated set of $2N$ bands reads $\text{Ch} = \text{Ch}_+ + \text{Ch}_-$. Even if the total Chern number is zero, we can still have nonzero chiral Chern number $\text{Ch}_+ - \text{Ch}_-$, which forbids the construction of the exponentially-localized Wannier functions with strictly local \mathcal{C} in the real space. See details in Appendix. D. The nonzero chiral Chern number $\text{Ch}_+ - \text{Ch}_-$ can occur even if there is $C_{2z}\mathcal{T}$ symmetry, but a stable anomaly cannot be protected by $C_{2z}\mathcal{T}$ alone.

In practice, the nonzero value of $\text{Ch}_+ - \text{Ch}_-$ can be indicated by the total winding number of the chiral protected band-touching points at zero energy. Chiral symmetry can protect stable band touching points at zero energy in 2D [66], labeled \mathbf{k}_l . The robustness of the band touching points is indicated by their nonzero chiral-protected winding numbers, labelled by W_l . As elabo-

rated in Appendix. D, we prove that

$$\sum_l W_l = \text{Ch}_+ - \text{Ch}_-. \quad (3)$$

Therefore, if $\sum_l W_l \neq 0$, a Wannier obstruction exists for any isolated chiral-symmetric set of $2N$ bands, indicating a stable anomaly protected by chiral symmetry. Continuously deforming $h(\mathbf{k})$ cannot change $\sum_l W_l$, unless the continuous deformation involves making $h(\mathbf{k})$ into a vanishing matrix. Using Eq. (3), we can conclude that the single-valley spinless single-particle Hamiltonian of twisted bilayer graphene in the chiral limit [65] has chiral-protected anomaly, since it has two Dirac cones at zero energy whose total winding number is 2.

The twisted checkerboard model in the chiral limit proposed in Ref. [67] has a stable anomaly protected by chiral symmetry. The model consists of two layers of checkerboard lattice with lattice constant 1; each layer of the checkerboard system has two atoms (A and B) in one unit cell. For one individual layer, the model is parameterized by two hoppings t and t' (Fig. 3(a)). Its low-energy physics at half filling happens around M point with an effective Hamiltonian $h_0(\mathbf{p}) = tp_x p_y \sigma_x + t'(p_x^2 + p_y^2) \sigma_y$ in the basis of $(\tilde{c}_{\mathbf{p},+}^\dagger, \tilde{c}_{\mathbf{p},-}^\dagger) = (c_{\mathbf{p},A}^\dagger - ic_{\mathbf{p},B}^\dagger, -ic_{\mathbf{p},A}^\dagger + c_{\mathbf{p},B}^\dagger)/\sqrt{2}$. The effective Hamiltonian carries a chiral winding number 2 with chiral operator σ_z , and the quadratic touching is pinned by C_{4z} symmetry of the system—the chiral winding number 2 only guarantees two linear touching points without pinning their positions (see Appendix. [E].) The moiré model is built from low-energy models around M from both layers, which reads

$$h_{\mathbf{r}} = \begin{pmatrix} h_0(-i\nabla_{\mathbf{r}}) & W(\mathbf{r}) \\ W^\dagger(\mathbf{r}) & h_0(-i\nabla_{\mathbf{r}}) \end{pmatrix} \otimes s_0, \quad (4)$$

where the basis is $(\psi_{\mathbf{r},t}^\dagger, \psi_{\mathbf{r},b}^\dagger)$ with

$$\psi_{\mathbf{r},l}^\dagger = (\psi_{\mathbf{r},l,+, \uparrow}^\dagger, \psi_{\mathbf{r},l,+, \downarrow}^\dagger, \psi_{\mathbf{r},l,-, \uparrow}^\dagger, \psi_{\mathbf{r},l,-, \downarrow}^\dagger), \quad (5)$$

$l = t, b$ labels the layer,

$$W(\mathbf{r}) = 2 \sum_{i=1}^2 T_i \cos(\mathbf{r} \cdot \mathbf{q}_i) + 2 \sum_{i=1}^4 T'_i \cos(\mathbf{r} \cdot \mathbf{g}_i), \quad (6)$$

$\mathbf{q}_n = C_{4z}^{n-1} \frac{k_\theta}{\sqrt{2}} (1, 1)^T$ with $n = 1, 2, 3, 4$ (see \mathbf{q}_1 in Fig. 3(c)), $\mathbf{g}_i = \mathbf{b}_{M,i} + \mathbf{q}_1$ with $i = 1, 2$, $\mathbf{g}_i = C_{4z} \mathbf{g}_{i-2}$ with $i = 3, 4$, $k_\theta = 2\sqrt{2}\pi \sin(\frac{\theta}{2})$, $\mathbf{b}_{M,1} = \mathbf{q}_1 + \mathbf{q}_4$, $\mathbf{b}_{M,2} = \mathbf{q}_1 + \mathbf{q}_2$. Just like the original BM model [15], the intralayer potential in Eq. (4) is neglected for simplicity. In practice, we choose T and T' to have the following forms which preserve chiral symmetry: $T_1 = \sigma_z T_2 \sigma_z = w_1 \sigma_x$ and $T'_1 = T'_2 = w'_1 \sigma_x$ with $T'_3 = T'_4 = \sigma_z T'_1 \sigma_z$. Besides chiral symmetry, the moiré model has spin $\text{SU}(2)$, spinless C_{4z} , spinless C_{2x} , \mathcal{T} , moiré-lattice translations, and an effective m_z symmetry that exchange two layers. (See

Appendix. [E] for detailed expressions.) We do not have valleys here since the moiré model is constructed from the monolayer M points which are time-reversal symmetric. If we set $w_1 = w'_1 = 0$, we have two quadratic touching points (from two layers) at the zero energies at Γ_M and M_M in the moiré Brillouin zone, and each of it has chiral winding number 2, adding up to a total chiral winding number of $\sum_l W_l = 4$. The nonzero total chiral winding number indicates a stable anomaly, which holds for nonzero w_1 and w'_1 due to the presence of chiral symmetry.

The stable topology of the nearly flat bands with concentrated curvature present in this model are particularly suited for the construction of topological heavy fermion model [21]. To show this, we choose $t = 4/k_\theta^2$, $t' = 1.26/k_\theta^2$, $w_1 = 0.66$ and $w'_1 = -0.4$, resulting in nearly flat bands with nontrivial topology and concentrated chiral Berry curvature $F_+(\mathbf{k}) - F_-(\mathbf{k})$ as shown in Fig. 3(b-c). (The topology can also be indicated by the symmetry eigenvalues as discussed in Appendix. [E].) The concentrated chiral Berry curvature allows us to construct the exponentially-localized Wannier modes $f_{\mathbf{k},\alpha}$, $\alpha = 1, 2$ by combining states of nearly flat bands near zero energy and the states near X_M and Y_M from the remote bands (see Fig. 3(b)). The resulting f modes have the symmetry representations of $p_x - p_y$ orbitals at $1a$ position in the moiré unit cell. There are 6 low-energy states at X_M (or Y_M) per spin, and the construction of the f modes uses 2 of them; the remaining 4 states at X_M (or Y_M) per spin give rise to the itinerant c modes. The resulting heavy fermion model consists of three parts: the f -mode part with zero Hamiltonian, the c -mode part, and the $f - c$ coupling. The c -mode part reads

$$H_c = \sum_{\mathbf{p}} c_{X_M+\mathbf{p}}^\dagger h_{cc}^{X_M}(\mathbf{p}) \otimes s_0 c_{X_M+\mathbf{p}} + C_{4z} \text{ partner} , \quad (7)$$

where $c_{X_M+\mathbf{p}}^\dagger = (c_{X_M+\mathbf{p},1}^\dagger, c_{X_M+\mathbf{p},2}^\dagger, c_{X_M+\mathbf{p},3}^\dagger, c_{X_M+\mathbf{p},4}^\dagger) \otimes (\uparrow, \downarrow)$,

$$h_{cc}^{X_M}(\mathbf{p}) = \begin{pmatrix} m\sigma_x & iv_2[(p_x + p_y)\sigma_x + (p_x - p_y)\sigma_y] \\ h.c. & 0_{2 \times 2} \end{pmatrix} \quad (8)$$

to the linear order of \mathbf{p} , and the C_{4z} partner term stands for the Y_M Hamiltonian:

$$h_{cc}^{Y_M}(\mathbf{p}) = h_{cc}^{X_M}(C_{4z}^{-1}\mathbf{p}) . \quad (9)$$

For the spinless part of the basis $c_{X_M+\mathbf{p},\beta}^\dagger$ with $\beta = 1, \dots, 4$, $\beta = 1, 2$ have opposite spinless- C_{2z} eigenvalues than $\beta = 3, 4$, explaining the linear-in- \mathbf{p} terms that couple them. Combined with all other symmetries that leave X_M unchanged, $\beta = 1, 2$ furnish a reducible representation of them while $\beta = 3, 4$ furnish an irreducible representation, explaining the appearance of the mass term for $\beta = 1, 2$ but not for $\beta = 3, 4$ (see Appendix. [E]). The

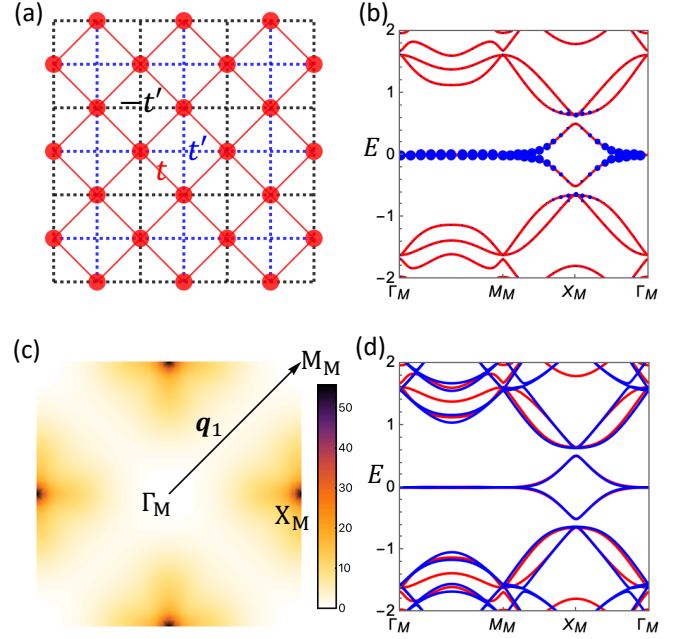


FIG. 3. (a) The monolayer checkerboard model parametrized by two hoppings proposed in Ref. [67]. (b) The band structure (red) of the twisted checkerboard model with $t = 4$, $t' = 1.26$, $w_1 = 0.66$ and $w'_1 = -0.4$. The blue dots mark the probability of the f modes. (c) The chiral Berry curvature $F_+(\mathbf{k}) - F_-(\mathbf{k})$ for the isolated set of two bands around zero energy in (b). (d) The comparison between the continuum-model band structure (red) and the heavy fermion-model band structure (blue).

$f - c$ coupling reads

$$H_{fc} = \sum_{\mathbf{p}} f_{\mathbf{p}}^\dagger h_{fc}^{X_M}(\mathbf{p}) c_{X_M+\mathbf{p}} e^{-\frac{|\mathbf{p}|^2 \lambda^2}{2}} + (C_{4z} \text{ partner}) + h.c. , \quad (10)$$

where $\lambda = 0.43a_M$ is square root of the Wannier spread of the f modes with a_M the moiré lattice constant, and

$$h_{fc}^{X_M}(\mathbf{p}) = \begin{pmatrix} iv_1(p_x\sigma_x + p_y\sigma_y) & \gamma(\sigma_x + \sigma_y) \end{pmatrix} . \quad (11)$$

From the tight-binding parameters and the Wannier states, we compute $v_1 = -0.52/k_\theta$, $\gamma = 0.45$, $m = 0.51$ and $v_2 = 1.53/k_\theta$. The heavy fermion bands in Fig. 3(d) match the continuum model remarkably well. At the interacting level, we project the Coulomb interaction to obtain an Anderson-“+” model with nine interaction terms. The largest term is the density-density Hubbard U for f modes which can be treated with Hartree Fock and DMFT methods. Other important terms, which can all be well-approximated in mean field, are the density-density interaction V/W among $c/f - c$ modes, and the flavor-dependent interactions J and K between f and c . They are listed in Appendix. E.

We specify that Ref. [21] studied the heavy fermion framework for a quadratic band touching model with a

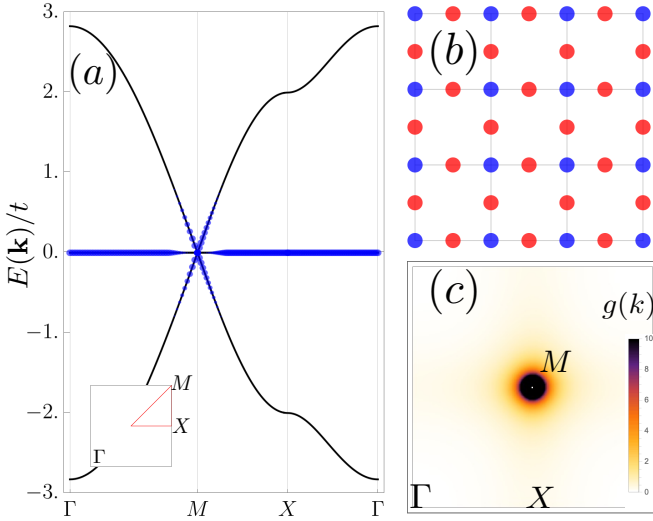


FIG. 4. Divergent quantum geometry of the Lieb lattice. The band structure (a) exhibits an exactly flat band protected by the bipartite lattice structure shown in (b) where the L/L' sublattice is red/blue respectively. A singular band crossing at the $M = (\pi, \pi)$ point results in divergent Fubini-Study metric (c) in the flat band, going as $g(M + \mathbf{k}) \rightarrow 1/|\mathbf{k}|^2$. Blue shading in (a) shows the weight of the heavy fermion wavefunction on the dispersive bands.

perfectly flat band protected by chiral symmetry. We have here complemented their analysis by uncovering the stable chiral-symmetric anomaly and obtaining the interaction Hamiltonian.

III. GAPLESS FLAT BAND MODELS

We now turn to a family of lattice models known as bipartite crystalline flat bands. These models support both gapped topological flat bands as well as flat bands which are degenerate with dispersive bands at isolated momenta, which will be our focus here. To introduce this family of models, we study the Lieb lattice (see Fig. 4a). In momentum space, the Hamiltonian can be written in bipartite form

$$h(\mathbf{k}) = 2t \begin{pmatrix} 0 & S^\dagger(\mathbf{k}) \\ S(\mathbf{k}) & 0 \end{pmatrix}, \quad S(\mathbf{k}) = \begin{pmatrix} \cos k_y/2 \\ \cos k_x/2 \end{pmatrix}. \quad (12)$$

There exist $N_L - N_{L'}$ flat bands in a general bipartite models if $S(\mathbf{k})$ is a rectangular matrix of dimensions $N_L \times N_{L'}$, where L and L' are the two sublattices of the crystal with N_L and $N_{L'}$ orbitals per unit cell respectively. The flat band wavefunction $U_0(\mathbf{k}) = (\psi(\mathbf{k}), 0)^T$ is supported only on the L sublattice and has exactly zero energy since there always exists a vector $\psi(\mathbf{k})$ such that $S^\dagger(\mathbf{k})\psi(\mathbf{k}) =$

0. In the Lieb lattice,

$$\psi(\mathbf{k}) = \left(-\cos \frac{k_x}{2}, \cos \frac{k_y}{2}\right)^T / \sqrt{\cos^2 \frac{k_x}{2} + \cos^2 \frac{k_y}{2}}. \quad (13)$$

This construction can be generalized to encompass realistic materials [5], identifying minimal models for flat and nearly bands away from zero energy.

At generic \mathbf{k} , the dimension of the null space of $S^\dagger(\mathbf{k})$ is $N_L - N_{L'} = 2 - 1 = 1$, but at high-symmetry points the nullity may be larger, indicating band touching points. Plainly, Eq. (12) shows a band touching occurs at $\mathbf{k} = (\pi, \pi)$, the M point at which $S^\dagger(\mathbf{k}) = 0$, as seen in the band structure in Fig. 4b. Its existence fundamentally obstructs a local, low-energy model of the flat band alone, even though most of the flat band is clearly separated from the dispersive bands. From Eq. (13), we see that

$$\psi(\mathbf{k}) \rightarrow (\cos \phi, -\sin \phi) \quad (14)$$

has a singular limit at the gap closing point, where $\mathbf{k} - M = |k|(\cos \phi, \sin \phi)$ and $|k| \rightarrow 0$. While the Berry curvature in this model is strictly zero due to $C_2\mathcal{T}$ symmetry rendering all eigenstates real, the quantum geometry of the model, measured by the Fubini-Study metric, is small away from M and is peaked (indeed, diverges) at the gap closing, as shown in Fig. 4c. This suggests that a topological heavy fermion model can overcome this obstruction.

The band structure in Fig. 4a shows a flat band with pierced by a dispersive bands. What is the low-energy theory at partial filling of the flat bands? Naively, one may expect a theory of Dirac-like electrons and coupled to the a localized s orbital in the atomic basis. Instead, we will show analytically that the low-energy degrees of freedom are a quadratic semi-metal with 2π Berry phase (unlike the linear, π Berry phase Dirac) and an obstructed atomic d -orbital (unlike the atomic basis). The (unitary) transformation of the microscopic degrees of freedom into this basis is accomplished through the heavy fermion framework.

Symmetries play a key role in identifying the low-energy degrees of freedom of the heavy fermion model. We will need the rotation symmetry $D[C_{4z}] = 1 \oplus \sigma_1$ and time-reversal $D[\mathcal{T}] = K$, obeying $D[g]h(\mathbf{k})D^\dagger[g] = h(g\mathbf{k})$, as well as the anti-commuting chiral symmetry $D[\Sigma] = 1 \oplus -\sigma_0$ obeying $D[\Sigma]h(\mathbf{k})D^\dagger[\Sigma] = -h(\mathbf{k})$. The combination of C_2 and \mathcal{T} ensures the Berry curvature is identically zero everywhere in the Brillouin zone when the bands are gapped. The irrep tables in this space group, $p41'$, are [68]

| | | | | |
|----------------------------|-----------|-------|-----------|------|
| $41'$ | $1 \ C_4$ | $21'$ | $1 \ C_2$ | (15) |
| Γ_1, M_1 | $1 \ 1$ | X_1 | $1 \ 1$ | |
| Γ_2, M_2 | $1 \ -1$ | X_2 | $1 \ -1$ | |
| $\Gamma_3\Gamma_4, M_3M_4$ | $2 \ 0$ | | | |

The band touching at the M point is protected by these symmetries. Ref. [5] has shown that the irreps of

the flat band are given by the formal subtraction of the representations of the two sublattices

$$\mathcal{B}_0 = \mathcal{B}_L \ominus \mathcal{B}_{L'} = \Gamma_2 + X_1 + (M_3 M_4 \ominus M_2) \quad (16)$$

where $\mathcal{B}_L = \Gamma_1 \oplus \Gamma_2 + X_1 \oplus X_2 + M_3 M_4$ and $\mathcal{B}_{L'} = \Gamma_1 + X_2 + M_2$ can be found on the Bilbao crystallographic server[68]. The incompatibility of the M irrep subtraction is interpreted as a gapless point. In fact, these representations identify a unique atomic (localized) representation available at low energy. At the Γ, X points, the dispersive bands are far away in energy from the flat band so the only accessible irreps are Γ_2, X_1 . There is only a single one-band atomic representation consistent with these irreps:

$$\Gamma_2 + X_1 + M_2 = B_{1a} \uparrow G \quad (17)$$

where B_{1a} is a $d_{x^2-y^2}$ -orbital at the origin — importantly off the sites of the L and L' sublattices. This is the representation of the low-energy heavy fermion. The M_2 irrep is induced from the L' sublattice, meaning the wavefunction of the heavy fermion obeys $U_f(\mathbf{k} = M) = (1, 0, 0)$. This requires mixing into the dispersive band Hilbert space since the flat band wavefunction (carrying the Γ_2, X_1 irreps) is entirely supported on the L sublattice. Thus the heavy fermion wavefunction takes the simple form

$$U_f(\mathbf{k}) = U_0(\mathbf{k}) \cos \theta(\mathbf{k}) + (1, 0, 0)^T \sin \theta(\mathbf{k}) \quad (18)$$

where the band mixing is parameterized by $\theta(\mathbf{k})$. $\theta(M) = \pi/2$ and decays to zero away from M . We can choose $\theta(\mathbf{k})$ such that the heavy fermion is maximally localized[69] in position space in order to obtain an Anderson-“+” model where Hubbard-like interactions are predominantly carried by the heavy fermion, and correlations are local. Usually one first uses numerical routines such as Wannier90 to accomplish this task, or relies on gaussian approximations for the Wannier states [33]. Remarkably, we now show it is possible to solve for $\theta(\mathbf{k})$ analytically. This is likely to generalize to other bipartite models with band touchings, as the L and L' support of the flat band and touching point as well as ansatz in Eq. 18 generalize.

We form the Wannier state

$$f_{\mathbf{R}}^\dagger = \sum_{\alpha} \int \frac{d^2 k}{(2\pi)^2} e^{i\mathbf{k} \cdot \mathbf{R}} c_{\mathbf{k}, \alpha}^\dagger U_{f, \alpha}(\mathbf{k}) \quad (19)$$

and compute its spread to be (see Appendix. F)

$$\frac{1}{2} \langle r^2 \rangle = \int \frac{d^2 k}{(2\pi)^2} \left(\frac{1}{2} (\nabla \theta)^2 + \frac{1}{2} g(\mathbf{k}) \cos^2 \theta \right) \quad (20)$$

using the fact that a smooth $C_2\mathcal{T}$ -symmetric band can be chosen real with vanishing Berry connection. Here

$$g(\mathbf{k}) = \frac{1}{2} \text{Tr} (\nabla P)^2 = \frac{1 - \cos k_x \cos k_y}{2(2 + \cos k_x + \cos k_y)^2} \quad (21)$$

is the Fubini-Study (quantum) metric of the flat band with projector $P = U_0 U_0^\dagger$, which diverges as $1/|k|^2$ for $\mathbf{k} = M + |k|(\cos \phi, \sin \phi)$. Only through mixing into the dispersive bands parameterized by $\sin^2 \theta$, which reaches 1 at M , can the Wannier spread of the heavy fermion be made finite. We now impose a cutoff $\Lambda \ll \pi$ around the M point, beyond which $\theta(\mathbf{k}) = 0$ and the heavy fermion wavefunction is supported strictly in the flat bands. This cutoff is analogous to the “energy window” employed in disentanglement algorithms, and physically corresponds to allowing band mixing only within the a range of energy given by the interaction. The cutoff $\Lambda \sim U/t$ restricts the heavy fermion to be supported on low-energy states only. Minimizing Eq. (20) now corresponds to an Euler-Lagrange problem with Dirichlet boundary conditions given by the action

$$\begin{aligned} S &= \int_{\Lambda} \frac{d^2 k}{(2\pi)^2} \left(\frac{1}{2} (\nabla \theta)^2 + \frac{1}{2k^2} \cos^2 \theta \right) \\ &= \int_{\Lambda} \frac{dt}{(2\pi)^2} \left(\frac{1}{2} \dot{\theta}^2 + \frac{1}{2} \cos^2 \theta \right) \end{aligned} \quad (22)$$

where in the last line we have taken $\theta(\mathbf{k}) = \theta(|\mathbf{k}|)$ since higher angular momentum dependence strictly increases the spread, and written $k = e^t$ to bring the action into the famous instanton form. Writing $\dot{\theta}^2 + \cos^2 \theta = (\dot{\theta} \pm \cos \theta)^2 \mp 2 \frac{d}{dt} \sin \theta$ allows us to saturate the Bogomol'nyi–Prasad–Sommerfield (BPS) bound [70], and find the absolute minimum with solution (see Appendix. F)

$$\cos \theta(\mathbf{k}) = \frac{2|\mathbf{k}|/\Lambda}{(|\mathbf{k}|/\Lambda)^2 + 1} \quad (23)$$

for $|\mathbf{k}| \leq \Lambda$ and $\theta(\mathbf{k}) = 0$ otherwise. Note that $\theta(\mathbf{k})$ and its first derivative are continuous at Λ , as can be seen in Fig. 5a. The real space Wannier wavefunction and its d -orbital character are shown in Fig. 5b. The theory of instantons is well developed and solutions are known for higher dimensional, non-abelian actions (see Ref. [71] and references therein), which may find other analogues in heavy-fermion problems.

The heavy fermion wavefunction carries the M_2 irrep, but the $M_3 M_4$ irrep must be carried by another particle, the conduction electrons. Their wavefunctions are easily obtained by looking at the two-dimensional orthogonal complement of $U_f(\mathbf{k})$, and fixing the gauge freedom with time-reversal symmetry (see Appendix. F). To leading order, we find

$$\gamma_{M+\mathbf{k}, c\pm}^\dagger = \sum_{\alpha} c_{M+\mathbf{k}, \alpha}^\dagger \left(\mp i\sqrt{2} \frac{k_x \pm ik_y}{\Lambda}, \mp \frac{i}{\sqrt{2}}, -\frac{1}{\sqrt{2}} \right)_{\alpha} \quad (24)$$

which are explicitly smooth, and have highest probability on the L sublattice (recall at the heavy fermion wavefunction is supported primarily on the L' sublattice within the cutoff). The Hamiltonian in the heavy fermion basis can

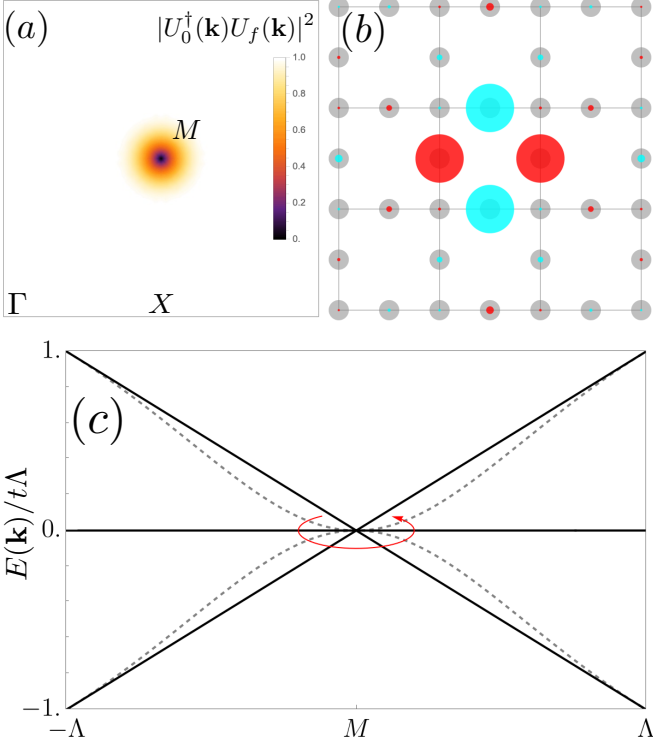


FIG. 5. Lieb lattice Heavy Fermion. (a) c -electron instanton-tunneling probability in the flat band. (b) Real-space Wannier function, whose d -orbital character is apparent from the sign structure (blue/red corresponds to \pm amplitude). The total probability on the L' sublattice is set by the cutoff Λ . (c) We show the decoupled HF and conduction electron bands (dashed) within Λ around the M point. The conduction electrons carry 2π Berry phase and are a topological semi-metal. Linear $f - c$ coupling restores the Lieb dispersion (black).

now be written in a $k.p$ expansion as ($k, \bar{k} = k_x \pm ik_y$)

$$h_{HF}(\mathbf{k}) = t \begin{pmatrix} -2i\bar{k}^2/\Lambda & \bar{k}/\sqrt{2} \\ 2ik^2/\Lambda & k/\sqrt{2} \\ k/\sqrt{2} & \bar{k}/\sqrt{2} & 0 \end{pmatrix} \quad (25)$$

in the basis $c_{\mathbf{k},+}, c_{\mathbf{k},-}, f_{\mathbf{k}}$. The heavy fermion description reveals the emergent degrees of freedom at low energies to be obstructed d -orbitals coupled to a double vortex topological semi-metal (see Fig. 5c).

We now consider the addition of Hubbard interactions

$$H_{int} = U \sum_{\mathbf{R}\alpha} n_{\mathbf{R}\alpha,\uparrow} n_{\mathbf{R}\alpha,\downarrow} \quad (26)$$

acting on the spin-degenerate bands. Since the HF basis is unitarily related to the band basis, it is simple to rotate between them and compute the periodic Anderson model, which we show in Appendix F. Let us recall that for a highly localized heavy fermion like in TBG, the largest interaction is an onsite Hubbard term, with nearest- and farther-neighbor interactions controlled by the Wannier

spread. A surprising feature that distinguishes the Lieb lattice from its continuum heavy fermion counterparts is that there is an obstruction to taking $\lambda \rightarrow 0$. This obstruction is easily explained through topological quantum chemistry[72]: the representation of the Lieb lattice f -mode is a d -orbital at a lattice vacancy, so its wavefunction must always be supported on the neighboring orbitals (see Fig. 5) which causes strong overlaps between the densities of neighboring f -modes. Hence the f -mode density-density interaction always has strong nearest-neighbor components, while farther-neighbor interactions will be suppressed due to the localized Wannier wavefunction. Approximating the Wannier state by keeping only its largest 4 amplitudes (the central 4 d -wave like lobes), we find the f - f interaction takes the form

$$H_U = U \sum_{\mathbf{R}\alpha} \bar{n}_{\mathbf{R},\alpha,\uparrow}^f \bar{n}_{\mathbf{R},\alpha,\downarrow}^f \approx \frac{U}{4} \sum_{\langle \mathbf{R}\mathbf{R}' \rangle} n_{\langle \mathbf{R}\mathbf{R}' \rangle,\uparrow} n_{\langle \mathbf{R}\mathbf{R}' \rangle,\downarrow} \quad (27)$$

where $\bar{n}_{\mathbf{R},\alpha,\sigma}^f$ is the projection of $n_{\mathbf{R},\alpha,\sigma}$ to the f -modes, $f_{\langle \mathbf{R}\mathbf{R}' \rangle,\sigma}^\dagger = \frac{f_{\mathbf{R},\sigma}^\dagger + f_{\mathbf{R}',\sigma}^\dagger}{\sqrt{2}}$ is a bond-centered heavy fermion, $n_{\langle \mathbf{R}\mathbf{R}' \rangle,\sigma} = f_{\langle \mathbf{R}\mathbf{R}' \rangle,\sigma}^\dagger f_{\langle \mathbf{R}\mathbf{R}' \rangle,\sigma}$ is its density, and $\langle \mathbf{R}\mathbf{R}' \rangle$ denotes all f -mode nearest neighbors on the square lattice. The physical meaning of the symmetry obstruction to an onsite Hubbard f -mode term is the following: while the tight-binding Hubbard interaction is onsite, it is smeared out in the low-energy degrees of freedom due to the quantum geometry of the heavy fermion. This shows that the effective model at low energies is dramatically altered from the original tight-binding description.

We remark that f -mode sector $\bar{H}^f = H_U$ is an analytically tractable strong coupling problem. This is because projected Hubbard Hamiltonians with flat bands have exactly solvable groundstates [27] and low-energy excitations [29], where the minimal Fubini-Study metric [73] is known to generate the mass of the collective bosonic modes (the spin wave for repulsive interactions, and the Cooper pair for attractive interactions) [74–78]. Projecting the Lieb lattice onto the f -mode basis yields such a projected Hubbard Hamiltonian since the f -modes have zero kinetic energy in Eq. (25). However, the hybridization with the conduction electrons cannot be neglected, and the full interacting Hamiltonian

$$H_{int} = H_U + H_W + H_J + \dots \quad (28)$$

contains additional interactions between the f and c modes, including the f -density/ c -density interaction $H_W \sim f^\dagger f c^\dagger c$ the exchange interaction $H_J \sim f^\dagger c c^\dagger f$, which are usually decoupled in mean-field. (The dots in Eq. 28 refer to odd-parity f -terms and the conduction electron Coulomb repulsion which are typically neglected see Appendix F). Together, these terms form an Anderson-“+” model in the low-energy Hilbert space, which can be approached from various directions. The importance of quantum geometry in the Lieb lattice has

been studied in seminal work on flat band superconductivity [79], and reveals strongly correlated behavior consistent with the phenomenology of heavy fermions [80]. Although our focus is on the partially filled flat band for $U < t$, the heavy fermion representation is simply a unitary rewriting of the model, and can potentially shed light on other densities and parameter regimes of the model [81].

IV. GENERAL ARGUMENT FOR HEAVY FERMION REPRESENTATIONS OF FLAT BANDS WITH CONCENTRATED QUANTUM GEOMETRY

We have shown that flat Bands with concentrated non-abelian Berry curvature in moiré systems, or concentrated Fubini-Study metric in the Lieb lattice, are accompanied by dispersive bands whose gap is smallest where the curvature or metric is largest. These systems admit a heavy fermion representation and serve to illustrate the broader proposal that narrow band systems with strongly peaked quantum geometry are candidates for heavy fermion systems.

Let us recall the two obstacles to an exponentially localized Wannier basis with physical symmetry representations in a given set of bands. The first obstacle arises from symmetry considerations: if the momentum space irreps of the band cannot be induced from atomic limits [72], then no such Wannier basis with physical symmetry representations exists. The second obstacle is quantum geometric: the Wannier spread is lower bounded by the integrated Fubini-Study metric [69], becoming infinite if the bands carry a nonzero Chern number [82] (see Ref. [83, 84]) or are gapless, as in e.g. the Lieb lattice. These obstacles are intrinsic properties of the Hilbert space of the bands. They cannot be removed without mixing into nearby bands, necessitating a heavy fermion description.

Symmetries are crucial for restricting the possible f -modes. In all the cases studied so far, the symmetries are powerful enough to uniquely identify candidate f -modes: the $p_x - p_y$ orbitals in TBG and twisted checkerboard, and the $d_{x^2-y^2}$ orbital in the Lieb lattice. It is worth noting that a class of line graph lattices [5, 9, 85, 86] such as the kagome are ruled out as heavy fermion candidates by symmetry.

The existence of irrep-compatible f -modes is a necessary but not sufficient condition, since the quantum geometric obstruction must also be overcome. We will now present a criterion to estimate the f -mode spread and determine whether a heavy fermion description is appropriate.

Given a projector $P_S(\mathbf{k}) = \sum_{n \in S} U_n(\mathbf{k}) U_n^\dagger(\mathbf{k})$ onto a set of bands indexed by S , their abelian Fubini-Study metric is [87]

$$g_S(\mathbf{k}) = \frac{1}{2} \text{Tr} \partial_i P_S(\mathbf{k}) \partial_i P_S(\mathbf{k}) \geq 0 \quad (29)$$

where the momentum index i is implicitly summed over. Since $P_S(\mathbf{k})$ is gauge-invariant, $g_S(\mathbf{k})$ can be computed without choosing a gauge. Picking S to be the set of narrow bands, a large value of $g_S(\mathbf{k})$ at its peak prevents a highly localized f -mode by lower-bounding the spread of any possible Wannier functions formed in S . However, by including a set of low-energy dispersive bands D , it may be possible to find a more localized Wannier function if $g_{S \oplus D}(\mathbf{k}) < g_S(\mathbf{k})$, noting that $P_{S \oplus D} = P_S + P_D$, but $g_{S \oplus D} \neq g_S + g_D$. We propose a simple estimate for the total Wannier spread λ_f^2 of the f -mode

$$\lambda_f^2 \approx \Omega \int \frac{d^2 k}{(2\pi)^2} \min\{g_S(\mathbf{k}), g_{S \oplus D}(\mathbf{k})\} \quad (30)$$

where Ω is the unit cell area. λ_f^2 reflects the possibility of reducing the Wannier obstruction by mixing into the dispersive bands if the enlarged Hilbert space $S \oplus D$ reduces the Fubini-Study metric. Fig. 6 shows $g_S, g_{S \oplus D}$ for TBG and the twisted checkerboard model, demonstrating how the inclusion of the nearby dispersive bands can remove the strong peak in $g_S(\mathbf{k})$. For TBG, this estimate gives $0.29a_M$ compared to the Wannier90 value $0.3a_M$, and for twisted checkerboard, this estimate gives $0.45a_M$ compared to $0.42a_M$. The good numerical agreement between these estimates and the Wannier90 results is evidence that the localization properties of different Hilbert spaces, captured by Eq. (30), control the existence of a heavy fermion (assuming there is no symmetry obstruction). Further understanding can be gleaned from the Lieb lattice, where g_S diverges at the gap closing point whereas $g_{S \oplus D}$ vanishes, since $S \oplus D$ is the entire single-particle Hilbert space whose projector is the identity. One can verify from the value of the instanton action at its BPS bound that Eq. (30) is exact up to $\frac{\Lambda^2}{2\pi} \ll 1$. Although Eq. (30) is written in terms of the Fubini-Study metric, the inequality $g(\mathbf{k}) \geq |f(\mathbf{k})|$ [88, 89] ensures that small Fubini-Study metric also constrains the Berry curvature, $f(\mathbf{k})$.

Armed with an approximate value for the Wannier spread λ_f^2 , it is also possible to estimate the onsite Hubbard interaction strength via [35]

$$U \approx \frac{e^2}{\epsilon \lambda_f} \quad (31)$$

assuming a Coulomb interaction (with gate-screening length much larger than λ_f). Given the gap γ to the dispersive bands, we can determine the regime of the resulting Anderson model based on whether

$$\frac{\gamma}{U} = \frac{\gamma}{e^2/\epsilon a} \frac{\lambda_f}{a} \quad (32)$$

is less than 1 (heavy fermion regime) or greater than 1 (projected regime). Here a is the lattice constant, and $e^2/(\epsilon a)$ is the Coulomb energy scale. In TBG, using a value of $\epsilon = 6$ for the dielectric constant gives $\frac{\gamma}{e^2/\epsilon a} \sim 1$. Due to the strong localization of the f -modes, $\lambda_f/a \sim .3$

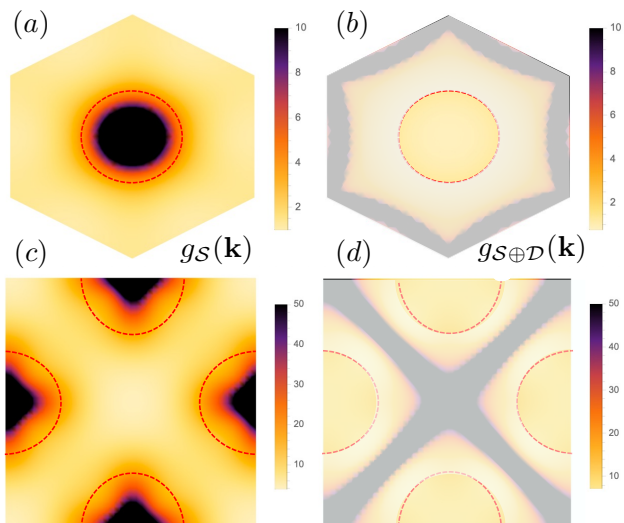


FIG. 6. Resolution of the quantum geometric obstruction to localized Wannier functions. The 2-band Fubini-Study metric for TBG (a) and twisted checkerboard (c) are peaked in the regions (dashed red) where the nearest 4 dispersive bands are closest. The 6-band Fubini-Study metric for TBG (b) and twisted checkerboard (d) shows no peak in these regions, demonstrating that mixing into the dispersive bands (within the low-energy, unshaded regions) can yield highly localized Wannier functions.

ensures $\frac{\gamma}{\ell}$ is firmly less than 1, putting TBG into the heavy fermion regime where local moment behavior is expected.

V. CONCLUSIONS

The low-energy description of a system can be very different from its microscopic model. Untangling these relevant degrees of freedom from the microscopic model is often the key to understanding their emergent properties, both intuitively and computationally. The formation of heavy fermions from the moiré coupling of two massless Dirac particles in TBG is a prototypical example of this phenomenon in interacting flat bands. In this work, we have studied a variety of other examples, from moiré systems to tight-binding lattices, and observed a simple pattern. While band theoretic considerations would forbid a local description of topological bands, we find that — if their quantum geometry is concentrated — a heavy fermion representation is possible by introducing metallic degrees of freedom to carry the obstruction. This single-particle description is extended to a periodic Anderson-“+” model incorporating interactions within this basis. The abundance of heavy fermions thus far revealed in topological, correlated quantum materials underscores the value in studying this class of models, and sets a direction for future research.

VI. ACKNOWLEDGEMENTS

The authors are grateful for important conversations and collaborations with Antoine Georges, Xi Dai, Andy Millis, Francisco Guinea, Roser Valentí, Giorgio Sangiovanni, Tim Wehling, Qimiao Si, Jian Kang, Dmitri K. Efetov, Keshav Singh, Liam Lau, Daniel Kaplan, Ryan Lee, Gautam Rai, Lorenzo Crippa, and Michael Scheer. This work was supported by Office of Basic Energy Sciences, Material Sciences and Engineering Division, U.S. Department of Energy (DOE) under Contracts No. DE-SC0016239 (B. A. B.), DE-FG02-99ER45790 (P. C.) and DE-SC0012704 (A. M. T.). J. H.-A. is supported by a Hertz Fellowship, with additional support from DOE Grant No. DE-SC0016239. J. Y. is supported by the Gordon and Betty Moore Foundation through Grant No. GBMF8685 towards the Princeton theory program and through the Gordon and Betty Moore Foundation’s EPIQS Initiative (Grant No. GBMF11070). D.C. acknowledges the hospitality of the Donostia International Physics Center, at which this work was carried out, and acknowledges support by the Simons Investigator Grant No. 404513, the Gordon and Betty Moore Foundation through Grant No. GBMF8685 towards the Princeton theory program, the Gordon and Betty Moore Foundation’s EPIQS Initiative (Grant No. GBMF11070), Office of Naval Research (ONR Grant No. N00014-20-1-2303), Global Collaborative Network Grant at Princeton University, BSF Israel US foundation No. 2018226, NSF-MERSEC (Grant No. MERSEC DMR 2011750). H.H. was supported by the European Research Council (ERC) under the European Union’s Horizon 2020 research and innovation program (Grant Agreement No. 101020833).

CONTENTS

| | |
|---|----|
| I. Introduction | 1 |
| II. Gapped Topological Bands | 2 |
| A. $C_{2z}T$ protected obstruction: Heavy Fermions in Twisted Bilayer Graphene | 2 |
| B. Chern bands with localized Berry curvature | 3 |
| C. Chiral-Symmetry-Protected Wannier Obstruction: Heavy Fermions in the Twisted Checkerboard | 4 |
| III. Gapless Flat Band Models | 6 |
| IV. General Argument For Heavy Fermion Representations of Flat Bands With Concentrated Quantum Geometry | 9 |
| V. Conclusions | 10 |
| VI. Acknowledgements | 10 |
| A. Twisted bilayer graphene | 12 |
| 1. Review of the Bistritzer-MacDonald model | 12 |
| a. Single-particle Hamiltonian | 12 |
| b. Many-body Hamiltonian | 13 |
| 2. Review of the topological heavy fermion model for TBG | 13 |
| a. The THF model fermions | 13 |
| b. The single-particle THF model | 15 |
| c. The interaction THF Hamiltonian | 15 |
| d. Berry Curvature of the TBG active bands | 16 |
| B. Analytical results within the THF model | 17 |
| 1. Flat-band wave functions | 18 |
| a. Analytical expression for the TBG flat-band wave functions | 18 |
| b. Analytical expressions for the TBG form factors | 19 |
| 2. The charge-one excitation spectrum of TBG in the $ \gamma > U_1$ limit | 20 |
| a. Charge-one excitation matrices | 21 |
| b. Analytical expressions for the charge-one excitation matrices of TBG | 22 |
| c. Flat-band projected limit of the THF model | 25 |
| C. Chern bands with localized Berry curvature | 29 |
| D. Chiral-Symmetry-Protected Stable Anomaly | 31 |
| E. Twisted Checkerboard Model | 33 |
| 1. Chiral-Symmetry Protected Stable Anomaly | 36 |
| 2. Heavy Fermion Model: Single-Particle | 37 |
| 3. Heavy Fermion Model: Interaction | 39 |
| a. $H_{int,1}$ | 40 |
| b. $H_{int,2}$ | 41 |
| c. $H_{int,3}$ | 41 |
| d. $H_{int,4}$ | 42 |
| e. $H_{int,5}$ | 43 |
| f. $H_{int,6}$ | 44 |
| g. $H_{int,7}$ | 44 |
| h. Summary of The Interaction | 45 |
| 4. Alternative Convention | 45 |
| F. Lieb Lattice and Analytical Wannier States from the Instanton Action | 46 |
| 1. Conduction electrons and Hamiltonian | 49 |
| 2. Anderson Model | 50 |
| References | 52 |

Appendix A: Twisted bilayer graphene

Twisted bilayer graphene (TBG) consist of two graphene layers rotated by a small angle θ relative to each other. Near the magic angle $\theta = 1.05^\circ$, flat bands emerge near charge neutrality, which gives rise to various exotic quantum phases, including correlated insulators and superconductivity. Extensive experimental efforts, including both transport [90–117] and spectroscopic measurements [118–132], have been taken to investigate the nature of these quantum phases. Concurrently, significant theoretical efforts have also been made towards constructing the microscopic models [59, 133–169], investigating experimental response [120, 170–178], understanding the topology [59, 153, 162, 179–184] and excitations [24, 185–191], elucidating the mechanism behind the correlated insulating states [22, 23, 120, 141, 154, 172, 187, 189–241], and superconductivity [183, 186, 218, 220, 221, 227, 230, 231, 233, 235, 241–268]. In this appendix, we briefly review both the Bistritzer-MacDonald (BM) model [15] and the topological heavy fermion (THF) model [33] of TBG.

1. Review of the Bistritzer-MacDonald model

In this section, we briefly review the Bistritzer-MacDonald (BM) model [15] of twisted bilayer graphene (TBG). Throughout this work, we use the notations introduced in Refs. [23, 24, 60, 149, 269–272]. We use $\hat{a}_{\mathbf{p},\alpha,s,l}^\dagger$ to denote the creation operator of an electron with momentum \mathbf{p} , spin $s = \uparrow, \downarrow$, sublattice index $\alpha = A, B$, and within the graphene layer $l = \pm$. We use \mathbf{K}_l to label the K point of the l -layer graphene Brillouin Zone (BZ), and use $\eta = \pm$ to denote the two valleys of graphene which corresponds to the momenta $\eta\mathbf{K}_\pm$. In addition, we introduce the following auxiliary vectors

$$\mathbf{q}_1 = k_\theta (0, -1)^T, \quad \mathbf{q}_2 = k_\theta \left(\frac{\sqrt{3}}{2}, \frac{1}{2} \right)^T, \quad \mathbf{q}_3 = k_\theta \left(-\frac{\sqrt{3}}{2}, \frac{1}{2} \right)^T, \quad (\text{A1})$$

where $k_\theta = |\mathbf{K}_+ - \mathbf{K}_-| = 2|\mathbf{K}_+| \sin \frac{\theta}{2}$. The reciprocal lattice of the moiré system is then given by

$$\begin{aligned} \mathcal{Q}_0 &= \mathbb{Z}\mathbf{b}_{M1} + \mathbb{Z}\mathbf{b}_{M2} \\ \mathbf{b}_{M1} &= \mathbf{q}_3 - \mathbf{q}_1, \quad \mathbf{b}_{M2} = \mathbf{q}_3 - \mathbf{q}_2, \end{aligned} \quad (\text{A2})$$

For future convenience, we also introduce $\mathcal{Q}_\pm = \mathcal{Q} \pm \mathbf{q}_1$. The corresponding moiré lattice vectors in the real space are defined as $\mathbf{a}_{M1} = \frac{2\pi}{3k_\theta} (\sqrt{3}, 1)$ and $\mathbf{a}_{M2} = \frac{2\pi}{3k_\theta} (-\sqrt{3}, 1)$.

a. Single-particle Hamiltonian

To define the Hamiltonian of TBG, we consider the following electron operators

$$\hat{c}_{\mathbf{k},\mathbf{Q},\alpha,\eta,s}^\dagger \equiv \hat{a}_{\eta\mathbf{K}_l+\mathbf{k}-\mathbf{Q},\alpha,s,l}^\dagger, \quad \text{for } \mathbf{Q} \in \mathcal{Q}_{\eta l}. \quad (\text{A3})$$

The single-particle Hamiltonian can then be written as [60, 149, 269]

$$\hat{H}_0^{\text{TBG}} = \sum_{\mathbf{k}} \sum_{\eta,\alpha,\beta,s} \sum_{\mathbf{Q},\mathbf{Q}' \in \mathcal{Q}_\pm} \left[h_{\mathbf{Q},\mathbf{Q}'}^{\text{TBG},\eta}(\mathbf{k}) \right]_{\alpha\beta} \hat{c}_{\mathbf{k},\mathbf{Q},\eta,\alpha,s}^\dagger \hat{c}_{\mathbf{k},\mathbf{Q}',\eta,\beta,s}, \quad (\text{A4})$$

We can decompose matrix $h_{\mathbf{Q},\mathbf{Q}'}^{\text{TBG},\eta}(\mathbf{k})$ into two parts, which correspond, respectively, to the original Dirac cone graphene Hamiltonian $h_{\mathbf{Q}}^{\text{D},\eta}(\mathbf{k})$ and the inter-layer coupling term $h_{\mathbf{Q},\mathbf{Q}'}^{\text{I},\eta}$

$$h_{\mathbf{Q},\mathbf{Q}'}^{\text{TBG},\eta}(\mathbf{k}) = h_{\mathbf{Q}}^{\text{D},\eta}(\mathbf{k}) \delta_{\mathbf{Q},\mathbf{Q}'} + h_{\mathbf{Q},\mathbf{Q}'}^{\text{I},\eta}. \quad (\text{A5})$$

For valley $+$, we have

$$h_{\mathbf{Q}}^{\text{D},+}(\mathbf{k}) = v_F (\mathbf{k} - \mathbf{Q}) \cdot \boldsymbol{\sigma}, \quad (\text{A6})$$

$$h_{\mathbf{Q},\mathbf{Q}'}^{\text{I},+} = \sum_{j=1}^3 T_j \delta_{\mathbf{Q},\mathbf{Q}' \pm \mathbf{q}_j}. \quad (\text{A7})$$

where v_F is the Fermi velocity of graphene, $\boldsymbol{\sigma} = (\sigma_x, \sigma_y)$ is the Pauli vector, and T_j characterizes the inter-layer tunneling with

$$T_j = w_0 \sigma_0 + w_1 \left[\sigma_x \cos \frac{2\pi(j-1)}{3} + \sigma_y \sin \frac{2\pi(j-1)}{3} \right], \quad \text{for } j = 1, 2, 3. \quad (\text{A8})$$

In this work, we take $w_1 = 110 \text{ meV}$, $v_F = 5.944 \text{ eV } \text{\AA}$, $|\mathbf{K}_+| = 1.703 \text{ \AA}^{-1}$, and vary $0 \leq w_0/w_1 \leq 1$. The Hamiltonian of valley $\eta = -$ can be obtained from the time-reversal transformation

$$h_{\mathbf{Q}, \mathbf{Q}'}^{\text{TBG}, -}(\mathbf{k}) = \sigma_x h_{-\mathbf{Q}, -\mathbf{Q}'}^{\text{TBG}, +}(-\mathbf{k}) \sigma_x. \quad (\text{A9})$$

b. Many-body Hamiltonian

For a double-gated experimental setup, the electron-electron interaction potential is given by [23, 269]

$$V(\mathbf{r}) = U_\xi \sum_{n=-\infty}^{\infty} \frac{(-1)^n}{\sqrt{(|\mathbf{r}|/\xi)^2 + n^2}} \quad \text{and} \quad V(\mathbf{q}) = (\pi U_\xi \xi^2) \frac{\tanh(|\mathbf{q}|\xi/2)}{|\mathbf{q}|\xi/2}, \quad (\text{A10})$$

where $U_\xi = \frac{e^2}{4\pi\epsilon_0\epsilon\xi} = 24 \text{ meV}$, $\epsilon = 6$ is the dielectric constant, and $\xi = 10 \text{ nm}$ is the distance between the two screening gates. The interaction term takes the form of [22, 25, 269]

$$\hat{H}_I^{\text{TBG}} = \frac{1}{2} \frac{1}{N_0 \Omega_0} \sum_{\mathbf{q}} \sum_{\mathbf{G} \in \mathcal{Q}_0} V(\mathbf{q} + \mathbf{G}) \delta\rho(-\mathbf{q} - \mathbf{G}) \delta\rho(\mathbf{q} + \mathbf{G}), \quad (\text{A11})$$

where the normal-ordered density operator $\delta\rho(\mathbf{q} + \mathbf{G})$ is defined as

$$\delta\rho(\mathbf{q} + \mathbf{G}) = \rho(\mathbf{q} + \mathbf{G}) - \frac{1}{2} \delta_{\mathbf{q}, \mathbf{0}} \delta_{\mathbf{G}, \mathbf{0}} = \sum_{\eta, \alpha, s} \sum_{\mathbf{k}} \sum_{\mathbf{Q} \in \mathcal{Q}_\pm} \left(\hat{c}_{\mathbf{k}+\mathbf{q}, \mathbf{Q}-\mathbf{G}, \alpha, \eta, s}^\dagger \hat{c}_{\mathbf{k}, \mathbf{Q}, \alpha, \eta, s} - \frac{1}{2} \delta_{\mathbf{q}, \mathbf{0}} \delta_{\mathbf{G}, \mathbf{0}} \right), \quad (\text{A12})$$

N_0 is the number of moiré unit cells, and Ω_0 is the area of a single moiré unit cell. The full TBG Hamiltonian is written as $\hat{H}^{\text{TBG}} = \hat{H}_0^{\text{TBG}} + \hat{H}_I^{\text{TBG}}$.

2. Review of the topological heavy fermion model for TBG

We now review the topological heavy fermion (THF) description [33, 35, 45, 49, 50, 171, 273–278] of the BM low-energy bands. The THF model resolves the stable topological obstruction of the entire BM model [25, 33, 58, 60, 279, 280] by introducing two fermionic species: “heavy” (f) and “conduction” (c) electrons. In contrast to the f -fermions, which form effective $p_x \pm ip_y$ orbitals localized at the moiré AA sites, the c -fermions are semi-metallic, dispersive, and form anomalous electronic bands.

a. The THF model fermions

In terms of the low-energy operators of the BM model introduced in Eq. (A3), the f -fermions are given in momentum space by

$$\hat{f}_{\mathbf{k}, \alpha, \eta, s}^\dagger = \sum_{\mathbf{Q}, \beta} v_{\mathbf{Q}\beta; \alpha}^\eta(\mathbf{k}) \hat{c}_{\mathbf{k}, \mathbf{Q}, \beta, \eta, s}^\dagger, \quad (\text{A13})$$

where $v_{\mathbf{Q}\beta; \alpha}^\eta(\mathbf{k})$ is the f -fermion momentum-space wave function in valley η , with $\alpha = 1, 2$ denotes the orbital quantum number. Although usually obtained numerically through a Wannierization and disentanglement procedure, the f -fermion wave function has an analytical approximation in terms of Gaussian profiles [33, 35]. Defining the Fourier transformation for the f -fermion wave functions,

$$v_{\mathbf{Q}\beta; \alpha}^\eta(\mathbf{k}) = \frac{1}{\sqrt{\Omega_0}} \int d^2r w_{l\beta; \alpha}^\eta(\mathbf{r}) e^{-i(\mathbf{k}-\mathbf{Q}) \cdot \mathbf{r}}, \quad \text{for } \mathbf{Q} \in \mathcal{Q}_{\eta l}, \quad (\text{A14})$$

$$w_{l\beta;\alpha}^\eta(\mathbf{r}) = \frac{1}{N_0\sqrt{\Omega_0}} \sum_{\mathbf{k}} \sum_{\mathbf{Q} \in \mathcal{Q}_{\eta l, \beta}} v_{\mathbf{Q}\beta;\alpha}^\eta(\mathbf{k}) e^{i(\mathbf{k}-\mathbf{Q}) \cdot \mathbf{r}}, \quad (\text{A15})$$

their real-space Wannier wave functions can be approximated by [33],

$$w_{l1;1}^\eta(\mathbf{r}) = \frac{\alpha_1}{\sqrt{2\pi\lambda_1^2}} e^{i\frac{\pi}{4}l\eta - \frac{r^2}{2\lambda_1^2}}, \quad w_{l2;1}^\eta(\mathbf{r}) = -l \frac{\alpha_2}{\sqrt{2}} \frac{r_x + i\eta r_y}{\lambda_2^2 \sqrt{\pi}} e^{i\frac{\pi}{4}l\eta - \frac{r^2}{2\lambda_2^2}}, \quad (\text{A16})$$

$$w_{l1;2}^\eta(\mathbf{r}) = l \frac{\alpha_2}{\sqrt{2}} \frac{r_x - i\eta r_y}{\lambda_2^2 \sqrt{\pi}} e^{-i\frac{\pi}{4}l\eta - \frac{r^2}{2\lambda_2^2}}, \quad w_{l2;2}^\eta(\mathbf{r}) = \frac{\alpha_1}{\sqrt{2\pi\lambda_1^2}} e^{-i\frac{\pi}{4}l\eta - \frac{r^2}{2\lambda_1^2}}, \quad (\text{A17})$$

where the amplitudes α_1 and α_2 , as well as the spreads λ_1 and λ_2 have been obtained both numerically and analytically across a large parameter regime [33, 35]. In momentum-space across a large parameter regime [4, 12]. In momentum-space the approximations from Eqs. (A16) and (A17) can be, the approximations from Eqs. (A16) and (A17) can be computed using Eq. (A15)

$$v_{\mathbf{Q}1;1}^{(\eta)}(\mathbf{k}) = \alpha_1 \sqrt{\frac{2\pi\lambda_1^2}{\Omega_0 \mathcal{N}_{f,\mathbf{k}}}} e^{i\frac{\pi}{4}\zeta_{\mathbf{Q}} - \frac{1}{2}(\mathbf{k}-\mathbf{Q})^2 \lambda_1^2},$$

$$v_{\mathbf{Q}2;1}^{(\eta)}(\mathbf{k}) = \alpha_2 \sqrt{\frac{2\pi\lambda_2^4}{\Omega_0 \mathcal{N}_{f,\mathbf{k}}}} \zeta_{\mathbf{Q}} [i\eta(k_x - Q_x) - (k_y - Q_y)] e^{i\frac{\pi}{4}\zeta_{\mathbf{Q}} - \frac{1}{2}(\mathbf{k}-\mathbf{Q})^2 \lambda_2^2}, \quad (\text{A18})$$

$$v_{\mathbf{Q}1;2}^{(\eta)}(\mathbf{k}) = \alpha_2 \sqrt{\frac{2\pi\lambda_2^4}{\Omega_0 \mathcal{N}_{f,\mathbf{k}}}} \zeta_{\mathbf{Q}} [-i\eta(k_x - Q_x) - (k_y - Q_y)] e^{-i\frac{\pi}{4}\zeta_{\mathbf{Q}} - \frac{1}{2}(\mathbf{k}-\mathbf{Q})^2 \lambda_2^2},$$

$$v_{\mathbf{Q}2;2}^{(\eta)}(\mathbf{k}) = \alpha_1 \sqrt{\frac{2\pi\lambda_1^2}{\Omega_0 \mathcal{N}_{f,\mathbf{k}}}} e^{-i\frac{\pi}{4}\zeta_{\mathbf{Q}} - \frac{1}{2}(\mathbf{k}-\mathbf{Q})^2 \lambda_1^2}. \quad (\text{A19})$$

In Eqs. (A18) and (A19), we have introduced the normalization factor $\mathcal{N}_{f,\mathbf{k}}$, which can be determined to be

$$\mathcal{N}_{f,\mathbf{k}} = \alpha_1^2 \frac{2\pi\lambda_1^2}{\Omega_0} \sum_{\mathbf{Q}} e^{-(\mathbf{k}-\mathbf{Q})^2 \lambda_1^2} + \alpha_2^2 \frac{2\pi\lambda_2^4}{\Omega_0} \sum_{\mathbf{Q}} (\mathbf{k}-\mathbf{Q})^2 e^{-(\mathbf{k}-\mathbf{Q})^2 \lambda_2^2}. \quad (\text{A20})$$

In order to correctly capture the strong topology of the system, Ref. [33] also introduces four anomalous c -electrons around the Γ_M point. The c -fermion operators are defined according to

$$\hat{c}_{\mathbf{k},a,\eta,s}^\dagger = \sum_{\mathbf{Q},\beta} \tilde{u}_{\mathbf{Q}\beta;a}^\eta(\mathbf{k}) \hat{c}_{\mathbf{k},\mathbf{Q},\beta,\eta,s}^\dagger, \quad \text{for } 1 \leq a \leq 4. \quad (\text{A21})$$

In Eq. (A21), a indexes the four c -electron states (for each spin and valley), while $\tilde{u}_{\mathbf{Q}\beta;a}^\eta(\mathbf{k})$ denotes their wave function. The $\hat{c}_{\mathbf{k},a,\eta,s}^\dagger$ fermions have a large kinetic energy away from the Γ_M point, and as a result, they are only defined for momenta below a certain cutoff $|\mathbf{k}| < \Lambda_c$, and their wave function in the proximity of the Γ_M point can be approximated by [33]

$$\tilde{u}_{\mathbf{Q}\beta;a}^\eta(\mathbf{k}) \approx \tilde{u}_{\mathbf{Q}\beta;a}^\eta(\mathbf{0}). \quad (\text{A22})$$

Analytical expressions for c -electron wave functions were found in Ref. [35]. These were not directly derived from the BM model approximations [35, 149]. The approximations for the wave functions at $\mathbf{k} = \mathbf{0}$ are given by [35]

$$\tilde{u}_{\mathbf{Q}1;1}^{(\eta)}(\mathbf{0}) = -\alpha_{c1} \lambda_{c1} \sqrt{\frac{2\pi}{\Omega_0 \mathcal{N}_{c1}}} e^{-i\frac{\pi}{4}\zeta_{\mathbf{Q}} - \frac{1}{2}\mathbf{Q}^2 \lambda_{c1}^2}, \quad \tilde{u}_{\mathbf{Q}2;1}^{(\eta)}(\mathbf{0}) = \alpha_{c2} \lambda_{c2}^3 \sqrt{\frac{\pi}{\Omega_0 \mathcal{N}_{c1}}} (i\eta Q_x + Q_y)^2 e^{-i\frac{\pi}{4}\zeta_{\mathbf{Q}} - \frac{1}{2}\mathbf{Q}^2 \lambda_{c2}^2}, \quad (\text{A23})$$

$$\tilde{u}_{\mathbf{Q}1;2}^{(\eta)}(\mathbf{0}) = \alpha_{c2} \lambda_{c2}^3 \sqrt{\frac{\pi}{\Omega_0 \mathcal{N}_{c2}}} (-i\eta Q_x + Q_y)^2 e^{i\frac{\pi}{4}\zeta_{\mathbf{Q}} - \frac{1}{2}\mathbf{Q}^2 \lambda_{c2}^2}, \quad \tilde{u}_{\mathbf{Q}2;2}^{(\eta)}(\mathbf{0}) = -\alpha_{c1} \lambda_{c2} \sqrt{\frac{2\pi}{\Omega_0 \mathcal{N}_{c2}}} e^{i\frac{\pi}{4}\zeta_{\mathbf{Q}} - \frac{1}{2}\mathbf{Q}^2 \lambda_{c1}^2}, \quad (\text{A24})$$

$$\tilde{u}_{\mathbf{Q}1;3}^{(\eta)}(\mathbf{0}) = \alpha_{c3} \lambda_{c3}^2 \sqrt{\frac{2\pi}{\Omega_0 \mathcal{N}_{c3}}} \zeta_{\mathbf{Q}} (-i\eta Q_x + Q_y) e^{-i\frac{\pi}{4}\zeta_{\mathbf{Q}} - \frac{1}{2}\mathbf{Q}^2 \lambda_{c3}^2}, \quad \tilde{u}_{\mathbf{Q}2;3}^{(\eta)}(\mathbf{0}) = \alpha_{c4} \lambda_{c4}^3 \sqrt{\frac{\pi}{\Omega_0 \mathcal{N}_{c3}}} (-i\eta Q_x + Q_y)^2 e^{-i\frac{\pi}{4}\zeta_{\mathbf{Q}} - \frac{1}{2}\mathbf{Q}^2 \lambda_{c4}^2}, \quad (\text{A25})$$

$$\tilde{u}_{\mathbf{Q}1;4}^{(\eta)}(\mathbf{0}) = \alpha_{c4} \lambda_{c4}^3 \sqrt{\frac{\pi}{\Omega_0 \mathcal{N}_{c4}}} (i\eta Q_x + Q_y)^2 e^{i\frac{\pi}{4}\zeta_{\mathbf{Q}} - \frac{1}{2}\mathbf{Q}^2 \lambda_{c4}^2}, \quad \tilde{u}_{\mathbf{Q}2;4}^{(\eta)}(\mathbf{0}) = \alpha_{c3} \lambda_{c3}^2 \sqrt{\frac{2\pi}{\Omega_0 \mathcal{N}_{c4}}} \zeta_{\mathbf{Q}} (i\eta Q_x + Q_y) e^{i\frac{\pi}{4}\zeta_{\mathbf{Q}} - \frac{1}{2}\mathbf{Q}^2 \lambda_{c3}^2}, \quad (\text{A26})$$

where we have used the sublattice factor $\zeta_{\mathbf{Q}} = +1$ ($\zeta_{\mathbf{Q}} = -1$) for $\mathbf{Q} \in \mathcal{Q}_+$ ($\mathbf{Q} \in \mathcal{Q}_-$). These expressions are also extended for small momenta around the Γ_M point using Eq. (A22) [33]. For $\theta = 1.05^\circ$ and $w_0/w_1 = 0.8$, the parameters appearing in Eqs. (A23) to (A26) have been fitted to the numerical solution and are given by [35]

$$\alpha_{c1} = 0.3958, \quad \alpha_{c2} = 0.9183, \quad \mathcal{N}_{c1} = \mathcal{N}_{c2} = 1.2905, \quad \lambda_{c1} = 0.2194|\mathbf{a}_{M1}|, \quad \lambda_{c2} = 0.3299|\mathbf{a}_{M1}|, \quad (\text{A27})$$

$$\alpha_{c3} = 0.9257, \quad \alpha_{c4} = 0.3783, \quad \mathcal{N}_{c3} = \mathcal{N}_{c4} = 1.1102, \quad \lambda_{c3} = 0.2430|\mathbf{a}_{M1}|, \quad \lambda_{c4} = 0.2241|\mathbf{a}_{M1}|. \quad (\text{A28})$$

b. The single-particle THF model

The single-particle THF model Hamiltonian for TBG is obtained by projecting the low-energy fermions from Eq. (A3) into the THF model basis via the approximation

$$\hat{c}_{\mathbf{k},\mathbf{Q},\beta,\eta,s}^\dagger \approx \begin{cases} \sum_{\alpha} v_{\mathbf{Q}\beta;\alpha}^{*\eta}(\mathbf{k}) \hat{f}_{\mathbf{k},\alpha,\eta,s}^\dagger + \sum_a \tilde{u}_{\mathbf{Q}\beta;a}^{*\eta}(\mathbf{k}) \hat{c}_{\mathbf{k},a,\eta,s}^\dagger & \text{for } |\mathbf{k}| \leq \Lambda_c, \\ \sum_{\alpha} v_{\mathbf{Q}\beta;\alpha}^{*\eta}(\mathbf{k}) \hat{f}_{\mathbf{k},\alpha,\eta,s}^\dagger & \text{for } |\mathbf{k}| > \Lambda_c. \end{cases} \quad (\text{A29})$$

and reads as

$$\begin{aligned} H_0^{\text{TBG}} = & \sum_{\substack{|\mathbf{k}| \leq \Lambda_c \\ \eta,s}} \left[\sum_{a,a'} h_{aa'}^{cc,\eta}(\mathbf{k}) \hat{c}_{\mathbf{k},a,\eta,s}^\dagger \hat{c}_{\mathbf{k},a',\eta,s} + \left(\sum_{a,\alpha} h_{a\alpha}^{cf,\eta}(\mathbf{k}) \hat{c}_{\mathbf{k},a,\eta,s}^\dagger \hat{f}_{\mathbf{k},\alpha,\eta,s} + \text{h.c.} \right) \right] \\ & + \sum_{\substack{\mathbf{k},\alpha,\alpha' \\ \eta,s}} h_{\alpha\alpha'}^{ff,\eta}(\mathbf{k}) \hat{f}_{\mathbf{k},\alpha,\eta,s}^\dagger \hat{f}_{\mathbf{k},\alpha',\eta,s}. \end{aligned} \quad (\text{A30})$$

In Eq. (A30), “+h.c.” denotes the addition of the Hermitian conjugate. In order to differentiate the BM and THF model Hamiltonians, the former are always denoted with a hat. The matrix blocks appearing in Eq. (A30) are given by [33]

$$h^{cc,\eta}(\mathbf{k}) = \begin{pmatrix} 0 & v_*(\eta k_x \sigma_0 + i k_y \sigma_z) \\ v_*(\eta k_x \sigma_0 - i k_y \sigma_z) & M \sigma_z \end{pmatrix}, \quad (\text{A31})$$

$$h^{cf,\eta}(\mathbf{k}) = \begin{pmatrix} \gamma \sigma_0 + v'_*(\eta k_x \sigma_x + k_y \sigma_y) \\ v''_*(\eta k_x \sigma_x - k_y \sigma_y) \end{pmatrix} e^{-\frac{|\mathbf{k}|^2 \lambda^2}{2}}, \quad (\text{A32})$$

$$h^{ff,\eta}(\mathbf{k}) = 0, \quad (\text{A33})$$

with 0 denoting the zero 2×2 (per spin per valley) matrix. The single-particle parameters appearing in Eqs. (A31) and (A32) depend on the parameters of the BM model of TBG and have been obtained both numerically and analytically across a vast range of twist angles θ and tunneling ratios w_0/w_1 [33, 35]. For $\theta = 1.05^\circ$, $w_0/w_1 = 0.8$, and the BM model parameters chosen around Eq. (A5), $\lambda = 0.3375|\mathbf{a}_{M1}|$, $\gamma = -24.75 \text{ meV}$, $M = 3.697 \text{ meV}$, $v_* = -4.303 \text{ eV \AA}$, $v'_* = 1.623 \text{ eV \AA}$, and $v''_* = -0.0332 \text{ eV \AA}$.

c. The interaction THF Hamiltonian

The THF interaction Hamiltonian was derived by directly projecting density operator from Eq. (A12) with the aid of Eq. (A29). Ref. [33] has shown that the resulting expression can be simplified to a sum of just seven terms which depend on only six parameters and the Coulomb interaction potential from Eq. (A10)

$$H_I^{\text{TBG}} = H_{U_1} + H_W + H_V + H_J + H_{U_2} + H_{\bar{J}} + H_K. \quad (\text{A34})$$

The seven terms of Eq. (A34) are given by

$$H_{U_1} = \frac{U_1}{2} \sum_{\mathbf{R}} \sum_{\substack{\alpha,\eta,s \\ \alpha',\eta',s'}} : \hat{f}_{\mathbf{R},\alpha',\eta',s'}^\dagger \hat{f}_{\mathbf{R},\alpha,\eta,s}^\dagger :: \hat{f}_{\mathbf{R},\alpha,\eta,s} \hat{f}_{\mathbf{R},\alpha',\eta',s'}, \quad (\text{A35})$$

$$H_W = \frac{1}{N_0} \sum_{\mathbf{k}_1} \sum_{\substack{\mathbf{q} \\ |\mathbf{k}_2| \leq \Lambda_c}} \sum_{\substack{\alpha, \eta, s \\ a', \eta', s'}} W_{a'} : \hat{f}_{\mathbf{k}_1 + \mathbf{q}, \alpha, \eta, s}^\dagger \hat{f}_{\mathbf{k}_1, \alpha, \eta, s} :: \hat{c}_{\mathbf{k}_2 - \mathbf{q}, a', \eta', s'}^\dagger \hat{c}_{\mathbf{k}_2, a', \eta', s'} :, \quad (\text{A36})$$

$$H_V = \frac{1}{2\Omega_0 N_0} \sum_{|\mathbf{k}_1|, |\mathbf{k}_2| \leq \Lambda_c} \sum_{\substack{\mathbf{q} \\ |\mathbf{k}_1 + \mathbf{q}|, |\mathbf{k}_2 + \mathbf{q}| \leq \Lambda_c}} \sum_{\substack{a, \eta, s \\ a', \eta', s'}} V(\mathbf{q}) : \hat{c}_{\mathbf{k}_1 + \mathbf{q}, a', \eta', s'}^\dagger \hat{c}_{\mathbf{k}_1, a', \eta', s'} :: \hat{c}_{\mathbf{k}_2 - \mathbf{q}, a, \eta, s}^\dagger \hat{c}_{\mathbf{k}_2, a, \eta, s} :, \quad (\text{A37})$$

$$H_J = -\frac{J}{2N_0} \sum_{\mathbf{k}_1} \sum_{\substack{\mathbf{q} \\ |\mathbf{k}_2| \leq \Lambda_c}} \sum_{\substack{\alpha, \eta, s \\ a', \eta', s'}} \left[\eta \eta' + (-1)^{\alpha + \alpha'} \right] : \hat{f}_{\mathbf{k}_1 + \mathbf{q}, \alpha', \eta', s'}^\dagger \hat{f}_{\mathbf{k}_1, \alpha, \eta, s} :: \hat{c}_{\mathbf{k}_2 - \mathbf{q}, \alpha + 2, \eta, s}^\dagger \hat{c}_{\mathbf{k}_2, \alpha' + 2, \eta', s'} :, \quad (\text{A38})$$

$$H_{U_2} = \frac{U_2}{2} \sum_{\langle \mathbf{R}, \mathbf{R}' \rangle} \sum_{\substack{\alpha, \eta, s \\ \alpha', \eta', s'}} : \hat{f}_{\mathbf{R}', \alpha', \eta', s'}^\dagger \hat{f}_{\mathbf{R}, \alpha', \eta', s'} :: \hat{f}_{\mathbf{R}, \alpha, \eta, s}^\dagger \hat{f}_{\mathbf{R}, \alpha, \eta, s} :, \quad (\text{A39})$$

$$H_{\bar{J}} = -\frac{J}{4N_0} \sum_{|\mathbf{k}_1|, |\mathbf{k}_2| \leq \Lambda_c} \sum_{\mathbf{q}} \sum_{\substack{\alpha, \eta, s \\ a', \eta', s'}} \left[\eta \eta' - (-1)^{\alpha + \alpha'} \right] \hat{f}_{\mathbf{k}_1 + \mathbf{q}, \alpha', \eta', s'}^\dagger \hat{f}_{\mathbf{k}_2 - \mathbf{q}, \alpha, \eta, s}^\dagger \hat{c}_{\mathbf{k}_2, \alpha + 2, \eta, s} \hat{c}_{\mathbf{k}_1, \alpha' + 2, \eta', s'} + \text{h.c.} \quad (\text{A40})$$

$$H_K = \frac{K}{N_0 \Omega_0} \sum_{|\mathbf{k}_1|, |\mathbf{k}_2|, |\mathbf{k}_3| \leq \Lambda_c} \sum_{\substack{\alpha, \eta, s \\ \eta', s'}} \eta \eta' \left(\hat{c}_{\mathbf{k}_1, \bar{\alpha}, \eta, s}^\dagger \hat{c}_{\mathbf{k}_3, \alpha + 2, \eta, s} \hat{f}_{\mathbf{k}_1 - \mathbf{k}_2 - \mathbf{k}_3, \alpha, \eta', s'}^\dagger \hat{c}_{\mathbf{k}_2, \alpha + 2, \eta', s'} \right. \\ \left. - \hat{f}_{\mathbf{k}_2 + \mathbf{k}_3 - \mathbf{k}_1, \alpha, \eta', s'}^\dagger \hat{c}_{\mathbf{k}_2, \alpha + 2, \eta', s'} \hat{c}_{\mathbf{k}_1, \bar{\alpha} + 2, \eta, s}^\dagger \hat{c}_{\mathbf{k}_3, \alpha, \eta, s} \right) + \text{h.c.} \quad (\text{A41})$$

where $\bar{\alpha} = 3 - \alpha$. These terms represent various interactions within the THF model: onsite and nearest-neighbor repulsions between f -electrons (H_{U_1} and H_{U_2}), Coulomb interactions among c -electrons (H_V), density-density and exchange interactions between f and c electrons (H_W and H_J), and interactions involving hybridization ($H_{\bar{J}}$ and H_K). H_K is usually neglected as it does not conserve the f number, which bears a large energy cost when $U > |\gamma|$. When $U < |\gamma|$, the formalism changes, and the Coulomb interaction must be projected into the flat bands, giving rise to the projected strong interaction picture [23–25, 269, 281, 282]. The normal ordering of an operator \mathcal{O} subtracts its expectation value in the charge neutral ground state, $|G_0\rangle$, which is defined such that

$$\begin{aligned} \langle G_0 | \hat{f}_{\mathbf{k}, \alpha, \eta, s}^\dagger \hat{f}_{\mathbf{k}', \alpha', \eta', s'} | G_0 \rangle &= \frac{1}{2} \delta_{\mathbf{k}, \mathbf{k}'} \delta_{\alpha \alpha'} \delta_{\eta \eta'} \delta_{ss'}, \\ \langle G_0 | \hat{c}_{\mathbf{k}, a, \eta, s}^\dagger \hat{c}_{\mathbf{k}', a', \eta', s'} | G_0 \rangle &= \frac{1}{2} \delta_{\mathbf{k}, \mathbf{k}'} \delta_{aa'} \delta_{\eta \eta'} \delta_{ss'}, \\ \langle G_0 | \hat{f}_{\mathbf{k}, \alpha, \eta, s}^\dagger \hat{c}_{\mathbf{k}', a', \eta', s'} | G_0 \rangle &= \langle G_0 | \hat{c}_{\mathbf{k}, a, \eta, s}^\dagger \hat{f}_{\mathbf{k}', \alpha', \eta', s'} | G_0 \rangle = 0. \end{aligned} \quad (\text{A42})$$

Additionally, in Eq. (A39), $\langle \mathbf{R}, \mathbf{R}' \rangle$ denotes nearest-neighbor lattice sites. For $\theta = 1.05^\circ$, $w_0/w_1 = 0.8$, as well as the relative permittivity and screening length chosen around Eq. (A10), the six interaction parameters ($W_1 = W_2$ and $W_3 = W_4$ follows by symmetry [33]) are given by [33]

$$\begin{aligned} U_1 &= 57.95 \text{ meV}, & J &= 16.38 \text{ meV}, & W_1 &= W_2 = 44.03 \text{ meV}, \\ U_2 &= 2.239 \text{ meV}, & K &= 4.887 \text{ meV}, & W_3 &= W_4 = 50.2 \text{ meV}, \end{aligned} \quad (\text{A43})$$

while the c - c interaction potential is the same as in Eq. (A10).

d. Berry Curvature of the TBG active bands

For each spin s and valley η , the active TBG bands near charge neutrality can be recombined into Chern- (± 1) bands [58, 269, 279], whose operators are denoted by $\hat{d}_{\mathbf{k}, \zeta, \eta, s}^\dagger$. Specifically, $\hat{d}_{\mathbf{k}, \zeta, \eta, s}^\dagger$ creates a state of spin s in valley η within the Chern band with Chern number $\zeta \cdot \eta$. In terms of the TBG low-energy operators from Eq. (A3), the Chern-band operators are defined according to

$$\hat{d}_{\mathbf{k}, \zeta, \eta, s}^\dagger = \sum_{\mathbf{Q}, \beta} U_{\mathbf{Q}, \beta; \eta}^\zeta(\mathbf{k}) \hat{c}_{\mathbf{k}, \mathbf{Q}, \beta, \eta, s}^\dagger, \quad (\text{A44})$$

with $U_{\mathbf{Q}, \beta; \eta}^\zeta(\mathbf{k})$ being the corresponding Chern-band wave function.

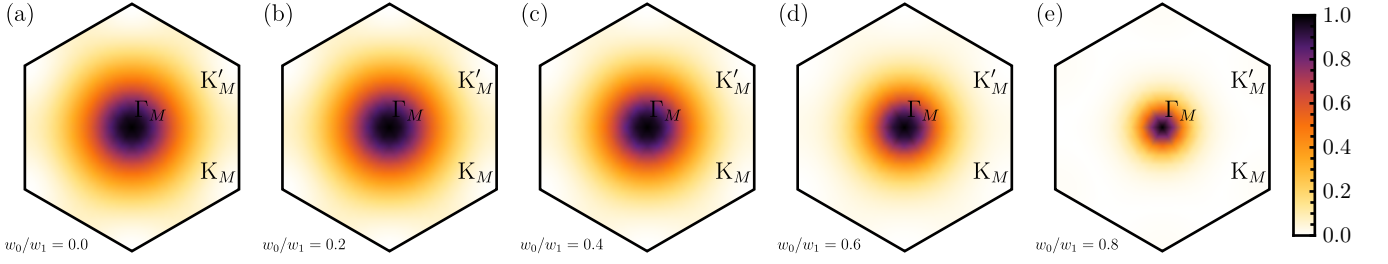


FIG. 7. Berry curvature $\Omega^{+,+}(\mathbf{k})$ of the Chern-(+1) band of TBG within valley $\eta = +$ at the magic angle $\theta = 1.05^\circ$. The BM model parameters we employ are listed below Eq. (A8). (a)-(e) illustrate the effects of varying the tunneling amplitude ratio (indicated below each panel) from the unrealistic chiral limit $w_0/w_1 = 0$ [61] to the more realistic value $w_0/w_1 = 0.8$. The Berry curvature is plotted in arbitrary units, as indicated by the accompanying colorbar.

The Berry curvature of the TBG active Chern bands can be defined in terms of the corresponding projector. Letting

$$[P^{\zeta,\eta}(\mathbf{k})]_{\alpha\mathbf{Q};\beta\mathbf{Q}'} = U_{\mathbf{Q}\alpha;\eta}^{\zeta}(\mathbf{k}) U_{\mathbf{Q}'\beta;\eta}^{*\zeta}(\mathbf{k}) \quad (\text{A45})$$

be the projector into the Chern band corresponding to $\hat{d}_{\mathbf{k},\zeta,\eta,s}^\dagger$, the associated Berry curvature is given by

$$\Omega^{\zeta,\eta}(\mathbf{k}) = -i \sum_{\mu,\nu} \epsilon^{\mu\nu} \text{Tr} [P^{\zeta,\eta}(\mathbf{k}) \partial_{k^\mu} P^{\zeta,\eta}(\mathbf{k}) \partial_{k^\nu} P^{\zeta,\eta}(\mathbf{k})], \quad (\text{A46})$$

where $\epsilon^{\mu\nu}$ is the two-dimensional Levi-Civita symbol with $\epsilon^{xx} = \epsilon^{yy} = 0$ and $\epsilon^{xy} = -\epsilon^{yx} = 0$.

In Fig. 7, we plot the distribution of the Berry curvature for the TBG Chern bands at the magic angle, across a range of tunneling ratios $0 \leq w_0/w_1 \leq 0.8$. For the realistic value $w_0/w_1 = 0.8$, the Berry curvature is concentrated near the Γ_M point. Conversely, as we approach the chiral limit ($w_0/w_1 = 0$) [61], the Berry curvature becomes more evenly distributed across the moiré BZ. This uniform spread of the Berry curvature can be directly linked to the largely increased f - c hybridization in the chiral limit [33, 35].

Appendix B: Analytical results within the THF model

In Ref. [35], it was shown that around the magic angle, the flat and closest remote bands of TBG within the single-particle BM model are extremely well-fitted by the THF model for a wide range of angles and tunneling amplitude ratios. It was, however, argued that the direct utility of the THF model is dependent on a separation of scales between the f - c hybridization (γ) and the onsite Hubbard repulsion of the f -electrons (U_1) [35], where the magnitude of the latter should be larger than the former. In this case, a *real-space* description of TBG is possible, in which the f -electrons form local moments [33, 45, 49, 50, 171, 273–278].

Conversely, when $|\gamma| > U_1$, a real-space description of the interaction terms is no longer useful, as the large f - c hybridization does not allow the polarization of the f -fermions to minimize the onsite Hubbard repulsion H_{U_1} . Because in the $|\gamma| > U_1$ limit, the energy scale of the interaction is smaller than the gap between the active and remote TBG, a flat-band-projected approach constitutes a more realistic formulation of the problem [23, 282]. Such a description involves the so-called TBG form factors – overlaps between the active TBG band wave functions at different momenta [269]. The TBG form factors can easily be computed numerically, but in order to obtain them analytically, the expressions of the active TBG wave functions are necessary. Obtaining the latter is an impossible task in the original BM model with a large number of bands, but becomes tractable within the THF formalism.

In this appendix, we show that in the $|\gamma| > U_1$ limit, the single-particle THF model can still be employed to derive analytical expressions for the TBG flat-band wave functions. We then show how the latter can be used to compute the TBG form factors analytically. In turn, this enables us to analytically obtain the charge-one excitations of TBG using the method introduced by Ref. [24]. Finally, we also show that for $|\gamma| > U_1$, a flat-band projected limit of the THF model can be defined, wherein the charge-one excitations of TBG around charge neutrality can also be obtained analytically. This confirms the conceptual utility of the THF model not just in the $|\gamma| < U_1$ limit, but also in the opposite limit $|\gamma| > U_1$.

1. Flat-band wave functions

In the THF model, the wave functions of the flat bands can be obtained analytically within the zero-bandwidth limit, which is defined when $v'_\star = v''_\star = 0$, and $M = 0$ [33]. In this limit, the model exhibits an additional symmetry, which Ref. [33] dubs “chiral symmetry”. Notably, the chiral symmetry of the THF model within the zero-bandwidth limit is *different* from the chiral sublattice symmetry of the TBG BM model in the $w_0/w_1 = 0$ limit [61]. This can be seen by noting that in the $w_0/w_1 = 0$ limit, the active TBG Chern bands are eigenstates of the chiral sublattice operator and are, therefore, graphene sublattice-polarized. However, the active TBG Chern bands, obtained analytically from the THF model in its zero-bandwidth limit [33] are not polarized on the single-layer graphene sublattices. As a result, the analytical expression for the TBG flat bands obtained with the THF model in zero-bandwidth limit are still a good approximation of the realistic TBG bands.

a. Analytical expression for the TBG flat-band wave functions

Working in the zero-bandwidth limit, the single-particle Hamiltonian from Eq. (A30) can be diagonalized analytically. The fermion operators $\hat{d}_{\mathbf{k},\zeta,\eta,s}^\dagger$ ($\zeta = \pm$) and $\hat{b}_{\mathbf{k},j,\eta,s}^\dagger$ ($j = \pm 1, \pm 2$), corresponding to the Chern band eigenstates of the active bands introduced in Eq. (A44) and to the remote-band eigenstates, respectively, are given in the THF model basis by

$$\begin{aligned}\hat{d}_{\mathbf{k},+, \eta, s}^\dagger &= g_{\mathbf{k}} e^{i\eta\theta_{\mathbf{k}}} \hat{f}_{\mathbf{k},1,\eta,s}^\dagger - \eta h_{\mathbf{k}} \hat{c}_{\mathbf{k},3,\eta,s}^\dagger, \\ \hat{b}_{\mathbf{k},+1,\eta,s}^\dagger &= \frac{1}{\sqrt{2}} \left(h_{\mathbf{k}} \hat{f}_{\mathbf{k},1,\eta,s}^\dagger - \hat{c}_{\mathbf{k},1,\eta,s}^\dagger + \eta g_{\mathbf{k}} e^{-i\eta\theta_{\mathbf{k}}} \hat{c}_{\mathbf{k},3,\eta,s}^\dagger \right), \\ \hat{b}_{\mathbf{k},+2,\eta,s}^\dagger &= \frac{1}{\sqrt{2}} \left(h_{\mathbf{k}} \hat{f}_{\mathbf{k},1,\eta,s}^\dagger + \hat{c}_{\mathbf{k},1,\eta,s}^\dagger + \eta g_{\mathbf{k}} e^{-i\eta\theta_{\mathbf{k}}} \hat{c}_{\mathbf{k},3,\eta,s}^\dagger \right), \\ \hat{d}_{\mathbf{k},-, \eta, s}^\dagger &= g_{\mathbf{k}} e^{-i\eta\theta_{\mathbf{k}}} \hat{f}_{\mathbf{k},2,\eta,s}^\dagger - \eta h_{\mathbf{k}} \hat{c}_{\mathbf{k},4,\eta,s}^\dagger, \\ \hat{b}_{\mathbf{k},-1,\eta,s}^\dagger &= \frac{1}{\sqrt{2}} \left(h_{\mathbf{k}} \hat{f}_{\mathbf{k},2,\eta,s}^\dagger - \hat{c}_{\mathbf{k},2,\eta,s}^\dagger + \eta g_{\mathbf{k}} e^{i\eta\theta_{\mathbf{k}}} \hat{c}_{\mathbf{k},4,\eta,s}^\dagger \right), \\ \hat{b}_{\mathbf{k},-2,\eta,s}^\dagger &= \frac{1}{\sqrt{2}} \left(h_{\mathbf{k}} \hat{f}_{\mathbf{k},2,\eta,s}^\dagger + \hat{c}_{\mathbf{k},2,\eta,s}^\dagger + \eta g_{\mathbf{k}} e^{i\eta\theta_{\mathbf{k}}} \hat{c}_{\mathbf{k},4,\eta,s}^\dagger \right),\end{aligned}\tag{B1}$$

where

$$g_{\mathbf{k}} = \frac{v_\star |\mathbf{k}|}{\sqrt{|v_\star \mathbf{k}|^2 + \gamma^2 e^{-|\mathbf{k}|^2 \lambda^2}}}, \quad h_{\mathbf{k}} = \frac{\gamma e^{-|\mathbf{k}|^2 \lambda^2 / 2}}{\sqrt{|v_\star \mathbf{k}|^2 + \gamma^2 e^{-|\mathbf{k}|^2 \lambda^2}}}, \quad \text{and} \quad e^{i\theta_{\mathbf{k}}} = \frac{k_x + i k_y}{|\mathbf{k}|}.\tag{B2}$$

In the resulting band-basis, the single-particle Hamiltonian can then be written simply as

$$H_0^{\text{TBG}} = \sum_{\mathbf{k},j,\eta,s} \sqrt{\gamma^2 e^{-|\mathbf{k}|^2 \lambda^2} + v_\star^2 |\mathbf{k}|^2} (2|j| - 3) \hat{b}_{\mathbf{k},j,\eta,s}^\dagger \hat{b}_{\mathbf{k},j,\eta,s}.\tag{B3}$$

For simplicity, in Eq. (B1), we restricted the c -electrons' momenta to the first moiré BZ. In the generic case that includes all the c -electrons with momenta $|\mathbf{k}| < \Lambda_c$, the $\hat{d}_{\mathbf{k},\zeta,\eta,s}^\dagger$ operators are given by

$$\hat{d}_{\mathbf{k},+, \eta, s}^\dagger = \frac{1}{\sqrt{\mathcal{N}_{\mathbf{k}}}} \hat{f}_{\mathbf{k},1,\eta,s}^\dagger - \frac{1}{\sqrt{\mathcal{N}_{\mathbf{k}}}} \sum_{|\mathbf{k}+\mathbf{G}| < \Lambda_c} \frac{\gamma e^{-\frac{1}{2}\lambda^2 |\mathbf{k}+\mathbf{G}|^2} / v_\star}{\eta(k_x + G_x) + i(k_y + G_y)} \hat{c}_{\mathbf{k}+\mathbf{G},3,\eta,s}^\dagger,\tag{B4}$$

$$\hat{d}_{\mathbf{k},-, \eta, s}^\dagger = \frac{1}{\sqrt{\mathcal{N}_{\mathbf{k}}}} \hat{f}_{\mathbf{k},2,\eta,s}^\dagger - \frac{1}{\sqrt{\mathcal{N}_{\mathbf{k}}}} \sum_{|\mathbf{k}+\mathbf{G}| < \Lambda_c} \frac{\gamma e^{-\frac{1}{2}\lambda^2 |\mathbf{k}+\mathbf{G}|^2} / v_\star}{\eta(k_x + G_x) - i(k_y + G_y)} \hat{c}_{\mathbf{k}+\mathbf{G},4,\eta,s}^\dagger,\tag{B5}$$

where the normalization prefactor reads as

$$\mathcal{N}_{\mathbf{k}} = 1 + \sum_{|\mathbf{k}+\mathbf{G}| < \Lambda_c} \frac{\gamma^2 e^{-\lambda^2 |\mathbf{k}+\mathbf{G}|^2} / v_\star^2}{|\mathbf{k} + \mathbf{G}|^2}.\tag{B6}$$

We remind the reader that the operator $d_{\mathbf{k},\zeta,\eta,s}^\dagger$ corresponds to a Chern band with Chern number $\zeta \cdot \eta$. It is worth noting that, for the valley $\eta = +$, the $\hat{d}_{\mathbf{k},\zeta,\eta,s}^\dagger$ operator is the same as the Chern-band operator introduced by Ref. [269]. However, in valley $\eta = -$, the $\hat{d}_{\mathbf{k},\zeta,-,s}^\dagger$ operator introduced here corresponds to the $\hat{d}_{\mathbf{k},-\zeta,-,s}^\dagger$ one of Ref. [269].

The wave function of the TBG flat bands can, therefore, be expressed *analytically* in terms of the f - and c -electron operators. The latter also admit analytical expressions given by Eqs. (A16), (A17) and (A23) to (A26). In turn, this enables one to obtain the active band TBG wave functions analytically within the plane wave basis from Eq. (A3), a result which is not otherwise directly available from the BM model.

By combining Eqs. (A13), (A21) and (B1), we can express the electron operators of the flat TBG Chern bands in terms of the the low-energy TBG operators from Eq. (A3) as

$$\begin{aligned}\hat{d}_{\mathbf{k},+,\eta,s}^\dagger &= g_{\mathbf{k}} e^{i\eta\theta_{\mathbf{k}}} \sum_{\mathbf{Q},\beta} v_{\mathbf{Q}\beta;1}^\eta(\mathbf{k}) \hat{c}_{\mathbf{k},\mathbf{Q},\beta,\eta,s}^\dagger - \eta h_{\mathbf{k}} \sum_{\mathbf{Q},\beta} \tilde{u}_{\mathbf{Q}\beta;3}^\eta(\mathbf{0}) \hat{c}_{\mathbf{k},\mathbf{Q},\beta,\eta,s}^\dagger, \\ \hat{d}_{\mathbf{k},-,\eta,s}^\dagger &= g_{\mathbf{k}} e^{-i\eta\theta_{\mathbf{k}}} \sum_{\mathbf{Q},\beta} v_{\mathbf{Q}\beta;2}^\eta(\mathbf{k}) \hat{c}_{\mathbf{k},\mathbf{Q},\beta,\eta,s}^\dagger - \eta h_{\mathbf{k}} \sum_{\mathbf{Q},\beta} \tilde{u}_{\mathbf{Q}\beta;4}^\eta(\mathbf{0}) \hat{c}_{\mathbf{k},\mathbf{Q},\beta,\eta,s}^\dagger.\end{aligned}\quad (\text{B7})$$

Comparing with Eq. (A44), we can directly identify the Chern band wave functions

$$U_{\mathbf{Q}\beta;\eta}^\zeta(\mathbf{k}) = e^{i\eta\zeta\theta_{\mathbf{k}}} g_{\mathbf{k}} v_{\mathbf{Q}\beta;\zeta}^\eta(\mathbf{k}) - \eta h_{\mathbf{k}} \tilde{u}_{\mathbf{Q}\beta;i_\zeta}^\eta(\mathbf{0}), \quad (\text{B8})$$

where, for simplicity, we have denoted $i_{\zeta=+} = 3$, $i_{\zeta=-} = 4$.

b. Analytical expressions for the TBG form factors

Another useful quantity which can be obtained analytically using Eq. (B8) are the TBG form factors corresponding to the active bands. The latter arise when projecting the TBG density operator into the Chern-band basis. Specifically, the projected TBG density operator is given by

$$\delta\rho(\mathbf{q}) = \sum_{\mathbf{k},\eta,s} \sum_{\zeta,\zeta'} M_{\zeta\zeta'}^{(\eta)}(\mathbf{k}, \mathbf{k} + \mathbf{q}) \left(\hat{d}_{\mathbf{k}+\mathbf{q},\zeta,\eta,s}^\dagger \hat{d}_{\mathbf{k},\zeta',\eta,s} - \frac{1}{2} \delta_{\mathbf{q},\mathbf{0}} \right), \quad (\text{B9})$$

where the corresponding form factors are defined by

$$M_{\zeta\zeta'}^{(\eta)}(\mathbf{k}, \mathbf{k}') = \sum_{\mathbf{Q},\beta} U_{\mathbf{Q}\beta;\eta}^{*\zeta}(\mathbf{k}) U_{\mathbf{Q}\beta;\eta}^{\zeta'}(\mathbf{k}'). \quad (\text{B10})$$

The form factors can be calculated via Eq. (B8). Approximately, we find that

$$M_{\zeta\zeta'}^{(\eta)}(\mathbf{k}, \mathbf{k}') \approx \sum_{\mathbf{Q},\beta} \left(g_{\mathbf{k}} g_{\mathbf{k}'} e^{-i\theta_{\mathbf{k}}\zeta - i\theta_{\mathbf{k}'}\zeta'} v_{\mathbf{Q}\beta;\zeta}^{*\eta}(\mathbf{k}) v_{\mathbf{Q}\beta;\zeta'}^\eta(\mathbf{k}') + h_{\mathbf{k}} h_{\mathbf{k}'} \tilde{u}_{\mathbf{Q}\beta;i_\zeta}^{*\eta}(\mathbf{0}) \tilde{u}_{\mathbf{Q}\beta;i_{\zeta'}}^\eta(\mathbf{0}) \right), \quad (\text{B11})$$

where we have dropped the cross-terms $v_{\mathbf{Q}\beta;\zeta}^{*\eta}(\mathbf{k}) \tilde{u}_{\mathbf{Q}\beta;i_{\zeta'}}^\eta(\mathbf{0})$ and $v_{\mathbf{Q}\beta;\zeta}^\eta(\mathbf{k}') \tilde{u}_{\mathbf{Q}\beta;i_\zeta}^{*\eta}(\mathbf{0})$. In general, the f - and c -fermions wave functions are orthogonal at any momentum \mathbf{k} in the moiré BZ

$$\sum_{\mathbf{Q},\beta} v_{\mathbf{Q}\beta;\zeta}^{*\eta}(\mathbf{k}) \tilde{u}_{\mathbf{Q}\beta;i_\zeta}^\eta(\mathbf{k}) = 0, \quad (\text{B12})$$

Coupled with the approximation $\tilde{u}_{\mathbf{Q}\beta,i}(\mathbf{k}) \approx \tilde{u}_{\mathbf{Q}\beta,i}(\mathbf{0})$ from Eq. (A22), this implies that the cross-terms should approximately vanish. Using also the orthonormal condition for the c -electron wave functions at the Γ_M point, $\sum_{\mathbf{Q},\beta} \tilde{u}_{\mathbf{Q}\beta;i_\zeta}^{*\eta}(\mathbf{0}) \tilde{u}_{\mathbf{Q}\beta;i_{\zeta'}}^\eta(\mathbf{0}) = \delta_{\zeta,\zeta'}$, we find that

$$M_{\zeta\zeta'}^{(\eta)}(\mathbf{k}, \mathbf{k}') \approx \sum_{\mathbf{Q},\beta} \left(g_{\mathbf{k}} g_{\mathbf{k}'} e^{-i(\theta_{\mathbf{k}} - \theta_{\mathbf{k}'})\zeta} v_{\mathbf{Q}\beta;\zeta}^{*\eta}(\mathbf{k}) v_{\mathbf{Q}\beta;\zeta'}^\eta(\mathbf{k}') + h_{\mathbf{k}} h_{\mathbf{k}'} \delta_{\zeta,\zeta'} \right). \quad (\text{B13})$$

To further simplify the expression from Eq. (B13), we now compute the sum $\sum_{\mathbf{Q},\beta} v_{\mathbf{Q}\beta;\zeta}^{*\eta}(\mathbf{k}) v_{\mathbf{Q}\beta;\zeta'}^\eta(\mathbf{k}')$ using the analytical formulae for the f -electron wave functions from Eqs. (A18) and (A19). Additionally, we approximate the summation over \mathbf{Q} by an integral according to

$$\sum_{\mathbf{Q}} \rightarrow \frac{\Omega_0}{2\pi^2} \int d^2Q. \quad (\text{B14})$$

This allows us to obtain

$$\begin{aligned}
& \sum_{\mathbf{Q},\beta} v_{\mathbf{Q}\beta,+}^{\eta}(\mathbf{k}) v_{\mathbf{Q}\beta,+}^{*\eta}(\mathbf{k}') \\
& \approx \frac{\Omega_0}{2\pi^2} \frac{2\pi}{\Omega_0 \sqrt{\mathcal{N}_{f,\mathbf{k}} \mathcal{N}_{f,\mathbf{k}'}}} \int d^2Q \left\{ \lambda_1^2 \alpha_1^2 e^{-(\mathbf{k}-\mathbf{Q})^2 \lambda_1^2/2 - (\mathbf{k}'-\mathbf{Q})^2 \lambda_1^2/2} \right. \\
& \quad \left. + \lambda_2^4 \alpha_2^2 e^{-(\mathbf{k}-\mathbf{Q})^2 \lambda_2^2/2 - (\mathbf{k}'-\mathbf{Q})^2 \lambda_2^2/2} [i\eta(k_x - Q_x) - (k_y - Q_y)] [-i\eta(k'_x - Q_x) - (k'_y - Q_y)] \right\} \\
& = \frac{1}{\sqrt{\mathcal{N}_{f,\mathbf{k}} \mathcal{N}_{f,\mathbf{k}'}}} \left[\alpha_1^2 e^{-\frac{|\mathbf{k}_1 - \mathbf{k}_2|^2 \lambda_1^2}{4}} + \alpha_2^2 \left(1 - \frac{|\mathbf{k}_1 - \mathbf{k}_2|^2 \lambda_1^2}{4} \right) e^{-\frac{|\mathbf{k}_1 - \mathbf{k}_2|^2 \lambda_2^2}{4}} \right], \tag{B15}
\end{aligned}$$

$$\begin{aligned}
& \sum_{\mathbf{Q},\beta} v_{\mathbf{Q}\beta,-}^{\eta}(\mathbf{k}) v_{\mathbf{Q}\beta,-}^{*\eta}(\mathbf{k}') \\
& \approx \frac{\Omega_0}{2\pi^2} \frac{2\pi}{\Omega_0 \sqrt{\mathcal{N}_{f,\mathbf{k}} \mathcal{N}_{f,\mathbf{k}'}}} \int d^2Q \left\{ \lambda_1^2 \alpha_1^2 e^{-(\mathbf{k}-\mathbf{Q})^2 \lambda_1^2/2 - (\mathbf{k}'-\mathbf{Q})^2 \lambda_1^2/2} \right. \\
& \quad \left. + \lambda_2^4 \alpha_2^2 e^{-(\mathbf{k}-\mathbf{Q})^2 \lambda_2^2/2 - (\mathbf{k}'-\mathbf{Q})^2 \lambda_2^2/2} [-i\eta(k_x - Q_x) - (k_y - Q_y)] [i\eta(k'_x - Q_x) - (k'_y - Q_y)] \right\} \\
& = \frac{1}{\sqrt{\mathcal{N}_{f,\mathbf{k}} \mathcal{N}_{f,\mathbf{k}'}}} \left[\alpha_1^2 e^{-\frac{|\mathbf{k}_1 - \mathbf{k}_2|^2 \lambda_1^2}{4}} + \alpha_2^2 \left(1 - \frac{|\mathbf{k}_1 - \mathbf{k}_2|^2 \lambda_1^2}{4} \right) e^{-\frac{|\mathbf{k}_1 - \mathbf{k}_2|^2 \lambda_2^2}{4}} \right], \tag{B16}
\end{aligned}$$

and

$$\begin{aligned}
& \sum_{\mathbf{Q},\beta} v_{\mathbf{Q}\beta,+}^{\eta}(\mathbf{k}) v_{\mathbf{Q}\beta,-}^{*\eta}(\mathbf{k}') \\
& \approx \frac{\Omega_0}{2\pi^2} \frac{2\pi}{\Omega_0 \sqrt{\mathcal{N}_{f,\mathbf{k}} \mathcal{N}_{f,\mathbf{k}'}}} \int d^2Q \alpha_1 \alpha_2 \lambda_1 \lambda_2^2 [-\eta(k'_x - Q_x) - i(k'_y - Q_y)] e^{-\frac{1}{2}(\mathbf{k}-\mathbf{Q})^2 \lambda_1^2 - \frac{1}{2}(\mathbf{k}'-\mathbf{Q})^2 \lambda_2^2} \\
& \quad + \frac{\Omega_0}{2\pi^2} \frac{2\pi}{\Omega_0 \sqrt{\mathcal{N}_{f,\mathbf{k}} \mathcal{N}_{f,\mathbf{k}'}}} \int d^2Q \alpha_1 \alpha_2 \lambda_1 \lambda_2^2 [-\eta(k_x - Q_x) - i(k_y - Q_y)] e^{-\frac{1}{2}(\mathbf{k}-\mathbf{Q})^2 \lambda_2^2 - \frac{1}{2}(\mathbf{k}'-\mathbf{Q})^2 \lambda_1^2} = 0, \tag{B17}
\end{aligned}$$

$$\sum_{\mathbf{Q},\beta} v_{\mathbf{Q}\beta,-}^{\eta}(\mathbf{k}) v_{\mathbf{Q}\beta,+}^{*\eta}(\mathbf{k}') = 0. \tag{B18}$$

Moreover, the continuum limit from Eq. (B14) enables us to approximate the normalization constant from Eq. (A20) and obtain

$$\mathcal{N}_{f,\mathbf{k}} \approx \frac{\Omega_0}{2\pi^2} \int d^2Q \left[\alpha_1^2 \frac{2\pi \lambda_1^2}{\Omega_0} e^{-(\mathbf{k}-\mathbf{Q})^2 \lambda_1^2} + \alpha_2^2 \frac{2\pi \lambda_2^4}{\Omega_0} (\mathbf{k}-\mathbf{Q})^2 e^{-(\mathbf{k}-\mathbf{Q})^2 \lambda_2^2} \right] = 1. \tag{B19}$$

As a result, we find that

$$\sum_{\mathbf{Q},\beta} v_{\mathbf{Q}\beta,\zeta}^{\eta}(\mathbf{k}) v_{\mathbf{Q}\beta,\zeta'}^{*\eta}(\mathbf{k}') \approx \delta_{\zeta,\zeta'} \frac{1}{\alpha_1^2 + \alpha_2^2} \left[\alpha_1^2 e^{-\frac{|\mathbf{k}-\mathbf{k}'|^2 \lambda_1^2}{4}} + \alpha_2^2 \left(1 - \frac{|\mathbf{k}-\mathbf{k}'|^2 \lambda_1^2}{4} \right) e^{-\frac{|\mathbf{k}-\mathbf{k}'|^2 \lambda_2^2}{4}} \right]. \tag{B20}$$

From Eq. (B13) and Eq. (B20), the TBG form factors can then be written as

$$M_{\zeta\zeta'}^{(\eta)}(\mathbf{k}, \mathbf{k}') = \delta_{\zeta,\zeta'} g_{\mathbf{k}} g_{\mathbf{k}'} e^{-i(\theta_{\mathbf{k}} - \theta_{\mathbf{k}'})\zeta} \left[\alpha_1^2 e^{-\frac{|\mathbf{k}-\mathbf{k}'|^2 \lambda_1^2}{4}} + \alpha_2^2 \left(1 - \frac{|\mathbf{k}-\mathbf{k}'|^2 \lambda_1^2}{4} \right) e^{-\frac{|\mathbf{k}-\mathbf{k}'|^2 \lambda_2^2}{4}} \right] + \delta_{\zeta,\zeta'} h_{\mathbf{k}} h_{\mathbf{k}'}. \tag{B21}$$

In the limit $\lambda_1 \approx \lambda_2$ (which holds approximately for TBG near magic angle), the form factors can be simplified to

$$M_{\zeta\zeta'}^{(\eta)}(\mathbf{k}, \mathbf{k}') \approx \delta_{\zeta,\zeta'} g_{\mathbf{k}} g_{\mathbf{k}'} e^{-i(\theta_{\mathbf{k}} - \theta_{\mathbf{k}'})\zeta} \left(1 - \frac{\alpha_2^2 |\mathbf{k}-\mathbf{k}'|^2 \lambda_1^2}{4} \right) e^{-\frac{|\mathbf{k}-\mathbf{k}'|^2 \lambda_1^2}{4}} + \delta_{\zeta,\zeta'} h_{\mathbf{k}} h_{\mathbf{k}'}. \tag{B22}$$

2. The charge-one excitation spectrum of TBG in the $|\gamma| > U_1$ limit

Armed with analytical expressions of the active TBG bands in both the THF model basis and the TBG plane wave basis, we now show that the charge-one excitations of TBG can be obtained analytically in the $|\gamma| > U_1$ limit. We

illustrate two different approaches to do so: one which leverages the results of Ref. [24] and employs the analytically derived TBG form factors from Eq. (B32), and another one in which we project the THF interaction Hamiltonian within the active TBG bands using the analytical eigenstates of the THF single-particle Hamiltonian obtained in Eq. (B1), within the zero-bandwidth limit.

a. Charge-one excitation matrices

As shown in Ref. [24], for the integer-filled exact ground states of TBG derived by Ref. [23], the charge-one excitation spectrum of TBG can be calculated directly, as we will review below. For a given exact eigenstate $|\varphi\rangle$ of the projected interaction H_I^{TBG} [23], the charge-one excitation is obtained by evaluating the following commutators [24]

$$\left[H_I^{\text{TBG}} - \mu \hat{N}, \hat{d}_{\mathbf{k},\zeta,\eta,s}^\dagger \right] |\varphi\rangle = \sum_{\zeta'} R_{\zeta'\zeta}^\eta(\mathbf{k}) \hat{d}_{\mathbf{k},\zeta',\eta,s}^\dagger |\varphi\rangle, \quad (\text{B23})$$

$$\left[H_I^{\text{TBG}} - \mu \hat{N}, \hat{d}_{\mathbf{k},\zeta,\eta,s} \right] |\varphi\rangle = \sum_{\zeta'} \tilde{R}_{\zeta'\zeta}^\eta(\mathbf{k}) \hat{d}_{\mathbf{k},\zeta',\eta,s} |\varphi\rangle, \quad (\text{B24})$$

where μ is the chemical potential and \hat{N} is defined as

$$\hat{N} = \sum_{\mathbf{k},\zeta,\eta,s} \hat{d}_{\mathbf{k},\zeta,\eta,s}^\dagger \hat{d}_{\mathbf{k},\zeta,\eta,s}. \quad (\text{B25})$$

The matrices $R_{\zeta'\zeta}^\eta(\mathbf{k})$ and $\tilde{R}_{\zeta'\zeta}^\eta(\mathbf{k})$ in Eqs. (B23) and (B24) are determined by the filling ν of the ground states $|\varphi\rangle$ and by the form factors of Eq. (B10). The explicit formulas are given below [24]

$$R_{\zeta'\zeta}^\eta(\mathbf{k}) = \frac{1}{2\Omega_0 N_0} \sum_{\mathbf{G} \in \mathcal{Q}_0} \left[\left(\sum_{\mathbf{q} \in \text{MBZ}, \zeta''} V(\mathbf{q} + \mathbf{G}) M_{\zeta''\zeta'}^{*(\eta)}(\mathbf{k} + \mathbf{q} + \mathbf{G}, \mathbf{k}) M_{\zeta''\zeta}^{(\eta)}(\mathbf{k} + \mathbf{q} + \mathbf{G}, \mathbf{k}) \right) + 2A_{-\mathbf{G}} \sqrt{V(\mathbf{G})} M_{\zeta'\zeta}^{(\eta)}(\mathbf{k} + \mathbf{G}, \mathbf{k}) \right] - \mu \delta_{\zeta',\zeta}, \quad (\text{B26})$$

$$\tilde{R}_{\zeta'\zeta}^\eta(\mathbf{k}) = \frac{1}{2\Omega_0 N_0} \sum_{\mathbf{G} \in \mathcal{Q}_0} \left[\left(\sum_{\mathbf{q} \in \text{MBZ}, \zeta''} V(\mathbf{q} + \mathbf{G}) M_{\zeta''\zeta'}^{(\eta)}(\mathbf{k} + \mathbf{q} + \mathbf{G}, \mathbf{k}) M_{\zeta''\zeta}^{*(\eta)}(\mathbf{k} + \mathbf{q} + \mathbf{G}, \mathbf{k}) \right) - 2A_{-\mathbf{G}} \sqrt{V(\mathbf{G})} M_{\zeta'\zeta}^{*(\eta)}(\mathbf{k} + \mathbf{G}, \mathbf{k}) \right] + \mu \delta_{\zeta',\zeta}, \quad (\text{B27})$$

where MBZ denotes the moiré BZ and $A_{\mathbf{G}}$ is defined as [24]

$$A_{\mathbf{G}} = \sqrt{V(\mathbf{G})} \sum_{\substack{\mathbf{k} \in \text{MBZ} \\ \zeta, \eta}} \frac{\nu}{4} M_{\zeta\zeta}^{(\eta)}(\mathbf{k} + \mathbf{G}, \mathbf{k}) = \sqrt{V(\mathbf{G})} \sum_{\mathbf{k} \in \text{MBZ}} \frac{\nu}{4} \text{Tr}[M(\mathbf{k} + \mathbf{G}, \mathbf{k})]. \quad (\text{B28})$$

Using the fact that the approximate TBG form factors from Eq. (B32) are diagonal in the Chern band basis, we find that the corresponding charge-one excitations are also diagonal in the same basis, *i.e.* $R_{\zeta'\zeta}^\eta(\mathbf{k}) = \delta_{\zeta',\zeta} R_{\zeta\zeta}^\eta(\mathbf{k})$ and $\tilde{R}_{\zeta'\zeta}^\eta(\mathbf{k}) = \delta_{\zeta',\zeta} \tilde{R}_{\zeta\zeta}^\eta(\mathbf{k})$ with

$$R_{\zeta\zeta}^\eta(\mathbf{k}) = \frac{1}{2\Omega_0 N_0} \sum_{\mathbf{G} \in \mathcal{Q}_0} \left[\left(\sum_{\mathbf{q} \in \text{MBZ}} V(\mathbf{q} + \mathbf{G}) M_{\zeta\zeta}^{*(\eta)}(\mathbf{k} + \mathbf{q} + \mathbf{G}, \mathbf{k}) M_{\zeta\zeta}^{(\eta)}(\mathbf{k} + \mathbf{q} + \mathbf{G}, \mathbf{k}) \right) + 2A_{-\mathbf{G}} \sqrt{V(\mathbf{G})} M_{\zeta\zeta}^{(\eta)}(\mathbf{k} + \mathbf{G}, \mathbf{k}) \right] - \mu, \quad (\text{B29})$$

$$\tilde{R}_{\zeta\zeta}^\eta(\mathbf{k}) = \frac{1}{2\Omega_0 N_0} \sum_{\mathbf{G} \in \mathcal{Q}_0} \left[\left(\sum_{\mathbf{q} \in \text{MBZ}} V(\mathbf{q} + \mathbf{G}) M_{\zeta\zeta}^{(\eta)}(\mathbf{k} + \mathbf{q} + \mathbf{G}, \mathbf{k}) M_{\zeta\zeta}^{*(\eta)}(\mathbf{k} + \mathbf{q} + \mathbf{G}, \mathbf{k}) \right) - 2A_{-\mathbf{G}} \sqrt{V(\mathbf{G})} M_{\zeta\zeta}^{*(\eta)}(\mathbf{k} + \mathbf{G}, \mathbf{k}) \right] + \mu. \quad (\text{B30})$$

At the same time, it is easy to see that $M_{(-\zeta)(-\zeta)}^{*(\eta)}(\mathbf{k}, \mathbf{k}') = M_{\zeta\zeta}^{(\eta)}(\mathbf{k}, \mathbf{k}')$, which implies that $A_{\mathbf{G}}$ is real and that $R_{\zeta\zeta}^{\eta}(\mathbf{k}) = R_{(-\zeta)(-\zeta)}^{*\eta}(\mathbf{k})$ and $\tilde{R}_{\zeta\zeta}^{\eta}(\mathbf{k}) = \tilde{R}_{(-\zeta)(-\zeta)}^{*\eta}(\mathbf{k})$. However, while the first term in each of Eqs. (B29) and (B30) is real, the second term is not manifestly so. Generically, the TBG form factors obey the hermiticity property $M_{\zeta\zeta'}^{(\eta)}(\mathbf{k}, \mathbf{k}') = M_{\zeta'\zeta}^{*(\eta)}(\mathbf{k}', \mathbf{k})$, which follows trivially from their definition in Eq. (B10). Together with the even symmetries of $A_{\mathbf{G}} = A_{-\mathbf{G}}$ and $V(\mathbf{G}) = V(-\mathbf{G})$, the hermiticity property of the form factors coupled with the periodicity in reciprocal space $M_{\zeta\zeta'}^{(\eta)}(\mathbf{k} + \mathbf{G}, \mathbf{k}' + \mathbf{G}) = M_{\zeta'\zeta}^{(\eta)}(\mathbf{k} + \mathbf{G}, \mathbf{k}' + \mathbf{G})$ is enough to guarantee the reality of the second term of each of Eqs. (B29) and (B30). However, the approximation in Eq. (B32) does not obey the periodicity property, which makes the charge-one excitation matrices nonhermitian at $\nu \neq 0$. For $\nu = 0$ (or alternatively when the so-called flat metric condition is imposed [24] at generic $\nu \neq 0$), $A_{\mathbf{G}} = 0$, which implies that the charge-one excitation matrices are proportional to the identity matrix (and are therefore *bona-fide* hermitian matrices).

b. Analytical expressions for the charge-one excitation matrices of TBG

We now provide asymptotic analytical expression for the charge-one excitation matrices at $\nu = 0$. The latter can be rewritten from Eqs. (B29) and (B30) as

$$\begin{aligned} R_{\zeta\zeta}^{\eta}(\mathbf{k}) &= \tilde{R}_{\zeta\zeta}^{\eta}(\mathbf{k}) = \frac{1}{2\Omega_0 N_0} \frac{\Omega_0 N_0}{(2\pi)^2} \sum_{\mathbf{G} \in \mathbf{Q}_0} \int_{\text{MBZ}} V(\mathbf{q} + \mathbf{G}) \left| M_{\zeta\zeta}^{(\eta)}(\mathbf{k} + \mathbf{q} + \mathbf{G}, \mathbf{k}) \right|^2 d^2 q \\ &= \frac{1}{8\pi^2} \int_{-\infty}^{\infty} \int_{-\infty}^{\infty} V(\mathbf{q} - \mathbf{k}) \left| M_{\zeta\zeta}^{(\eta)}(\mathbf{q}, \mathbf{k}) \right|^2 dq_x dq_y. \end{aligned} \quad (\text{B31})$$

To move forward, we need to make two simplifying assumptions. First, we consider the $\sqrt{|v_{\star}\mathbf{k}|^2 + \gamma^2 e^{-|\mathbf{k}|^2 \lambda^2}}$ denominator of the $g_{\mathbf{k}}$ and $h_{\mathbf{k}}$ functions from Eq. (B2), which appears in the expression of the form factors from Eq. (B32). For small values of $|\mathbf{k}|$ the exponential $e^{-|\mathbf{k}|^2 \lambda^2}$ is approximately 1. At large $|\mathbf{k}|$, $g_{\mathbf{k}}$ is already multiplied by decaying exponentials in Eq. (B32), while $h_{\mathbf{k}}$ itself contains a decaying exponential factor in the numerator. In other words, for large $|\mathbf{q}|$, the exact values of the $g_{\mathbf{q}}$ and $h_{\mathbf{q}}$ functions is unimportant, as they become exponentially suppressed in the form factors. As a result, we will ignore the exponential decay factor appearing in the denominators of the $g_{\mathbf{q}}$ and $h_{\mathbf{q}}$ functions in Eq. (B31) and approximate the form factor as

$$M_{\zeta\zeta}^{(\eta)}(\mathbf{k}, \mathbf{q}) = g_{\mathbf{k}} \tilde{g}_{\mathbf{q}} e^{-i(\theta_{\mathbf{k}} - \theta_{\mathbf{q}})\zeta} \left[\alpha_1^2 e^{-\frac{|\mathbf{k}-\mathbf{q}|^2 \lambda_1^2}{4}} + \alpha_2^2 \left(1 - \frac{|\mathbf{k}-\mathbf{q}|^2 \lambda_1^2}{4} \right) e^{-\frac{|\mathbf{k}-\mathbf{q}|^2 \lambda_2^2}{4}} \right] + h_{\mathbf{k}} \tilde{h}_{\mathbf{q}}, \quad (\text{B32})$$

where we have defined

$$\tilde{g}_{\mathbf{q}} \approx \frac{v_{\star} |\mathbf{q}|}{\sqrt{|v_{\star}\mathbf{q}|^2 + \gamma^2}} \quad \text{and} \quad \tilde{h}_{\mathbf{q}} = \frac{\gamma e^{-|\mathbf{q}|^2 \lambda^2 / 2}}{\sqrt{|v_{\star}\mathbf{q}|^2 + \gamma^2}}. \quad (\text{B33})$$

Additionally, we note that, while the form factor decays exponentially in $|\mathbf{q}|$, the screened Coulomb potential only decays polynomially over the same momentum scale. As a simple approximation, we can can therefore approximate the Coulomb potential to a constant

$$V(\mathbf{q} - \mathbf{k}) \approx U_{\xi} \pi \xi^2. \quad (\text{B34})$$

Finally, we note that the integrand in Eq. (B31) only depends on the the relative angle between \mathbf{k} and \mathbf{q} and their magnitudes. Letting $\mathbf{k} = (k, 0)$ and $\mathbf{q} = (q \cos \theta, q \sin \theta)$ without loss of generality, the charge-one excitation matrices become

$$R_{\zeta\zeta}^{\eta}(\mathbf{k}) = \frac{U_{\xi} \xi^2}{8\pi} \int_0^{\infty} q dq \int_0^{2\pi} d\theta \left(g_k^2 \tilde{g}_q^2 f^2(k, q, \theta) + h_k^2 \tilde{h}_q^2 + 2g_k h_k \tilde{g}_q \tilde{h}_q f(k, q, \theta) \cos \theta \right), \quad (\text{B35})$$

with

$$f(k, q, \theta) = \alpha_1^2 e^{-\frac{\lambda_1^2 (k^2 + q^2 - 2kq \cos \theta)}{4}} + \alpha_2^2 \left(1 - \frac{\lambda_1^2 (k^2 + q^2 - 2kq \cos \theta)}{4} \right) e^{-\frac{\lambda_2^2 (k^2 + q^2 - 2kq \cos \theta)}{4}}. \quad (\text{B36})$$

The integral over the angle in Eq. (B35) can be readily performed giving

$$R_{\zeta\zeta}^\eta(\mathbf{k}) = \frac{U_\xi \xi^2}{8\pi} \frac{1}{k^2 v_\star^2 + \gamma^2 e^{-\frac{k^2 \lambda^2}{2}}} \int_0^\infty \frac{q dq}{q^2 v_\star^2 + \gamma^2} F(k, q), \quad (\text{B37})$$

where we have defined

$$\begin{aligned} F(k, q) = & 2\pi\gamma^4 e^{-\lambda^2(k^2+q^2)} \\ & + 2\pi\alpha_1^4 k^2 q^2 v_\star^4 e^{-\frac{1}{2}\lambda_1^2(k^2+q^2)} I_0(k\lambda_1^2 q) \\ & + \frac{1}{8}\pi\alpha_2^4 k^2 q^2 v_\star^4 e^{-\frac{1}{2}\lambda_2^2(k^2+q^2)} (k^2\lambda_1^2 + \lambda_1^2 q^2 - 4)^2 I_0(k\lambda_2^2 q) \\ & + \pi\alpha_1^2 \alpha_2^2 k^2 q^2 v_\star^4 \left(-e^{-\frac{1}{4}(\lambda_1^2+\lambda_2^2)(k^2+q^2)}\right) (k^2\lambda_1^2 + \lambda_1^2 q^2 - 4) I_0\left(\frac{1}{2}k(\lambda_1^2 + \lambda_2^2)q\right) \\ & + 4\pi\alpha_1^2 \gamma^2 k q v_\star^2 e^{-\frac{1}{4}(2\lambda^2+\lambda_1^2)(k^2+q^2)} I_1\left(\frac{1}{2}k\lambda_1^2 q\right) \\ & - \frac{\pi\alpha_2^2 \gamma^2 k q v_\star^2 e^{-\frac{1}{4}(2\lambda^2+\lambda_2^2)(k^2+q^2)} (\lambda_1^2 (k^2\lambda_2^2 + \lambda_2^2 q^2 - 4) - 4\lambda_2^2)}{\lambda_2^2} I_1\left(\frac{1}{2}k\lambda_2^2 q\right) \\ & - \frac{\pi\alpha_2^4 k^3 \lambda_1^2 q^3 v_\star^4 e^{-\frac{1}{2}\lambda_2^2(k^2+q^2)} (\lambda_1^2 (k^2\lambda_2^2 + \lambda_2^2 q^2 - 1) - 4\lambda_2^2)}{2\lambda_2^2} I_1(k\lambda_2^2 q) \\ & + 2\pi\alpha_1^2 \alpha_2^2 k^3 \lambda_1^2 q^3 v_\star^4 e^{-\frac{1}{4}(\lambda_1^2+\lambda_2^2)(k^2+q^2)} I_1\left(\frac{1}{2}k(\lambda_1^2 + \lambda_2^2)q\right) \\ & + 2\pi\alpha_2^2 \gamma^2 k^2 \lambda_1^2 q^2 v_\star^2 e^{-\frac{1}{4}(2\lambda^2+\lambda_2^2)(k^2+q^2)} I_2\left(\frac{1}{2}k\lambda_2^2 q\right) \\ & + \frac{1}{2}\pi\alpha_2^4 k^4 \lambda_1^4 q^4 v_\star^4 e^{-\frac{1}{2}\lambda_2^2(k^2+q^2)} I_2(k\lambda_2^2 q), \end{aligned} \quad (\text{B38})$$

where $I_n(z)$ is the n -th order modified Bessel function of the first kind. For the first term of $F(k, q)$, the integral over q can be directly performed

$$\int_0^\infty 2\pi\gamma^4 e^{-\lambda^2(k^2+q^2)} \frac{q dq}{q^2 v_\star^2 + \gamma^2} = \frac{\pi\gamma^4 e^{-\lambda^2\left(k^2 - \frac{\gamma^2}{v_\star^2}\right)} \Gamma\left(0, \frac{\gamma^2 \lambda^2}{v_\star^2}\right)}{v_\star^2}. \quad (\text{B39})$$

For the other terms, we apply the following strategy. First, we expand the Bessel functions according to

$$I_n(z) = \sum_{m=0}^\infty \frac{1}{m!(m+n)!} \left(\frac{z}{2}\right)^{2m+n}, \quad \text{for } n \in \mathbb{N}, \quad (\text{B40})$$

which is equivalent to a power series expansion in q of $F(k, q)$. We find it easier to perform this step for each term of $F(k, q)$ separately. Consider the typical term in Eq. (B38), which has the form $\mathcal{C}(k)q^{n_1}e^{-\frac{\Lambda_1^2}{2}q^2}I_{n_2}\left(\frac{kq\Lambda_2^2}{2}\right)$, where $\mathcal{C}(k)$ is a function of k , $n_1, n_2 \in \mathbb{N}$, while Λ_1 and Λ_2 are combinations of λ , λ_1 , or λ_2 having dimension of length. For example, the second-to-last term of Eq. (B38) has this form with

$$\mathcal{C}(k) = 2\pi\alpha_2^2 \gamma^2 k^2 \lambda_1^2 v_\star^2 e^{-\frac{1}{4}(2\lambda^2+\lambda_2^2)k^2}, \quad (\text{B41})$$

$$n_1 = 2, \quad n_2 = 2, \quad \Lambda_1 = \sqrt{2\lambda^2 + \lambda_2^2}, \quad \Lambda_2 = \lambda_2^2. \quad (\text{B42})$$

Such a term can be integrated by first expanding the Bessel function according to Eq. (B40) and then integrating the resulting series in a term-by-term fashion

$$\begin{aligned} & \int_0^\infty \frac{q dq}{q^2 v_\star^2 + \gamma^2} \mathcal{C}(k) q^{n_1} e^{-\frac{\Lambda_1^2}{2}q^2} I_{n_2}\left(\frac{kq\Lambda_2^2}{2}\right) = \\ & = \frac{1}{v_\star^2} \mathcal{C}(k) \left| \frac{\gamma}{v_\star} \right|^{n_1} \int_0^\infty \frac{z dz}{1+z^2} z^{n_1} e^{-\frac{\Lambda_1^2 \gamma^2}{2v_\star^2} z^2} I_{n_2}\left(kz\Lambda_2^2 \left| \frac{\gamma}{2v_\star} \right| \right) \end{aligned}$$

$$\begin{aligned}
&= \frac{1}{v_\star^2} \mathcal{C}(k) \left| \frac{\gamma}{v_\star} \right|^{n_1} \sum_{m=0}^{\infty} \frac{1}{m!(m+n_2)!} \left(k \Lambda_2^2 \left| \frac{\gamma}{4v_\star} \right| \right)^{2m+n_2} \int_0^\infty \frac{z^{n_1+n_2+2m+1} dz}{1+z^2} e^{-\frac{\Lambda_1^2 \gamma^2}{2v_\star^2} z^2} \\
&= \frac{1}{v_\star^2} \mathcal{C}(k) \left| \frac{\gamma}{v_\star} \right|^{n_1} \sum_{m=0}^{\infty} \frac{\Gamma\left(\frac{n_1+n_2}{2} + m + 1\right)}{m!(m+n_2)!} \left(k \Lambda_2^2 \left| \frac{\gamma}{4v_\star} \right| \right)^{2m+n_2} \frac{1}{2} e^{\frac{\Lambda_1^2 \gamma^2}{2v_\star^2}} \Gamma\left(-\frac{n_1+n_2}{2} - m, \frac{\Lambda_1^2 \gamma^2}{4v_\star^2}\right). \tag{B43}
\end{aligned}$$

We now note that for all the terms in Eq. (B38), $\frac{\Lambda_1^2 \gamma^2}{2v_\star^2} \ll 1$, suggesting that the incomplete Gamma function can be expanded in the second argument. Moreover, we find that for all the terms in Eq. (B38) proportional to a Bessel function, $n_1 + n_2 \geq 2$ is even. As such, we can employ the following representation of the incomplete Gamma function

$$\Gamma(-m, z) = \frac{(-1)^m}{m!} \left[\Gamma(0, z) - e^{-z} \sum_{j=0}^{m-1} \frac{j!(-1)^j}{z^{j+1}} \right], \quad \text{for } m \in \mathbb{N}. \tag{B44}$$

For small z , the incomplete Gamma function has the following asymptotic form

$$\Gamma(-m, z) = \frac{1}{mz^m} + \begin{cases} \mathcal{O}(z^{-m+1}), & m \geq 1 \\ \mathcal{O}(\log z), & m = 1 \end{cases} \tag{B45}$$

which enables us to rewrite the integral in Eq. (B43) as

$$\begin{aligned}
&\int_0^\infty \frac{q dq}{q^2 v_\star^2 + \gamma^2} \mathcal{C}(k) q^{n_1} e^{-\frac{\Lambda_1^2}{2} q^2} I_{n_2} \left(\frac{k q \Lambda_2^2}{2} \right) = \\
&= \frac{1}{v_\star^2} \mathcal{C}(k) \left| \frac{\gamma}{v_\star} \right|^{n_1} \sum_{m=0}^{\infty} \frac{\Gamma\left(\frac{n_1+n_2}{2} + m + 1\right)}{m!(m+n_2)!} \left(k \Lambda_2^2 \left| \frac{\gamma}{4v_\star} \right| \right)^{2m+n_2} \\
&\quad \times \left[\frac{\left(\frac{\Lambda_1^2 \gamma^2}{2v_\star^2} \right)^{-\frac{n_1+n_2}{2}-m}}{n_1 + n_2 + 2m} + \mathcal{O} \left(\left(\frac{\Lambda_1^2 \gamma^2}{2v_\star^2} \right)^{-\frac{n_1+n_2}{2}-m+1} + \log \left(\frac{\Lambda_1^2 \gamma^2}{2v_\star^2} \right) \right) \right] \\
&= \frac{1}{v_\star^2} \mathcal{C}(k) \left| \frac{\gamma}{v_\star} \right|^{n_1} \sum_{m=0}^{\infty} \frac{\Gamma\left(\frac{n_1+n_2}{2} + m + 1\right)}{m!(m+n_2)!} \left(k \Lambda_2^2 \left| \frac{\gamma}{4v_\star} \right| \right)^{n_2} \left(\frac{k^2 \Lambda_2^2}{2\sqrt{2}} \right)^m \left(\frac{\Lambda_2}{\Lambda_1} \right)^m \left(\frac{\Lambda_1^2 \gamma^2}{2v_\star^2} \right)^m \\
&\quad \times \left[\frac{\left(\frac{\Lambda_1^2 \gamma^2}{2v_\star^2} \right)^{-\frac{n_1+n_2}{2}-m}}{n_1 + n_2 + 2m} + \mathcal{O} \left(\left(\frac{\Lambda_1^2 \gamma^2}{2v_\star^2} \right)^{-\frac{n_1+n_2}{2}-m+1} + \log \left(\frac{\Lambda_1^2 \gamma^2}{2v_\star^2} \right) \right) \right]. \tag{B46}
\end{aligned}$$

Keeping only the leading contribution in the small parameter $\frac{\Lambda_1^2 \gamma^2}{2v_\star^2}$, we can approximate the integral from Eq. (B43) as

$$\begin{aligned}
&\int_0^\infty \frac{q dq}{q^2 v_\star^2 + \gamma^2} \mathcal{C}(k) q^{n_1} e^{-\frac{\Lambda_1^2}{2} q^2} I_{n_2} \left(\frac{k q \Lambda_2^2}{2} \right) \approx \\
&\approx \frac{1}{v_\star^2} \mathcal{C}(k) \left| \frac{\gamma}{v_\star} \right|^{n_1} \sum_{m=0}^{\infty} \frac{\Gamma\left(\frac{n_1+n_2}{2} + m + 1\right)}{m!(m+n_2)!} \left(k \Lambda_2^2 \left| \frac{\gamma}{4v_\star} \right| \right)^{n_2} \left(\frac{k^2 \Lambda_2^2}{2\sqrt{2}} \right)^m \left(\frac{\Lambda_2}{\Lambda_1} \right)^m \frac{\left(\frac{\Lambda_1^2 \gamma^2}{2v_\star^2} \right)^{-\frac{n_1+n_2}{2}}}{n_1 + n_2 + 2m}. \tag{B47}
\end{aligned}$$

Finally, the series in Eq. (B47) can be re-summed into an elementary function. Performing this approximation for each term in Eq. (B38), we arrive at the following result

$$\begin{aligned}
&\frac{8\pi}{U_\xi \xi^2} \left(k^2 v_\star^2 + \gamma^2 e^{-\frac{k^2 \lambda^2}{2}} \right) R_{\zeta\zeta}^\eta(\mathbf{k}) \approx \\
&\approx \frac{\pi \gamma^4 e^{-\lambda^2 \left(k^2 - \frac{\gamma^2}{v_\star^2} \right)} \Gamma\left(0, \frac{\gamma^2 \lambda^2}{v_\star^2}\right)}{v_\star^2} \\
&+ \frac{\pi \alpha_2^4 k^2 \lambda_1^4 (k^4 \lambda_2^4 - 8k^2 \lambda_2^2 + 8) v_\star^2}{8\lambda_2^6}
\end{aligned}$$

$$\begin{aligned}
& - \frac{\pi \alpha_2^4 k^2 \lambda_1^2 (\lambda_1^2 \lambda_2^2 k^4 - 4 (\lambda_1^2 + \lambda_2^2) k^2 + 8) v_*^2}{4 \lambda_2^4} \\
& + \frac{2 \pi \alpha_2^2 \gamma^2 \lambda_1^2 e^{-\frac{1}{4} k^2 (2 \lambda^2 + \lambda_2^2)} \left(e^{\frac{k^2 \lambda_2^4}{8 \lambda^2 + 4 \lambda_2^2}} (4 \lambda_2^2 \lambda^2 (k^2 \lambda_2^2 - 8) + \lambda_2^4 (k^2 \lambda_2^2 - 8) - 32 \lambda^4) + 8 (2 \lambda^2 + \lambda_2^2)^2 \right)}{\lambda_2^4 (2 \lambda^2 + \lambda_2^2)^2} \\
& + \frac{2 \pi \alpha_1^2 \alpha_2^2 k^2 \lambda_1^2 (k^2 (\lambda_1^2 + \lambda_2^2) - 4) v_*^2}{(\lambda_1^2 + \lambda_2^2)^2} \\
& + \frac{2 \pi \alpha_1^4 k^2 v_*^2}{\lambda_1^2} \\
& + \frac{8 \pi \alpha_1^2 \gamma^2 e^{-\frac{1}{4} k^2 (2 \lambda^2 + \lambda_1^2)} \left(e^{\frac{k^2 \lambda_1^4}{8 \lambda^2 + 4 \lambda_1^2}} - 1 \right)}{\lambda_1^2} \\
& + \frac{\pi \alpha_2^4 k^2 (k^2 \lambda_1^2 - 4)^2 v_*^2}{8 \lambda_2^2} \\
& - \frac{2 \pi \alpha_2^2 \gamma^2 e^{-\frac{1}{4} k^2 (2 \lambda^2 + \lambda_2^2)} \left(e^{\frac{k^2 \lambda_2^4}{8 \lambda^2 + 4 \lambda_2^2}} - 1 \right) (\lambda_1^2 (k^2 \lambda_2^2 - 4) - 4 \lambda_2^2)}{\lambda_2^4} \\
& - \frac{2 \pi \alpha_1^2 \alpha_2^2 k^2 (k^2 \lambda_1^2 - 4) v_*^2}{\lambda_1^2 + \lambda_2^2}.
\end{aligned} \tag{B48}$$

To simplify the expression in Eq. (B48), we now take the approximation $\lambda_1 \approx \lambda_2 \approx \frac{\lambda}{\sqrt{2}}$, which holds approximately for TBG around the magic angle and realistic interlayer tunneling amplitudes $w_0/w_1 = 0.8$. Coupled with the normalization condition $\alpha_1^2 + \alpha_2^2 = 1$, this enables us to obtain the following approximate expression for the charge-one excitation matrix

$$\begin{aligned}
& \frac{k^2 v_*^2 + \gamma^2 e^{-\frac{k^2 \lambda^2}{2}}}{U_\xi \xi^2} R_{\zeta\zeta}^\eta(\mathbf{k}) \approx \\
& \approx \frac{\pi \gamma^4 e^{-\lambda^2 \left(k^2 - \frac{\gamma^2}{v_*^2} \right)} \Gamma\left(0, \frac{\gamma^2 \lambda^2}{v_*^2}\right)}{v_*^2} \\
& + \frac{-25 \gamma^2 e^{-\frac{5}{8} k^2 \lambda^2} (\alpha_1^2 (k^2 \lambda^2 + 8) - k^2 \lambda^2) + 8 \gamma^2 e^{-\frac{3}{8} k^2 \lambda^2} (\alpha_1^2 (2 k^2 \lambda^2 + 25) - 2 k^2 \lambda^2) + 25 (\alpha_1^4 + 1) k^2 v_*^2}{100 \lambda^2}.
\end{aligned} \tag{B49}$$

The simplified expression in Eq. (B49) readily explains the shape of the charge-one excitation spectrum around charge neutrality

$$\frac{8 R_{\zeta\zeta}^\eta(\mathbf{k})}{U_\xi \xi^2} = \begin{cases} \frac{2(\alpha_1^4 + 1)}{\lambda^2}, & \text{for } k \rightarrow \infty \\ k^2 \left(\frac{2}{25} \left(-4 \alpha_1^2 + \frac{25(\alpha_1^4 + 1) v_*^2}{\gamma^2 \lambda^2} + 9 \right) - e^{\frac{\gamma^2 \lambda^2}{v_*^2}} \Gamma\left(0, \frac{\gamma^2 \lambda^2}{v_*^2}\right) \right) + \frac{\gamma^2 e^{\frac{\gamma^2 \lambda^2}{v_*^2}} \Gamma\left(0, \frac{\gamma^2 \lambda^2}{v_*^2}\right)}{v_*^2}, & \text{for } k \approx 0 \end{cases}. \tag{B50}$$

We benchmark the analytical expressions for the TBG form factors from Eq. (B32) by computing the charge-one excitation dispersion of TBG. We focus on charge neutrality, where the dispersion is identical for both the electron- and hole-excitations and compute the corresponding charge-one excitation matrices both exactly using Eqs. (B29) and (B30) and analytically using the asymptotic expression derived in Eq. (B49). The resulting charge-one excitation dispersion is shown in Fig. 8 and qualitatively agrees with the numerical results of Ref. [24].

c. Flat-band projected limit of the THF model

The THF model has been used in Refs. [33, 45, 49, 50, 171, 273–278] to obtain many of the properties of TBG in the limit $U_1 > |\gamma|$. In this section, we discuss the opposite limit – the flat-band projected limit of the THF model –

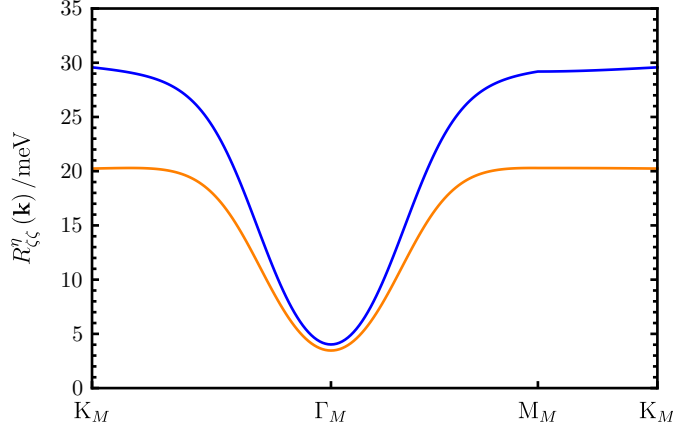


FIG. 8. Charge-one excitations of TBG above the $\nu = 0$ correlated insulators computed with the analytical form-factor expression from Eq. (B32). We take $\theta = 1.05^\circ$ and $w_0/w_1 = 0.5$ for which the relevant THF model parameters are given by $\alpha_1 = 0.9208$, $\alpha_2 = 0.3901$, $\lambda = 0.533|\mathbf{a}_{M1}|$, $\lambda_1 = 0.2268|\mathbf{a}_{M1}|$, $\lambda_2 = 0.2089|\mathbf{a}_{M1}|$, $|\gamma| = 65.78 \text{ meV}$, and $U_1 = 37.61 \text{ meV}$ (such that the condition $|\gamma| > U_1$ is satisfied). The blue line show the dispersion computed using the formula from Eqs. (B29) and (B30), while the orange line corresponds to its analytical asymptotic expression from Eq. (B49).

which is valid for $U_1 < |\gamma|$. Within this parameter regime, the remote bands are effectively gapped degrees of freedom and the interaction THF Hamiltonian can be projected into the active TBG bands. We will show that in the limit $U_1 < |\gamma|$, the THF model remains a reliable mapping of the TBG problem, which captures the essential physics of the system, even though the interaction cannot be treated locally anymore, due to the heavy mixing between the c - and f -electrons.

In what follows, we analytically obtain the charge- (± 1) excitation of the system around integer fillings, in the limit of $v'_\star = v''_\star = 0$, $M = 0$ and $U_1 < |\gamma|$. As already discussed near Eq. (B1), the single-particle Hamiltonian of the system can be solved analytically. For $U_1 < |\gamma|$, the remote bands corresponding to $\hat{b}_{\mathbf{k},j,\eta,s}^\dagger$ are high-energy degrees of freedom, being separated from the active TBG bands by $|\gamma|$. At integer fillings $-4 \leq \nu \leq +4$, the ground states of the system were shown to be Slater determinants obtained by fully filling the TBG Chern bands [23]

$$|\Psi_\nu\rangle = \prod_{\mathbf{k}} \prod_{n=1}^{\nu+4} \hat{d}_{\mathbf{k},\zeta_n,\eta_n,s_n}^\dagger |\text{RB}\rangle. \quad (\text{B51})$$

where $\{\zeta_n, \eta_n, s_n\}_n$ are $(\nu + 4)$ flavor indices arbitrarily sorted in n and $|\text{RB}\rangle$ is the Slater determinant state corresponding to the fully occupied remote bands with negative energy

$$|\text{RB}\rangle = \prod_{\mathbf{k}} \prod_{\eta,s,|j|=1} \hat{b}_{\mathbf{k},j,\eta,s}^\dagger |0\rangle. \quad (\text{B52})$$

For the given ground state, we can then obtain the charge ± 1 excitation via the Hartree-Fock approximation [33, 50]. In the Hartree-Fock approach, we can rewrite the interacting Hamiltonian as

$$H_{I,\text{MF}} = \sum_{\substack{i,\eta,s \\ i',\eta',s'}} h_{i\eta s; i'\eta' s'}^{I,\text{MF}}(\mathbf{k}) \hat{\gamma}_{\mathbf{k},i,\eta,s}^\dagger \hat{\gamma}_{\mathbf{k},i',\eta',s'}, \quad (\text{B53})$$

where we have introduced the following operators to simplify the notations

$$\hat{\gamma}_{\mathbf{k},\eta,i,s}^\dagger \equiv \begin{cases} \hat{c}_{\mathbf{k},\eta,i,s}^\dagger, & \text{for } 1 \leq i \leq 4 \\ \hat{f}_{\mathbf{k},\eta,i-4,s}^\dagger, & \text{for } 5 \leq i \leq 6 \end{cases}. \quad (\text{B54})$$

We consider the full THF interacting Hamiltonian from Eq. (A34), but follow Ref. [203] and only consider the Hartree contribution stemming from H_V , but otherwise include both the Hartree and Fock contributions stemming from the other terms. The Hartree-Fock Hamiltonian is then characterized by the following matrix [50]

$$h_{i\eta s; i'\eta' s'}^{I,\text{MF}}(\mathbf{k}) = \sum_{\alpha=1}^2 \left(U_1 \nu_f + 3U_2 \nu_f + \frac{1}{N_0} \sum_{a=1}^4 W_a \sum_{\mathbf{k}'} \sum_{\eta'',s''} \varrho_{a\eta''s''; a\eta''s''}(\mathbf{k}') \right) \delta_{(\alpha+4)i} \delta_{(\alpha+4)i'} \delta_{\eta\eta'} \delta_{ss'}$$

$$\begin{aligned}
& + \sum_{a=1}^4 (V(\mathbf{0})\nu_c + W_a\nu_f) \delta_{ai} \delta_{ai'} \delta_{\eta\eta'} \delta_{ss'} \\
& - \frac{U}{N_0} \sum_{\alpha, \alpha'=1}^2 \delta_{(\alpha+4)i} \delta_{(\alpha'+4)i'} \sum_{\mathbf{k}'} \varrho_{i'\eta's';i\eta s}(\mathbf{k}') \\
& + \frac{U_2}{N_0} \sum_{\mathbf{k}'} \sum_{n=0}^5 \cos((\mathbf{k} - \mathbf{k}') \cdot C_{6z}^m \mathbf{a}_{M_1}) \varrho_{i'\eta's';i\eta s}(\mathbf{k}') \\
& - \sum_{\alpha=1}^2 \sum_{a'=1}^4 \frac{W_{a'}}{N_0} [\delta_{(\alpha+4)i} \delta_{a'i'} + \delta_{(\alpha+4)i'} \delta_{a'i}] \sum_{\mathbf{k}'} \varrho_{i'\eta's';i\eta s}(\mathbf{k}') \\
& + \frac{1}{N_0} \sum_{\substack{i_1, \eta_1, \sigma_1 \\ i_2, \eta_2, \sigma_2}} (\mathcal{J}_{i_1 \eta_1 s_1; i_2 \eta_2 s_2; i \eta s; i' \eta' s'} + \mathcal{J}_{i \eta s; i' \eta' s'; i_1 \eta_1 s_1; i_2 \eta_2 s_2}) \sum_{\mathbf{k}'} \varrho_{i_1 \eta_1 s_1; i_2 \eta_2 s_2}(\mathbf{k}') \\
& - \frac{1}{N_0} \sum_{\substack{i_1, \eta_1, \sigma_1 \\ i_2, \eta_2, \sigma_2}} (\mathcal{J}_{i_1 \eta_1 s_1; i' \eta' s'; i \eta s; i_2 \eta_2 s_2} + \mathcal{J}_{i \eta s; i_2 \eta_2 s_2; i_1 \eta_1 s_1; i' \eta' s'}) \sum_{\mathbf{k}'} \varrho_{i_1 \eta_1 s_1; i_2 \eta_2 s_2}(\mathbf{k}'), \tag{B55}
\end{aligned}$$

where the interaction tensor is defined as

$$\begin{aligned}
\mathcal{J}_{i_1 \eta_1 s_1; i_2 \eta_2 s_2; i_3 \eta_3 s_3; i_4 \eta_4 s_4} & = -\frac{J}{2} \sum_{\substack{\alpha, \alpha'=1 \\ \eta, \eta'}}^2 [\eta\eta' + (-1)^{\alpha+\alpha'}] \delta_{(\alpha+4)i_1} \delta_{(\alpha'+4)i_2} \delta_{(\alpha'+2)i_3} \delta_{(\alpha+2)i_4} \delta_{\eta\eta_1} \delta_{\eta'\eta_2} \delta_{\eta'\eta_3} \delta_{\eta\eta_4} \delta_{s_1 s_4} \delta_{s_2 s_3} \\
& - \frac{J}{4} \sum_{\substack{\alpha, \alpha'=1 \\ \eta, \eta'}}^2 [\eta\eta' - (-1)^{\alpha+\alpha'}] \delta_{(\alpha+4)i_1} \delta_{(\alpha'+2)i_2} \delta_{(\alpha'+4)i_3} \delta_{(\alpha+2)i_4} \delta_{\eta\eta_1} \delta_{\eta'\eta_2} \delta_{\eta'\eta_3} \delta_{\eta\eta_4} \delta_{s_1 s_4} \delta_{s_2 s_3} \\
& - \frac{J}{4} \sum_{\substack{\alpha, \alpha'=1 \\ \eta, \eta'}}^2 [\eta\eta' - (-1)^{\alpha+\alpha'}] \delta_{(\alpha+4)i_2} \delta_{(\alpha'+2)i_1} \delta_{(\alpha'+4)i_4} \delta_{(\alpha+2)i_3} \delta_{\eta\eta_1} \delta_{\eta'\eta_2} \delta_{\eta'\eta_3} \delta_{\eta\eta_4} \delta_{s_1 s_4} \delta_{s_2 s_3} \\
& + \frac{K}{\Omega_0} \sum_{\alpha=1}^2 \sum_{\eta\eta'} \eta\eta' [\delta_{\bar{\alpha}i_1} \delta_{(\alpha+2)i_2} \delta_{(\alpha+4)i_3} \delta_{(\alpha+2)i_4} \delta_{\eta\eta_1} \delta_{\eta\eta_2} \delta_{\eta'\eta_3} \delta_{\eta'\eta_4} \delta_{s_1 s_2} \delta_{s_3 s_4} \\
& - \delta_{(\alpha+4)i_1} \delta_{(\alpha+2)i_2} \delta_{(\bar{\alpha}+2)i_3} \delta_{\alpha i_4} \delta_{\eta\eta_1} \delta_{\eta\eta_2} \delta_{\eta'\eta_3} \delta_{\eta'\eta_4} \delta_{s_1 s_2} \delta_{s_3 s_4}] \\
& + \frac{K}{\Omega_0} \sum_{\alpha=1}^2 \sum_{\eta\eta'} \eta\eta' [\delta_{\bar{\alpha}i_4} \delta_{(\alpha+2)i_3} \delta_{(\alpha+4)i_2} \delta_{(\alpha+2)i_1} \delta_{\eta\eta_4} \delta_{\eta\eta_3} \delta_{\eta'\eta_2} \delta_{\eta'\eta_1} \delta_{s_1 s_2} \delta_{s_3 s_4} \\
& - \delta_{(\alpha+4)i_4} \delta_{(\alpha+2)i_3} \delta_{(\bar{\alpha}+2)i_2} \delta_{\alpha i_1} \delta_{\eta\eta_4} \delta_{\eta\eta_3} \delta_{\eta'\eta_2} \delta_{\eta'\eta_1} \delta_{s_1 s_2} \delta_{s_3 s_4}] \tag{B56}
\end{aligned}$$

The Hartree-Fock Hamiltonian also depends on the density matrix of the system

$$\varrho_{i\eta s; i'\eta' s'}(\mathbf{k}) = \left\langle : \hat{\gamma}_{\mathbf{k}, i, \eta, s}^\dagger \hat{\gamma}_{\mathbf{k}, i', \eta', s'} : \right\rangle, \tag{B57}$$

and the filling of the f -electrons (ν_f) and c -electrons (ν_c)

$$\nu_c = \frac{1}{N_0} \sum_{i=1}^4 \sum_{\mathbf{k}, \eta, \sigma} \varrho_{i\eta\sigma; i\eta\sigma}(\mathbf{k}) \quad \text{and} \quad \nu_f = \frac{1}{N_0} \sum_{i=5}^6 \sum_{\mathbf{k}, \eta, \sigma} \varrho_{i\eta\sigma; i\eta\sigma}(\mathbf{k}). \tag{B58}$$

The total filling of the system is $\nu = \nu_f + \nu_c$.

For the Slater-determinant ground states from Eq. (B51), we can directly compute the density matrix using Eq. (B57) and then diagonalize the Hartree-Fock Hamiltonian to get the charge- (± 1) excitation spectra. Here, we also provide the density matrix for different integer fillings. We find that the density matrix is diagonal in the valley and spin spaces with

$$\varrho_{i\eta s; i'\eta' s'}(\mathbf{k}) = \delta_{\eta, \eta'} \delta_{s, s'} \varrho_{\eta, s; i, j} \tag{B59}$$

where $\varrho_{\eta,s,ij}$ is the density matrix of valley η spin s block. For each block, we have four cases corresponding to four different density matrices. The four cases are: (1) filling zero $\hat{d}_{\mathbf{k},\zeta,\eta,s}^\dagger$ electrons ($\varrho_{\eta,s,ij}^{\text{empty}}(\mathbf{k})$); (2) filling one $\hat{d}_{\mathbf{k},+, \eta,s}^\dagger$ electron for each \mathbf{k} ($\varrho_{\eta,s,ij}^+(\mathbf{k})$); (3) filling one $\hat{d}_{\mathbf{k},-, \eta,s}^\dagger$ electron for each \mathbf{k} ($\varrho_{\eta,s,ij}^-(\mathbf{k})$); (4) filling one $\hat{d}_{\mathbf{k},+, \eta,s}^\dagger$ electron and one $\hat{d}_{\mathbf{k},-, \eta,s}^\dagger$ electron for each \mathbf{k} ($\varrho_{\eta,s,ij}^{+-}(\mathbf{k})$). The corresponding density matrices are

$$\varrho_{\eta,s}^{\text{empty}}(\mathbf{k}) = \begin{pmatrix} 0 & 0 & -\frac{1}{2}\eta g_{\mathbf{k}} e^{-i\eta\theta_{\mathbf{k}}} & 0 & -\frac{h_{\mathbf{k}}}{2} & 0 \\ 0 & 0 & 0 & -\frac{1}{2}\eta g_{\mathbf{k}} e^{i\eta\theta_{\mathbf{k}}} & 0 & -\frac{h_{\mathbf{k}}}{2} \\ -\frac{1}{2}\eta g_{\mathbf{k}} e^{i\eta\theta_{\mathbf{k}}} & 0 & \frac{g_{\mathbf{k}}^2-1}{2} & 0 & \frac{1}{2}\eta g_{\mathbf{k}} h_{\mathbf{k}} e^{i\eta\theta_{\mathbf{k}}} & 0 \\ 0 & -\frac{1}{2}\eta g_{\mathbf{k}} e^{-i\eta\theta_{\mathbf{k}}} & 0 & \frac{g_{\mathbf{k}}^2-1}{2} & 0 & \frac{1}{2}\eta g_{\mathbf{k}} h_{\mathbf{k}} e^{-i\eta\theta_{\mathbf{k}}} \\ -\frac{h_{\mathbf{k}}}{2} & 0 & \frac{1}{2}\eta g_{\mathbf{k}} h_{\mathbf{k}} e^{-i\eta\theta_{\mathbf{k}}} & 0 & \frac{h_{\mathbf{k}}^2-1}{2} & 0 \\ 0 & -\frac{h_{\mathbf{k}}}{2} & 0 & \frac{1}{2}\eta g_{\mathbf{k}} h_{\mathbf{k}} e^{i\eta\theta_{\mathbf{k}}} & 0 & \frac{h_{\mathbf{k}}^2-1}{2} \end{pmatrix} \quad (\text{B60})$$

$$\varrho_{\eta,s}^+(\mathbf{k}) = \begin{pmatrix} 0 & 0 & -\frac{1}{2}\eta g_{\mathbf{k}} e^{-i\eta\theta_{\mathbf{k}}} & 0 & -\frac{h_{\mathbf{k}}}{2} & 0 \\ 0 & 0 & 0 & -\frac{1}{2}\eta g_{\mathbf{k}} e^{i\eta\theta_{\mathbf{k}}} & 0 & -\frac{h_{\mathbf{k}}}{2} \\ -\frac{1}{2}\eta g_{\mathbf{k}} e^{i\eta\theta_{\mathbf{k}}} & 0 & \frac{1}{2}h_{\mathbf{k}}^2 & 0 & -\frac{1}{2}\eta g_{\mathbf{k}} h_{\mathbf{k}} e^{i\eta\theta_{\mathbf{k}}} & 0 \\ 0 & -\frac{1}{2}\eta g_{\mathbf{k}} e^{-i\eta\theta_{\mathbf{k}}} & 0 & \frac{g_{\mathbf{k}}^2-1}{2} & 0 & \frac{1}{2}\eta g_{\mathbf{k}} h_{\mathbf{k}} e^{-i\eta\theta_{\mathbf{k}}} \\ -\frac{h_{\mathbf{k}}}{2} & 0 & -\frac{1}{2}\eta g_{\mathbf{k}} h_{\mathbf{k}} e^{-i\eta\theta_{\mathbf{k}}} & 0 & \frac{g_{\mathbf{k}}^2}{2} & 0 \\ 0 & -\frac{h_{\mathbf{k}}}{2} & 0 & \frac{1}{2}\eta g_{\mathbf{k}} h_{\mathbf{k}} e^{i\eta\theta_{\mathbf{k}}} & 0 & \frac{h_{\mathbf{k}}^2-1}{2} \end{pmatrix} \quad (\text{B61})$$

$$\varrho_{\eta,s}^-(\mathbf{k}) = \begin{pmatrix} 0 & 0 & -\frac{1}{2}\eta g_{\mathbf{k}} e^{-i\eta\theta_{\mathbf{k}}} & 0 & -\frac{h_{\mathbf{k}}}{2} & 0 \\ 0 & 0 & 0 & -\frac{1}{2}\eta g_{\mathbf{k}} e^{i\eta\theta_{\mathbf{k}}} & 0 & -\frac{h_{\mathbf{k}}}{2} \\ -\frac{1}{2}\eta g_{\mathbf{k}} e^{i\eta\theta_{\mathbf{k}}} & 0 & \frac{g_{\mathbf{k}}^2-1}{2} & 0 & \frac{1}{2}\eta g_{\mathbf{k}} h_{\mathbf{k}} e^{i\eta\theta_{\mathbf{k}}} & 0 \\ 0 & -\frac{1}{2}\eta g_{\mathbf{k}} e^{-i\eta\theta_{\mathbf{k}}} & 0 & \frac{1}{2}h_{\mathbf{k}}^2 & 0 & -\frac{1}{2}\eta g_{\mathbf{k}} h_{\mathbf{k}} e^{-i\eta\theta_{\mathbf{k}}} \\ -\frac{h_{\mathbf{k}}}{2} & 0 & \frac{1}{2}\eta g_{\mathbf{k}} h_{\mathbf{k}} e^{-i\eta\theta_{\mathbf{k}}} & 0 & \frac{h_{\mathbf{k}}^2-1}{2} & 0 \\ 0 & -\frac{h_{\mathbf{k}}}{2} & 0 & -\frac{1}{2}\eta g_{\mathbf{k}} h_{\mathbf{k}} e^{i\eta\theta_{\mathbf{k}}} & 0 & \frac{g_{\mathbf{k}}^2}{2} \end{pmatrix} \quad (\text{B62})$$

$$\varrho_{\eta,s}^{+-}(\mathbf{k}) = \begin{pmatrix} 0 & 0 & -\frac{1}{2}\eta g_{\mathbf{k}} e^{-i\eta\theta_{\mathbf{k}}} & 0 & -\frac{h_{\mathbf{k}}}{2} & 0 \\ 0 & 0 & 0 & -\frac{1}{2}\eta g_{\mathbf{k}} e^{i\eta\theta_{\mathbf{k}}} & 0 & -\frac{h_{\mathbf{k}}}{2} \\ -\frac{1}{2}\eta g_{\mathbf{k}} e^{i\eta\theta_{\mathbf{k}}} & 0 & \frac{1}{2}h_{\mathbf{k}}^2 & 0 & -\frac{1}{2}\eta g_{\mathbf{k}} h_{\mathbf{k}} e^{i\eta\theta_{\mathbf{k}}} & 0 \\ 0 & -\frac{1}{2}\eta g_{\mathbf{k}} e^{-i\eta\theta_{\mathbf{k}}} & 0 & \frac{1}{2}h_{\mathbf{k}}^2 & 0 & -\frac{1}{2}\eta g_{\mathbf{k}} h_{\mathbf{k}} e^{-i\eta\theta_{\mathbf{k}}} \\ -\frac{h_{\mathbf{k}}}{2} & 0 & -\frac{1}{2}\eta g_{\mathbf{k}} h_{\mathbf{k}} e^{-i\eta\theta_{\mathbf{k}}} & 0 & \frac{1}{2}g_{\mathbf{k}}^2 & 0 \\ 0 & -\frac{h_{\mathbf{k}}}{2} & 0 & -\frac{1}{2}\eta g_{\mathbf{k}} h_{\mathbf{k}} e^{i\eta\theta_{\mathbf{k}}} & 0 & \frac{1}{2}g_{\mathbf{k}}^2 \end{pmatrix} \quad (\text{B63})$$

Using the above density matrices, one can directly obtain the charge-(± 1) excitations by diagonalizing the corresponding Hartree-Fock Hamiltonian obtained using Eq. (B55).

In Fig. 9, we show the charge-(± 1) excitation at fillings integer filling $-3 \leq \nu \leq 0$ of THF model for $w_0/w_1 = 0.5$. For this tunneling ratio, the Hubbard interaction $U_1 = 37.61 \text{ meV}$ is smaller than the f - c hybridization strength $|\gamma| = 65.78 \text{ meV}$. For the other parameters, we employed [33]

$$v_* = -4.774 \text{ eV } \text{\AA}, \quad v'_* = 0, \quad M = 0, \quad \lambda = 0.5330 |\mathbf{a}_{M1}| \\ W_1 = W_2 = 44.06 \text{ meV}, \quad W_3 = W_4 = 48.35 \text{ meV}, \quad J = 23.75 \text{ meV}, \quad K = 5.11 \text{ meV}, \quad U_2 = 3.709 \text{ meV} \quad (\text{B64})$$

The ground states we considered in Fig. 9 are

$$|\Psi_{\nu=-3}\rangle = \prod_{\mathbf{k}} \hat{d}_{\mathbf{k},+, \uparrow}^\dagger |\text{RB}\rangle, \quad |\Psi_{\nu=-2}\rangle = \prod_{\mathbf{k}} \hat{d}_{\mathbf{k},+, \uparrow}^\dagger \hat{d}_{\mathbf{k},-, \uparrow}^\dagger |\text{RB}\rangle, \\ |\Psi_{\nu=-1}\rangle = \prod_{\mathbf{k}} \hat{d}_{\mathbf{k},+, \uparrow}^\dagger \hat{d}_{\mathbf{k},-, \uparrow}^\dagger \hat{d}_{\mathbf{k},+, \downarrow}^\dagger |\text{RB}\rangle, \quad |\Psi_{\nu=0}\rangle = \prod_{\mathbf{k}} \hat{d}_{\mathbf{k},+, \uparrow}^\dagger \hat{d}_{\mathbf{k},-, \uparrow}^\dagger \hat{d}_{\mathbf{k},+, \downarrow}^\dagger \hat{d}_{\mathbf{k},-, \downarrow}^\dagger |\text{RB}\rangle. \quad (\text{B65})$$

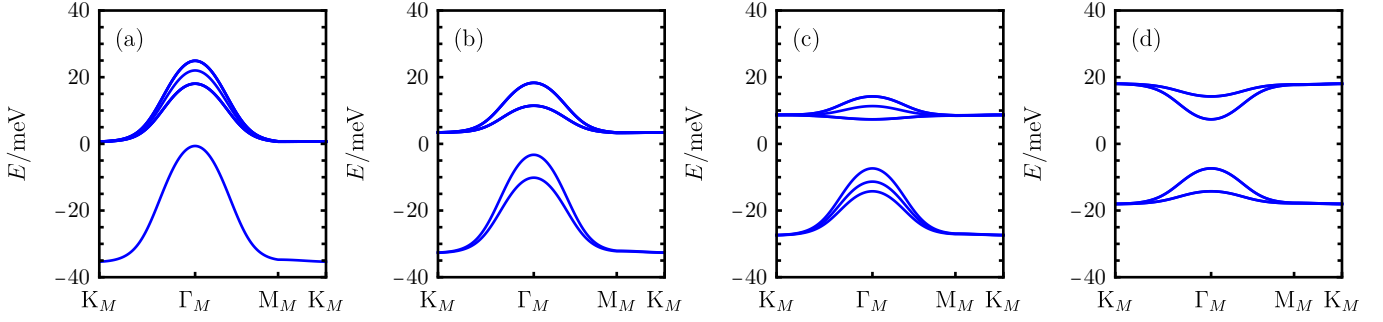


FIG. 9. Charge-(± 1) excitations at $w_0/w_1 = 0.5$ with $\nu = -3$ (a), $\nu = -2$ (b), $\nu = -1$ (c) and $\nu = 0$ (d).

Appendix C: Chern bands with localized Berry curvature

In this appendix, we discuss the heavy fermion description of a model with gapped Chern bands with concentrated Berry curvature. Our simple sp -orbital model consists of one s orbital and one p_z orbital both located at the $1a$ Wyckoff position of the square lattice. We take the following non-interacting Hamiltonian featuring both inversion symmetry and time-reversal symmetry[63]

$$H_0 = \sum_{\mathbf{k}, \sigma} \psi_{\mathbf{k}, \sigma}^\dagger h_{\mathbf{k}}^\sigma \psi_{\mathbf{k}, \sigma}, \quad \text{with} \quad \psi_{\mathbf{k}, \sigma} = \begin{bmatrix} \hat{f}_{\mathbf{k}, \sigma} & \hat{c}_{\mathbf{k}, \sigma} \end{bmatrix}^T$$

$$h_{\mathbf{k}}^\sigma = \begin{bmatrix} \epsilon_s & t_{sp} [\sigma \sin(k_y) - i \sin(k_x)] \\ t_{sp} [\sigma \sin(k_y) + i \sin(k_x)] & \epsilon_p - t_p [\cos(k_x) + \cos(k_y)] \end{bmatrix}, \quad (\text{C1})$$

where $\hat{f}_{\mathbf{k}, \sigma}^\dagger$ ($\hat{c}_{\mathbf{k}, \sigma}^\dagger$) creates a s (p_z)-orbital electron at momentum \mathbf{k} with spin σ . ϵ_s, ϵ_p denote the onsite energy of the s and p orbitals, respectively. At the same time, t_{sp} is the hopping between two orbitals and t_p denotes the hopping of between the p_z orbitals. As a result of the time-reversal symmetry, the spin- \uparrow and spin- \downarrow bands are degenerate in this model.

We consider the situation where $|t_p| \gg |t_{sp}|$, $\epsilon_p = 2t_p - \Delta\epsilon$ with $|\Delta\epsilon| \ll |t_p|$, and $\epsilon_s = 0$. The resulting band structure is shown in Fig. 10(a) for $\Delta\epsilon/t_p = -0.2$ and $t_{sp}/t_p = 0.1$ and features a flat band and a dispersive band, both being doubly-degenerate.

We now discuss the band structure of the system. In the limit $t_{sp} \rightarrow 0$, the p orbitals develop a dispersive band with the band minimum at the Γ point and dispersion

$$\epsilon_{p, \mathbf{k}} = t_p [2 - \cos(k_x) - \cos(k_y)] - \Delta\epsilon \approx -\Delta\epsilon + \frac{t_p |\mathbf{k}|^2}{2} \quad (\text{C2})$$

In this limit, the s orbitals form a perfectly flat trivial band. After introducing a non-zero t_{sp} , the atomic s orbitals and the dispersive p orbitals hybridize near the Γ point and a band inversion happens therein. Performing a leading-order expansion in \mathbf{k} of the p -orbital dispersion and of the s - p orbital hybridization, the single-particle Hamiltonian from Eq. (C1) can be approximated to

$$H_0 \approx \sum_{|\mathbf{k}| < \Lambda_c, \sigma} \left(-\Delta\epsilon + \frac{t_p |\mathbf{k}|^2}{2} \right) \hat{c}_{\mathbf{k}, \sigma}^\dagger \hat{c}_{\mathbf{k}, \sigma} + \frac{t_{sp}}{\sqrt{N}} \sum_{|\mathbf{k}| < \Lambda_c, \mathbf{R}, \sigma} \left[e^{-i\mathbf{k} \cdot \mathbf{R}} (\sigma k_y + i k_x) \hat{c}_{\mathbf{k}, \sigma}^\dagger \hat{f}_{\mathbf{R}, \sigma} + \text{h.c.} \right]. \quad (\text{C3})$$

where N is the number of unit cells. We have also introduced a momentum cutoff Λ_c for the c electrons, since the electron with large momenta are high-energy degrees of freedom and can be dropped. In practice, we can set the cutoff to the edge of the BZ. From Eq. (C3), it becomes evident that the system is equivalent to a heavy-fermion model, characterized by the hybridization between atomic f -electrons (s orbitals) and dispersive c electrons (p orbitals).

The eigenvalues of the single-particle Hamiltonian near the Γ point are

$$E_{\mathbf{k}, 1}^\sigma \approx -\Delta\epsilon + \frac{t_p \Delta\epsilon + 2t_{sp}^2}{2\Delta\epsilon} |\mathbf{k}|^2, \quad E_{\mathbf{k}, 2} \approx \frac{t_{sp}^2}{\Delta\epsilon} |\mathbf{k}|^2, \quad (\text{C4})$$

with the corresponding eigenvectors being given by

$$\begin{aligned}
U_{\mathbf{k},1}^\sigma &\approx \frac{1}{\sqrt{2\sqrt{\frac{s_{\mathbf{k}}^2}{4} + t_{sp}^2|\mathbf{k}|^2} \left[\sqrt{\frac{s_{\mathbf{k}}^2}{4} + t_{sp}^2|\mathbf{k}|^2} - \frac{s_{\mathbf{k}}}{2} \right]}} \left[\frac{s_{\mathbf{k}}}{2} - \sqrt{\frac{s_{\mathbf{k}}^2}{4} + t_{sp}^2|\mathbf{k}|^2} t_{sp} (ik_x + \sigma k_y) \right] \\
U_{\mathbf{k},2}^\sigma &\approx \frac{1}{\sqrt{2\sqrt{\frac{s_{\mathbf{k}}^2}{4} + t_{sp}^2|\mathbf{k}|^2} \left[\sqrt{\frac{s_{\mathbf{k}}^2}{4} + t_{sp}^2|\mathbf{k}|^2} + \frac{s_{\mathbf{k}}}{2} \right]}} \left[\frac{s_{\mathbf{k}}}{2} + \sqrt{\frac{s_{\mathbf{k}}^2}{4} + t_{sp}^2|\mathbf{k}|^2} t_{sp} (ik_x + \sigma k_y) \right]
\end{aligned} \tag{C5}$$

where $s_{\mathbf{k}} = -\Delta\epsilon + t_p|\mathbf{k}|^2/2$. It is easy to see that at the Γ point, the lowest bands are formed by the p_z orbital with $U_{\mathbf{k}=0,1}^\sigma = [0, 1]$. As we move away Γ point, the lowest bands acquire more and more s -orbital weight. At large momenta $|\mathbf{k}|$, the p_z orbitals form high-energy bands, and the lowest-energy bands are mostly formed by the s orbitals.

We can also estimate the bandwidths of the bands. We first consider the lowest-energy bands. At the high-symmetry points, we have

$$E_{0,1}^\sigma = -\Delta\epsilon, \quad E_{(0,\pi),1}^\sigma = E_{(\pi,0),1}^\sigma \approx 0, \quad E_{(\pi,\pi),1}^\sigma \approx 0 \tag{C6}$$

where, away from Γ point, the lowest-energy bands are mostly formed by s orbitals with energy $\epsilon_s = 0$. Therefore the bandwidth of the lowest-energy bands are $\sim |\Delta\epsilon|$. For the high-energy bands, the energies at high-symmetry points are

$$E_{0,2}^\sigma = 0, \quad E_{(0,\pi),2}^\sigma = E_{(\pi,0),2}^\sigma \approx t_p, \quad vE_{(\pi,\pi),2}^\sigma \approx 2t_p \tag{C7}$$

where away from Γ point, the high-energy bands are mostly formed by p_z orbitals with energy $-\Delta\epsilon + t_p[2 - \cos(k_x) - \cos(k_y)] \approx t_p[2 - \cos(k_x) - \cos(k_y)]$. Therefore, the high-energy bands have bandwidth $\sim 2|t_p|$. Thus, our current model comprises a two-fold degenerate narrow band with bandwidth $\sim |\Delta\epsilon|$ and a two-fold degenerate dispersive band with bandwidth $\sim 2|t_p|$.

We now show that the two-fold degenerate low-energy narrow bands have Chern number ± 1 for spin- \uparrow / \downarrow . Since the system has inversion symmetry, it is sufficient to check the inversion eigenvalues of the lowest-energy band at high symmetry points $(0,0), (0,\pi), (\pi,0), (\pi,\pi)$. At the $\Gamma = (0,0)$ point, the narrow bands are formed by p_z orbitals and have -1 inversion eigenvalues. At the $(0,\pi), (\pi,0), (\pi,\pi)$ points, the narrow bands are formed by s orbitals with $+1$ inversion eigenvalue. Therefore, the two-fold degenerate narrow bands have Chern number ± 1 due to the band inversion at the Γ point.

Since the band inversion happens near the Γ point, we also analyze the Berry curvature near Γ point. We can calculate the Berry curvature of the lowest bands near Γ point using Eq. (C5), which gives

$$\Omega(\mathbf{k}) \approx \frac{8(2\Delta\epsilon + |\mathbf{k}|^2 t_p) t_{sp}^2}{\left[\left(-2\Delta\epsilon + t_p^2 |\mathbf{k}|^2 \right)^2 + 16|\mathbf{k}|^2 t_{sp}^2 \right]^{3/2}} \tag{C8}$$

We can observe that, at large momentum the Berry curvature decays as $\frac{t_{sp}^2}{t_p^2 |\mathbf{k}|}$. Since $|t_{sp}/t_p| \ll 1$, the Berry curvature quickly goes to zero at large momenta. In Fig. 10(b), we also show the numerically computed Berry curvature distribution, where we observe the Berry curvature concentrates near Γ point.

We can also introduce interactions to our current model. Here, we consider onsite Hubbard interactions for the s (U) and p (V) orbitals, as well as onsite repulsion between the two orbitals (W). The interaction term can be written as

$$\begin{aligned}
H_I &= \sum_{\mathbf{R}} \frac{U}{2} \left(\sum_{\sigma} : \hat{f}_{\mathbf{R},\sigma}^\dagger \hat{f}_{\mathbf{R},\sigma} : \right)^2 + \sum_{\mathbf{R}, |\mathbf{k}| < \Lambda_c, |\mathbf{k}+\mathbf{q}| < \Lambda_c} \frac{W e^{i\mathbf{q}\cdot\mathbf{R}}}{N} \left(\sum_{\sigma} : \hat{f}_{\mathbf{R},\sigma}^\dagger \hat{f}_{\mathbf{R},\sigma} : \right) \left(\sum_{\sigma'} : \hat{c}_{\mathbf{k},\sigma'}^\dagger \hat{c}_{\mathbf{k}+\mathbf{q},\sigma'} : \right) \\
&+ \sum_{|\mathbf{k}| < \Lambda_c, |\mathbf{k}+\mathbf{q}| < \Lambda_c, |\mathbf{k}'| < \Lambda_c, |\mathbf{k}'-\mathbf{q}| < \Lambda_c} \frac{V}{2N} \left(: \sum_{\sigma} \hat{c}_{\mathbf{k},\sigma}^\dagger \hat{c}_{\mathbf{k}+\mathbf{q},\sigma} : \right) \left(: \sum_{\sigma'} \hat{c}_{\mathbf{k}',\sigma'}^\dagger \hat{c}_{\mathbf{k}'-\mathbf{q},\sigma'} : \right)
\end{aligned} \tag{C9}$$

which takes a similar form to the interaction term of the THF model of TBG from Eq. (A34). For a given operator \hat{O} , we have also defined normal ordering as $: \hat{O} := \hat{O} - \langle \Phi_0 | \hat{O} | \Phi_0 \rangle$ with $|\Phi_0\rangle$ the ground state of the non-interacting

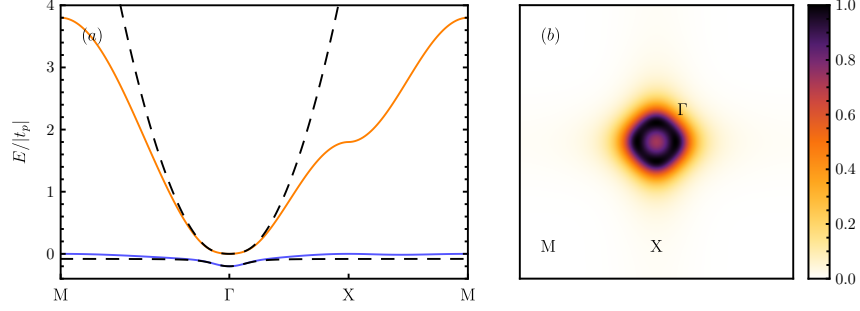


FIG. 10. Heavy-fermion model for Chern bands with localized Berry curvature. (a) shows the dispersion of the sp -orbital model defined in Eq. (C1) for $t_p = -1$, $t_s p = 0.1$, $\epsilon_s = 0$, and $\epsilon_p = 1.8$. The band structure features a doubly-degenerate narrow Chern band (blue) and a doubly-degenerate dispersive band (orange). The dashed lines correspond to the band structure of the corresponding approximate Hamiltonian from Eq. (C3). The berry curvature distributions of the narrow Chern band in arbitrary units is plotted in (b).

Hamiltonian. Finally, we mention that one could also consider the spinless case, where the only interaction term is the term proportional to W .

In summary, our current model yields two-fold degenerate narrow Chern bands near the Fermi energy, exhibiting concentrated Berry curvature near the Γ point. By including both the narrow Chern bands and the dispersive bands, the entire system can be effectively described by a heavy fermion model, as depicted by the single-particle Hamiltonian in Eq. (C1) (or Eq. (C3)). Here, the s orbitals correspond to localized f -electrons, while the p_z orbitals represent dispersive c -electrons. The flatness of the narrow bands arises from the localized nature of s orbitals (f -fermions), while the non-trivial topology emerges from the hybridization between s and p_z orbitals. Furthermore, after introducing interaction terms to the s and p orbitals, we could obtain a conventional interacting heavy fermion model. Thus we conclude that, in the case of flat Chern bands with concentrated Berry curvature, a heavy fermion description is still feasible.

Appendix D: Chiral-Symmetry-Protected Stable Anomaly

We now present the general discussion for chiral-symmetry-protected stable anomaly. Given a generic 2D single-particle matrix Hamiltonian $h(\mathbf{k})$ with chiral symmetry \mathcal{C} , *i.e.*, $\{\mathcal{C}, h(\mathbf{k})\} = 0$ and $\mathcal{C}^2 = 1$. Suppose

$$h(\mathbf{k} + \mathbf{G}) = V_{\mathbf{G}}^\dagger h(\mathbf{k}) V_{\mathbf{G}} \quad (\text{D1})$$

and

$$[V_{\mathbf{G}}, \mathcal{C}] = 0. \quad (\text{D2})$$

Let us focus on an isolated set of $2N$ bands whose energies are symmetric with respect to the zero energy. The eigenvectors ($U_{n,\mathbf{k}}$ with $n = 1, \dots, 2N$) of the isolated set of bands are compatible with \mathcal{C} , *i.e.*, the eigenvectors of the isolated set of bands furnish a rep of \mathcal{C} : $\mathcal{C}U_{n,\mathbf{k}} = \sum_{n'} U_{n',\mathbf{k}} [D_{\mathcal{C}}(\mathbf{k})]_{n'n}$ with $D_{\mathcal{C}}(\mathbf{k})$ unitary for any n and \mathbf{k} . Equivalently, the projection matrix $P(\mathbf{k})$ of the isolated set of $2N$ bands commutes with \mathcal{C} :

$$[\mathcal{C}, P(\mathbf{k})] = 0. \quad (\text{D3})$$

We can diagonalize $D_{\mathcal{C}}(\mathbf{k})$, which gives a “+1” subspace and a “−1” subspace, each of which has a dimension N . Specifically, we denote

$$D_{\mathcal{C}}(\mathbf{k})v_{\pm,i,\mathbf{k}} = \pm v_{\pm,i,\mathbf{k}} \text{ for } i=1,\dots,N, \quad (\text{D4})$$

and then we have

$$U_{\pm,i,\mathbf{k}} = \sum_n U_{n,\mathbf{k}} [v_{\pm,i,\mathbf{k}}]_n, \quad (\text{D5})$$

where

$$\mathcal{C}U_{\pm,i,\mathbf{k}} = \pm U_{\pm,i,\mathbf{k}}. \quad (\text{D6})$$

The projection matrix of the “ ± 1 ” subspace of the isolated set of $2N$ bands reads

$$P_{\pm}(\mathbf{k}) = \sum_{i=1,\dots,N} U_{\pm,i,\mathbf{k}} U_{\pm,i,\mathbf{k}}^{\dagger} . \quad (\text{D7})$$

Owing to Eq. (D2), $P_{\pm}(\mathbf{k} + \mathbf{G}) = V_{\mathbf{G}}^{\dagger} P_{\pm}(\mathbf{k}) V_{\mathbf{G}}$, which has the same behavior as $P(\mathbf{k})$. Combined with the fact that they are projection matrices of the smooth $P(\mathbf{k})$ for chiral eigenvalues $+$ and $-$, respectively, both $P_{+}(\mathbf{k})$ and $P_{-}(\mathbf{k})$ are globally smooth in the momentum space. Therefore, the Berry curvature of each subspace reads

$$F_{\pm}(\mathbf{k}) = \text{Tr} [P_{\pm}(\mathbf{k}) [\partial_{k_x} P_{\pm}(\mathbf{k}), \partial_{k_y} P_{\pm}(\mathbf{k})]] \quad (\text{D8})$$

which is smooth with $F_{\pm}(\mathbf{k} + \mathbf{G}) = F_{\pm}(\mathbf{k})$, leading to well-defined Chern numbers for $P_{\pm}(\mathbf{k})$:

$$\text{Ch}_{\pm} = \frac{1}{2\pi} \int d^2k F_{\pm}(\mathbf{k}) . \quad (\text{D9})$$

The total Chern number of the entire isolated set of $2N$ bands is

$$\text{Ch} = \text{Ch}_{+} + \text{Ch}_{-} . \quad (\text{D10})$$

Note that Eq. (D2) makes sure that Ch_{\pm} are well defined. If Eq. (D2) is violated by having $\{\mathcal{C}, V(\mathbf{b}_1)\} = 0$ with \mathbf{b}_1 one primitive reciprocal lattice vector, we have $\mathcal{C}P_{+}(\mathbf{k} - \mathbf{b}_1) = \mathcal{C}V_{\mathbf{b}_1}P_{+}(\mathbf{k})V_{\mathbf{b}_1}^{\dagger} = -P_{+}(\mathbf{k} - \mathbf{b}_1)$ and thus $F_{+}(\mathbf{k} + \mathbf{b}_1) = F_{-}(\mathbf{k})$, which cannot guarantee well-defined Ch_{\pm} .

If $\text{Ch} \neq 0$, it is impossible to construct exponentially-localized Wannier functions for them, which is the classic obstruction from the total Chern number [283]. Nevertheless, if $\text{Ch}_{\mathcal{C}} = \text{Ch}_{+} - \text{Ch}_{-} \neq 0$, it is also impossible to construct exponentially-localized Wannier functions for them while keeping the rep of \mathcal{C} strictly-onsite in the real space or momentum-independent in the momentum space, even if $\text{Ch} = 0$. To see this, let us assume we can rotate $U_{n,\mathbf{k}}$ to a set of globally smooth vectors $\zeta_{a,\mathbf{k}}$ with $a = 1, 2, \dots, 2N$, *i.e.*,

$$\zeta_{a,\mathbf{k}} = \sum_{n=1}^{2N} U_{n,\mathbf{k}} R_{na}(\mathbf{k}) \quad (\text{D11})$$

and all $\zeta_{a,\mathbf{k}}$ are globally smooth while $V_{\mathbf{G}}^{\dagger} \zeta_{a,\mathbf{k}} = \zeta_{a,\mathbf{k} + \mathbf{G}}$. We further assume the rep of \mathcal{C} furnished by $\zeta_{a,\mathbf{k}}$ is independent of \mathbf{k} (which means that the rep of \mathcal{C} is strictly-onsite in the real space), *i.e.*,

$$\mathcal{C}\zeta_{a,\mathbf{k}} = \sum_{a'} \zeta_{a',\mathbf{k}} [\tilde{D}_{\mathcal{C}}]_{a'a} . \quad (\text{D12})$$

Then, we can diagonalize $\tilde{D}_{\mathcal{C}}$:

$$\tilde{D}_{\mathcal{C}} \tilde{v}_{\pm,i} = \pm \tilde{v}_{\pm,i} \text{ for } i = 1, \dots, N , \quad (\text{D13})$$

and have

$$\zeta_{\pm,i,\mathbf{k}} = \sum_a \zeta_{a,\mathbf{k}} [\tilde{v}_{\pm,i}]_a . \quad (\text{D14})$$

Since $\zeta_{\pm,i,\mathbf{k}}$ are globally smooth and $V_{\mathbf{G}}^{\dagger} \zeta_{\pm,i,\mathbf{k}} = \zeta_{\pm,i,\mathbf{k} + \mathbf{G}}$, we have $\text{Ch}_{+} = \text{Ch}_{-} = 0$. As globally smooth $\zeta_{a,\mathbf{k}}$ give exponentially localized Wannier functions, we know nonzero $\text{Ch}_{\mathcal{C}} = \text{Ch}_{+} - \text{Ch}_{-} \neq 0$ forbids exponentially-localized Wannier functions with the rep of \mathcal{C} being strictly-onsite in the real space or momentum-independent in the momentum space, even if $\text{Ch} = 0$.

Now we present an alternative way to evaluate $\text{Ch}_{+} - \text{Ch}_{-}$. Suppose $h(\mathbf{k})$ has several isolated band-touching points at zero energy, labeled as \mathbf{k}_l . Then, for each node \mathbf{k}_l , we can define the chiral winding number W_l as

$$W_l = \frac{i}{2\pi} \int_{\partial D_l} d\mathbf{k} \cdot \text{Tr} [Q_{\mathbf{k}}^{-1} \nabla_{\mathbf{k}} Q_{\mathbf{k}}] , \quad (\text{D15})$$

where

$$[Q_{\mathbf{k}}]_{ii'} = U_{+,i,\mathbf{k}}^{\dagger} h(\mathbf{k}) U_{-,i',\mathbf{k}} , \quad (\text{D16})$$

D_l is a disk-like region that only includes \mathbf{k}_l , and ∂D_l is the boundary (with direction) of D_l . We now prove

$$\sum_l W_l = \text{Ch}_C = \text{Ch}_+ - \text{Ch}_- . \quad (\text{D17})$$

The proof is analogous to the proof for monopole Cooper pairing in Ref. [284]. As the first step of the proof, we define

$$\begin{aligned} \mathbf{v}_k &= \text{Tr} \left[\left(U_{-,k} Q_k^{-1} U_{+,k}^\dagger \right) i \nabla_k \left(U_{+,k} Q_k U_{-,k}^\dagger \right) \right] \\ &= \text{Tr} \left[U_{+,k}^\dagger i \nabla_k U_{+,k} \right] + \text{Tr} \left[Q_k^{-1} i \nabla_k Q_k \right] - \text{Tr} \left[U_{-,k}^\dagger i \nabla_k U_{-,k} \right] \\ &= \text{Tr} \left[Q_k^{-1} i \nabla_k Q_k \right] - \mathbf{A}_+(\mathbf{k}) + \mathbf{A}_-(\mathbf{k}) , \end{aligned} \quad (\text{D18})$$

where

$$U_{\pm,k} = \begin{pmatrix} U_{\pm,1,k} & U_{\pm,2,k} & \dots & U_{\pm,N,k} \end{pmatrix} , \quad (\text{D19})$$

and

$$\mathbf{A}_\pm(\mathbf{k}) = -i \text{Tr} \left[U_{\pm,k}^\dagger \nabla_k U_{\pm,k} \right] . \quad (\text{D20})$$

\mathbf{v}_k is smooth except at \mathbf{k}_l 's, since both $U_{+,k}^\dagger U_{+,k}$ and $U_{-,k}^\dagger U_{-,k}$ are smooth, and $Q_k^{-1} = U_{-,k}^\dagger h^{-1}(\mathbf{k}) U_{+,k}$. Moreover, $\mathbf{v}_{\mathbf{k}+\mathbf{G}} = \mathbf{v}_k$. The next step is to choose D_l such that (i) two D_l 's either have no intersection or intersect only on the boundaries, and (ii) $\cup_l D_l = 1BZ$. Then, we have

$$\frac{1}{2\pi} \sum_l \int_{\partial D_l} d\mathbf{k} \cdot \mathbf{v}_k = 0 , \quad (\text{D21})$$

since the integration always cancels along a line shared by two neighboring D_l 's. Combined with Eq. (D18), we have

$$\begin{aligned} & \frac{1}{2\pi} \sum_l \int_{\partial D_l} d\mathbf{k} \cdot [\text{Tr} [Q_k^{-1} i \nabla_k Q_k] - \mathbf{A}_+(\mathbf{k}) + \mathbf{A}_-(\mathbf{k})] \\ &= \sum_l W_l - \frac{1}{2\pi} \sum_l \int_{\partial D_l} d\mathbf{k} \cdot \mathbf{A}_+(\mathbf{k}) + \frac{1}{2\pi} \sum_l \int_{\partial D_l} d\mathbf{k} \cdot \mathbf{A}_-(\mathbf{k}) \\ &= \sum_l W_l - \frac{1}{2\pi} \sum_l \int_{D_l} dk^2 F_+(\mathbf{k}) + \frac{1}{2\pi} \sum_l \int_{D_l} dk^2 F_-(\mathbf{k}) \\ &= \sum_l W_l - \text{Ch}_+ + \text{Ch}_- = 0 , \end{aligned} \quad (\text{D22})$$

leading to Eq. (D17). In the derivation, we have used $F_\pm(\mathbf{k}) = \nabla_k \times \mathbf{A}_\pm(\mathbf{k})$, and used the fact that we can always choose $U_{\pm,k}$ to be smooth within one single D_l (as it is disk-like) to use Stoke's theorem for the second equality. We note that $U_{\pm,k}$ cannot be made globally smooth if Ch_\pm are nonzero.

Based on Eq. (D17), we know that as long as $\sum_l W_l$ is nonzero, any isolated set of $2N$ chiral-symmetric bands have chiral-protected Wannier obstruction, leading to a stable chiral-protected anomaly.

Appendix E: Twisted Checkerboard Model

This section contained more details on the twisted checkerboard model in Ref. [67], and the construction of the heavy fermion model of it. We specify that Ref. [21] studied the heavy fermion framework for a special quadratic band touching model clearly related to the twisted checkerboard model. We have here complemented their analysis by uncovering the stable chiral-symmetric anomaly and obtaining the interaction Hamiltonian.

The twisted checkerboard model in Ref. [67] is generated by stacking two checkerboard lattices with relative twisted angle θ . For each checkerboard lattice, the primitive lattice vectors read

$$\begin{aligned} \mathbf{a}_1 &= (1, 0) \\ \mathbf{a}_2 &= (0, 1) , \end{aligned} \quad (\text{E1})$$

where we have chosen the lattice constant to be 1, and the primitive reciprocal lattice vectors are

$$\begin{aligned} \mathbf{b}_1 &= (2\pi, 0) \\ \mathbf{b}_2 &= (0, 2\pi) . \end{aligned} \quad (\text{E2})$$

The Hamiltonian reads

$$H_{CBL} = \sum_{\mathbf{k}} \begin{pmatrix} c_{\mathbf{k},A}^\dagger & c_{\mathbf{k},B}^\dagger \end{pmatrix} h(\mathbf{k}) \otimes s_0 \begin{pmatrix} c_{\mathbf{k},A} \\ c_{\mathbf{k},B} \end{pmatrix} , \quad (\text{E3})$$

where

$$h(\mathbf{k}) = -4t \cos(k_x/2) \cos(k_y/2) \sigma_x + 2t' (\cos(k_x) - \cos(k_y)) \sigma_z , \quad (\text{E4})$$

$$c_{\mathbf{k},A/B}^\dagger = \begin{pmatrix} c_{\mathbf{k},A/B,\uparrow}^\dagger & c_{\mathbf{k},A/B,\downarrow}^\dagger \end{pmatrix} \quad (\text{E5})$$

with $\sigma_{0,x,y,z}$ are identity and Pauli matrices for the sublattice index, and $s_{0,x,y,z}$ are identity and Pauli matrices for the spin index. Furthermore, for any reciprocal lattice vector \mathbf{G} , we have

$$\begin{aligned} c_{\mathbf{k}+\mathbf{G},A}^\dagger &= c_{\mathbf{k},A}^\dagger \\ c_{\mathbf{k}+\mathbf{G},B}^\dagger &= c_{\mathbf{k},B}^\dagger e^{-i\mathbf{G} \cdot (\mathbf{a}_1 + \mathbf{a}_2)/2} \end{aligned} \quad (\text{E6})$$

With a basis transformation

$$\begin{pmatrix} \tilde{c}_{\mathbf{k},+}^\dagger & \tilde{c}_{\mathbf{k},-}^\dagger \end{pmatrix} = \begin{pmatrix} c_{\mathbf{k},A}^\dagger & c_{\mathbf{k},B}^\dagger \end{pmatrix} \frac{1}{\sqrt{2}} \begin{pmatrix} 1 & -i \\ -i & 1 \end{pmatrix} \otimes s_0 , \quad (\text{E7})$$

we get

$$H_{CBL} = \sum_{\mathbf{k}} \begin{pmatrix} \tilde{c}_{\mathbf{k},+}^\dagger & \tilde{c}_{\mathbf{k},-}^\dagger \end{pmatrix} \tilde{h}(\mathbf{k}) \otimes s_0 \begin{pmatrix} \tilde{c}_{\mathbf{k},+} \\ \tilde{c}_{\mathbf{k},-} \end{pmatrix} , \quad (\text{E8})$$

where

$$\tilde{h}(\mathbf{k}) = 4t \cos(k_x/2) \cos(k_y/2) \sigma_x + 2t' (\cos(k_x) - \cos(k_y)) \sigma_y . \quad (\text{E9})$$

The symmetry group of the checkerboard lattice model in Eq. (E8) is spanned by spin-charge $U(2)$, spinless C_{4z} , spinless C_{2x} , \mathcal{T} and lattice translations, where representations (reps) of C_{4z} , C_{2x} and \mathcal{T} are

$$\begin{aligned} C_{4z} \tilde{c}_{\mathbf{k}}^\dagger C_{4z}^{-1} &= \tilde{c}_{C_{4z}\mathbf{k}}^\dagger \sigma_x s_0 \\ C_{2x} \tilde{c}_{\mathbf{k}}^\dagger C_{2x}^{-1} &= \tilde{c}_{C_{2x}\mathbf{k}}^\dagger \sigma_0 s_0 \\ \mathcal{T} \tilde{c}_{\mathbf{k}}^\dagger \mathcal{T}^{-1} &= \tilde{c}_{-\mathbf{k}}^\dagger (-\sigma_y) i s_y . \end{aligned} \quad (\text{E10})$$

At $\mathbf{k} = (\pi, \pi) = \mathbf{M}$, the basis furnishes a 2D irrep of C_{4z} and C_{2x} symmetries:

$$\begin{aligned} C_{4z} \tilde{c}_{\mathcal{M}}^\dagger C_{4z}^{-1} &= \tilde{c}_{\mathbf{M}-\mathbf{b}_1}^\dagger \sigma_x s_0 = c_M^\dagger \sigma_z \frac{1}{\sqrt{2}} \begin{pmatrix} 1 & -i \\ -i & 1 \end{pmatrix} \sigma_x s_0 = \tilde{c}_{\mathcal{M}}^\dagger \frac{1}{2} \begin{pmatrix} 1 & i \\ i & 1 \end{pmatrix} \sigma_z \begin{pmatrix} 1 & -i \\ -i & 1 \end{pmatrix} \sigma_x s_0 = \tilde{c}_{\mathcal{M}}^\dagger (-i) \sigma_z s_0 \\ C_{2x} \tilde{c}_{\mathcal{M}}^\dagger C_{2x}^{-1} &= \tilde{c}_{\mathbf{M}-\mathbf{b}_2}^\dagger \sigma_0 s_0 = c_M^\dagger \sigma_z \frac{1}{\sqrt{2}} \begin{pmatrix} 1 & -i \\ -i & 1 \end{pmatrix} \sigma_0 s_0 = \tilde{c}_{\mathcal{M}}^\dagger \frac{1}{2} \begin{pmatrix} 1 & i \\ i & 1 \end{pmatrix} \sigma_z \begin{pmatrix} 1 & -i \\ -i & 1 \end{pmatrix} \sigma_0 s_0 = \tilde{c}_{\mathcal{M}}^\dagger \sigma_y s_0 . \end{aligned} \quad (\text{E11})$$

Therefore, $\tilde{h}(\mathcal{M})$ must be proportional to an identity matrix, which indeed is the case: $\tilde{h}(\mathcal{M}) = 0$ according to Eq. (E9). Away from \mathcal{M} , $\tilde{h}(\mathcal{M} + \mathbf{p})$ reads

$$\tilde{h}(\mathcal{M} + \mathbf{p}) = tp_x p_y \sigma_x + t'(p_x^2 + p_y^2) \sigma_y + O(p^4) . \quad (\text{E12})$$

The moiré model in the following is built from Eq. (E12) to the second order of p .

The basis of the moiré model is $\psi_{\mathbf{r},l,\sigma,s}^\dagger$, where $l = t, b$ labels the layer, $\sigma = A, B$ labels the sublattice, and $s = \uparrow, \downarrow$ labels the spin. Specifically,

$$\begin{aligned}\psi_{\mathbf{r},t,\sigma,s}^\dagger &= \frac{1}{\sqrt{N\Omega}} \sum_{\mathbf{p}} e^{i\mathbf{p}\cdot\mathbf{r}} \tilde{c}_{C_{\theta/2}M+\mathbf{p},\sigma,s}^\dagger \\ \psi_{\mathbf{r},b,\sigma,s}^\dagger &= \frac{1}{\sqrt{N\Omega}} \sum_{\mathbf{p}} e^{i\mathbf{p}\cdot\mathbf{r}} \tilde{c}_{C_{-\theta/2}M+\mathbf{p},\sigma,s}^\dagger\end{aligned}\quad (\text{E13})$$

where N is the number of moiré unit cells, and Ω is the area of the moiré unit cell. The model has moiré lattice translations generated by

$$\begin{aligned}\mathbf{a}_{M,1} &= \frac{\sqrt{2}\pi}{k_\theta} (1, 0)^T \\ \mathbf{a}_{M,2} &= \frac{\sqrt{2}\pi}{k_\theta} (0, 1)^T,\end{aligned}\quad (\text{E14})$$

where $k_\theta = 2\sqrt{2}\pi \sin(\frac{\theta}{2})$ and recall that the lattice constant of the underlying checkerboard lattice is set to 1. The moiré Hamiltonian in the real space reads

$$H = \int d^2r \begin{pmatrix} \psi_{\mathbf{r},t}^\dagger & \psi_{\mathbf{r},b}^\dagger \end{pmatrix} \begin{pmatrix} -t\partial_x\partial_y\sigma_x - t'(\partial_x^2 - \partial_y^2)\sigma_y & W(\mathbf{r}) \\ W^\dagger(\mathbf{r}) & -t\partial_x\partial_y\sigma_x - t'(\partial_x^2 - \partial_y^2)\sigma_y \end{pmatrix} \otimes s_0 \begin{pmatrix} \psi_{\mathbf{r},t} \\ \psi_{\mathbf{r},b} \end{pmatrix}, \quad (\text{E15})$$

where

$$\psi_{\mathbf{r},l}^\dagger = (\psi_{\mathbf{r},l,+, \uparrow}^\dagger, \psi_{\mathbf{r},l,+, \downarrow}^\dagger, \psi_{\mathbf{r},l,-, \uparrow}^\dagger, \psi_{\mathbf{r},l,-, \downarrow}^\dagger), \quad (\text{E16})$$

$$W(\mathbf{r}) = 2 \sum_{i=1}^2 T_i \cos(\mathbf{r} \cdot \mathbf{q}_i) + 2 \sum_{i=1}^4 T'_i \cos(\mathbf{r} \cdot \mathbf{g}_i), \quad (\text{E17})$$

$\mathbf{q}_n = C_{4z}^{n-1} \frac{k_\theta}{\sqrt{2}} (1, 1)^T$ with $n = 1, 2, 3, 4$ (see \mathbf{q}_1 in Fig. 3(c)), $\mathbf{g}_i = \mathbf{b}_{M,i} + \mathbf{q}_1$ with $i = 1, 2$, $\mathbf{g}_i = C_{4z}\mathbf{g}_{i-2}$ with $i = 3, 4$. The interlayer tunnelling chosen in Ref. [67] reads

$$T_1 = \sigma_z T_2 \sigma_z = w_1 \sigma_x, \quad (\text{E18})$$

and we added

$$T'_1 = T'_2 = w'_1 \sigma_x, \quad T'_3 = T'_4 = \sigma_z T'_1 \sigma_z \quad (\text{E19})$$

to allow more tunability of the model. The symmetry group of the model is spanned by spin SU(2), spinless C_{4z} , spinless C_{2x} , \mathcal{T} and moiré-lattice translations. It also has an effective m_z that exchanges the two layers, and chiral symmetry \mathcal{C} . (We neglect the identity term in T_1 and T_2 to achieve this.) The representations (reps) of the symmetries furnished by the basis are

$$\begin{aligned}C_{4z}\psi_{\mathbf{r},l}^\dagger C_{4z}^{-1} &= \psi_{C_{4z}\mathbf{r},l}^\dagger (-i\sigma_z s_0) \\ C_{2x}\psi_{\mathbf{r},l}^\dagger C_{2x}^{-1} &= \psi_{C_{2x}\mathbf{r},\bar{l}}^\dagger \sigma_y s_0 \\ \mathcal{T}\psi_{\mathbf{r},l}^\dagger \mathcal{T}^{-1} &= \psi_{\mathbf{r},l}^\dagger i\sigma_x i s_y \\ T_{\mathbf{R}_M}\psi_{\mathbf{r},l}^\dagger T_{\mathbf{R}_M}^{-1} &= e^{-i\mathbf{R}_M \cdot M_l} \psi_{\mathbf{r}+\mathbf{R}_M,l}^\dagger \\ m_z\psi_{\mathbf{r},l}^\dagger m_z^{-1} &= \psi_{\mathbf{r},\bar{l}}^\dagger \\ \mathcal{C}\psi_{\mathbf{r},l}^\dagger \mathcal{C}^{-1} &= \psi_{\mathbf{r},l}^\dagger \sigma_z s_0,\end{aligned}\quad (\text{E20})$$

where $\bar{l} = b/t$ if $l = t/b$, $M_t = C_{\theta/2}(\pi, \pi)^T$, and $M_b = C_{-\theta/2}(\pi, \pi)^T$.

In practical calculation, we always need to convert the model to the momentum spaces. To do so, we first define

$$\psi_{\mathbf{p},l,\sigma,s}^\dagger = \frac{1}{\sqrt{N\Omega}} \int d^2r e^{i\mathbf{p}\cdot\mathbf{r}} \psi_{\mathbf{r},l,\sigma,s}^\dagger, \quad (\text{E21})$$

where $\sigma = \pm$. The moiré reciprocal lattice vectors are $\{\mathbf{G}_M\} = (\mathbf{b}_{M,1} \ \mathbf{b}_{M,2}) \mathbb{Z}^2$, where $\mathbf{b}_{M,1} = \sqrt{2}k_\theta(1,0)^T$ and $\mathbf{b}_{M,2} = \sqrt{2}k_\theta(0,1)^T$. The \mathbf{Q} vectors for the two layers are

$$\begin{aligned} \mathcal{Q}_t &= \{\mathbf{G}_M\} + \mathbf{q}_1 \\ \mathcal{Q}_b &= \{\mathbf{G}_M\} \\ \mathcal{Q} &= \mathcal{Q}_t \cup \mathcal{Q}_b, \end{aligned} \quad (\text{E22})$$

and then we can define

$$\psi_{\mathbf{k},\mathbf{Q},\sigma,s}^\dagger = \psi_{\mathbf{k}-\mathbf{Q},l_{\mathbf{Q}},\sigma,s}^\dagger \quad (\text{E23})$$

with $l_{\mathbf{Q}} = l$ iff $\mathbf{Q} \in \mathcal{Q}_l$.

With those definitions, we have

$$H = \sum_{\mathbf{k} \in \text{MBZ}} \sum_{\mathbf{Q}, \mathbf{Q}'} \psi_{\mathbf{k},\mathbf{Q}}^\dagger \left[h_0(\mathbf{k} - \mathbf{Q}) \delta_{\mathbf{Q}\mathbf{Q}'} + \sum_{i=1}^2 T_i (\delta_{\mathbf{Q},\mathbf{Q}'+\mathbf{q}_i} + \delta_{\mathbf{Q},\mathbf{Q}'-\mathbf{q}_i}) + \sum_{i'=1}^4 T_{i'} (\delta_{\mathbf{Q},\mathbf{Q}'+\mathbf{g}_{i'}} + \delta_{\mathbf{Q},\mathbf{Q}'-\mathbf{g}_{i'}}) \right] \otimes s_0 \psi_{\mathbf{k},\mathbf{Q}'} , \quad (\text{E24})$$

where

$$h_0(\mathbf{p}) = tp_x p_y \tau_x + t'(p_x^2 - p_y^2) \tau_y. \quad (\text{E25})$$

The symmetry reps in the momentum space read

$$\begin{aligned} C_{4z} \psi_{\mathbf{k},\mathbf{Q}}^\dagger C_{4z}^{-1} &= \psi_{C_{4z}\mathbf{k}, C_{4z}\mathbf{Q}}^\dagger (-i\tau_z) s_0 \\ C_{2x} \psi_{\mathbf{k},\mathbf{Q}}^\dagger C_{2x}^{-1} &= \psi_{C_{2x}\mathbf{k}-C_{2x}\mathbf{Q}, \bar{l}_{\mathbf{Q}}}^\dagger \tau_y s_0 = \psi_{C_{2x}\mathbf{k}+\mathbf{q}_1-C_{2x}\mathbf{Q}-\mathbf{q}_1, l_{C_{2x}\mathbf{Q}+\mathbf{q}_1}}^\dagger \tau_y s_0 = \psi_{C_{2x}\mathbf{k}+\mathbf{q}_1, C_{2x}\mathbf{Q}+\mathbf{q}_1}^\dagger \tau_y s_0 \\ \mathcal{T} \psi_{\mathbf{k},\mathbf{Q}}^\dagger \mathcal{T}^{-1} &= \psi_{-\mathbf{k}, -\mathbf{Q}}^\dagger i\tau_x i s_y \\ m_z \psi_{\mathbf{k},\mathbf{Q}}^\dagger m_z^{-1} &= \psi_{\mathbf{k}+\mathbf{q}_1, \mathbf{Q}+\mathbf{q}_1}^\dagger \\ \mathcal{C} \psi_{\mathbf{k},\mathbf{Q}}^\dagger \mathcal{C}^{-1} &= \psi_{\mathbf{k},\mathbf{Q}}^\dagger \sigma_z s_0. \end{aligned} \quad (\text{E26})$$

In this basis, we see that the representation for C_{2x} changes the Bloch momentum. The reason is that C_{2x} changes $\mathbf{k} - \mathbf{Q}_t$ in the top layer to $C_{2x}\mathbf{k} - C_{2x}\mathbf{Q}_t$ in the second layer. However, \mathcal{Q}_t and \mathcal{Q}_b are both C_{2x} -invariant, and thus we have to shift $C_{2x}\mathbf{Q}_t$ by \mathbf{q}_1 to enter \mathcal{Q}_b , leading to the new separation $C_{2x}\mathbf{k} + \mathbf{q}_1 - C_{2x}\mathbf{Q}_t - \mathbf{q}_1$ in Eq. (E32). The same reasoning holds for m_z . The argument extends to any twisted bilayer rectangular/square systems (i) whose low-energy physics comes from M point and (ii) which has in-plane C_2 symmetries that flip two layers. In contrast, in TBG, the two \mathbf{Q} lattices of two layers are C_{2x} partners, and thus there is no momentum shift for C_{2x} there.

1. Chiral-Symmetry Protected Stable Anomaly

In this section, we discuss the stable anomaly of the moiré single-particle Hamiltonian in Eq. (E24) that is protected by the chiral symmetry. If we set $w_1 = w'_1 = 0$, we have two quadratic touching points (from two layers) at the zero energies at Γ_M and M_M in the moiré Brillouin zone, and each of it has chiral winding number 2, adding up to a total chiral winding number of $\sum_l W_l = 4$. The nonzero total chiral winding number indicates a stable anomaly, which holds for nonzero w_1 and w'_1 due to the presence of chiral symmetry.

The chiral-symmetry-protected anomaly should be reflected as nontrivial $\text{Ch}_+ - \text{Ch}_-$ for any chiral-symmetric set of even number of bands. To show this, we first choose

$$t = 4/k_\theta^2, \ t' = 1.26/k_\theta^2, \ w_1 = 0.66, \ w'_1 = -0.4, \quad (\text{E27})$$

whose band structure is shown in Fig. 11(b). We have $\text{Ch}_+ - \text{Ch}_- = 4$ for the isolated chiral-symmetric set of 2 bands in Fig. 11(b) around zero energies, as indicated by the Wilson loop spectrum in Fig. 11(c). We also plot the band structure for

$$t = 4/k_\theta^2, \ t' = 1.26/k_\theta^2, \ w_1 = 0.4, \ w'_1 = -0.4 \quad (\text{E28})$$

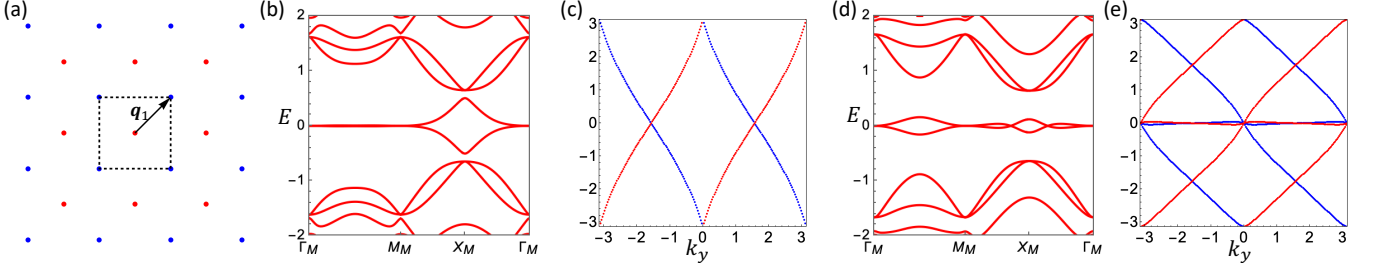


FIG. 11. (a) The red and blue dots are \mathcal{Q}_b and \mathcal{Q}_t , respectively, in Fig. E22. (b) and (d) show the band structures for the parameter set 1 in Eq. (E27) and set 2 in Eq. (E28), respectively. (c) and (e) show the chiral-resolved Wilson loop spectrum for the isolated chiral-symmetric set of 2 bands in (b) around zero energies and the isolated chiral-symmetric set of 6 bands in (d) around zero energies, respectively. The Wilson spectrum in the chiral-even (chiral-odd) subspace is in red (blue).

in Fig. 11(d), which has $\text{Ch}_+ - \text{Ch}_- = 4$ for the isolated chiral-symmetric set of 6 bands around zero energies, as indicated by the Wilson loop spectrum in Fig. 11(d).

The nonzero $\text{Ch}_+ - \text{Ch}_-$ can be indicated by the symmetries. Owing to the $C_{2z}\mathcal{T}$ symmetry, any isolated set of bands have zero total Chern number, and thus we always have $\text{Ch}_+ = -\text{Ch}_-$, which means we only need to indicate the nonzero Ch_+ . To do so, we look at C_{4z} eigenvalues at Γ_M and M_M , and C_{2z} eigenvalues at X_M . As a result, for the isolated chiral-symmetric set of 2 bands for Eq. (E27), the chiral-even subspace has $C_{4z} \doteq -i$ at Γ_M , $C_{4z} \doteq -i$ at M_M and $C_{2z} \doteq 1$ at X_M , which gives $i^{\text{Ch}_+} = (-i)(-i)1 = -1$; then we know $\text{Ch}_+ = 2 \bmod 4$, which is consistent with the Wilson loop in Fig. 11(c). Similarly, for the isolated chiral-symmetric set of 6 bands for Eq. (E28), the chiral-even subspace has $C_{4z} \sim \text{diag}(-i, i, -i)$ at Γ_M , $C_{4z} \sim \text{diag}(-i, i, -i)$ at M_M and $C_{2z} \sim \text{diag}(-1, -1, 1)$ at X_M , which gives $i^{\text{Ch}_+} = (-i)(-i)1 = -1 \Rightarrow \text{Ch}_+ = 2 \bmod 4$, which is consistent with the Wilson loop in Fig. 11(e).

2. Heavy Fermion Model: Single-Particle

The stable anomaly of the model forbids any local-chiral Wannierization for any chiral-symmetric set of bands. However, for the case of the nearly flat bands with concentrated curvature, we can resolve the issue via the construction of topological heavy fermion model [21].

To show this, we focus on the parameter set in Eq. (E27), where the near flat bands has concentrated $F_+(\mathbf{k}) - F_-(\mathbf{k})$ as shown in Fig. 3(c). Using *Wannier90*, we can construct the exponentially-localized Wannier functions by combining most states of nearly flat bands near the zero energy and the states near X_M and Y_M from the remote bands. The resultant f modes have the form

$$f_{\mathbf{k},\alpha,s}^\dagger = \sum_{\mathbf{Q}\sigma} \psi_{\mathbf{k},\mathbf{Q},\sigma,s}^\dagger [U_{f,\alpha}(\mathbf{k})]_{\mathbf{Q}\sigma} \quad (\text{E29})$$

with $\alpha = 1, 2$. The trial functions for the Wannierization were chosen as

$$\begin{aligned} [U_{f,1}(\mathbf{k})]_{\mathbf{Q}\sigma} &= \frac{1}{\sqrt{\Omega}} \sqrt{\pi\lambda^2} (1, i)_\alpha e^{-|\mathbf{k}-\mathbf{Q}|^2\lambda^2/2} (-)^{\mathbf{Q}} \\ [U_{f,2}(\mathbf{k})]_{\mathbf{Q}\sigma} &= \frac{1}{\sqrt{\Omega}} \sqrt{\pi\lambda^2} (-i, -1)_\alpha e^{-|\mathbf{k}-\mathbf{Q}|^2\lambda^2/2} (-)^{\mathbf{Q}}, \end{aligned} \quad (\text{E30})$$

where $(-)^{\mathbf{Q}} = 1$ for $\mathbf{Q} \in \mathcal{Q}_t$ and $(-)^{\mathbf{Q}} = -1$ for $\mathbf{Q} \in \mathcal{Q}_b$. The resultant Wannier function have the forms

$$w_{\alpha l\sigma}(\mathbf{r}) = \frac{1}{N\sqrt{\Omega}} \sum_{\mathbf{Q} \in \mathcal{Q}_l} e^{i(\mathbf{k}-\mathbf{Q})\cdot\mathbf{r}} [U_{f,\alpha}(\mathbf{k})]_{\mathbf{Q}\sigma}, \quad (\text{E31})$$

which has spread $(0.4285a_M)^2$ with a_M the moiré lattice constant. The symmetry reps furnished by $f_{\mathbf{k},\alpha,s}^\dagger$ are

$$\begin{aligned} C_{4z} f_{\mathbf{k}}^\dagger C_{4z}^{-1} &= f_{C_{4z}\mathbf{k}}^\dagger (-i\tau_z) s_0 \\ C_{2x} f_{\mathbf{k}}^\dagger C_{2x}^{-1} &= f_{C_{2x}\mathbf{k}+\mathbf{q}_1}^\dagger \tau_x s_0 \\ \mathcal{T} f_{\mathbf{k}}^\dagger \mathcal{T}^{-1} &= f_{-\mathbf{k}}^\dagger \tau_x i s_y \\ m_z f_{\mathbf{k}}^\dagger m_z^{-1} &= f_{\mathbf{k}+\mathbf{q}_1}^\dagger (-) \\ \mathcal{C} f_{\mathbf{k}}^\dagger \mathcal{C}^{-1} &= f_{\mathbf{k}}^\dagger \sigma_z s_0 , \end{aligned} \tag{E32}$$

indicating they have the same symmetry reps as $p_x \pm p_y$ at 1a position of the moiré unit cell.

The remaining c modes are localized around X_M and Y_M , which have the form

$$c_{X_M+\mathbf{q},\beta,s}^\dagger = \sum_{\mathbf{Q}\sigma} \psi_{X_M+\mathbf{q},\mathbf{Q},\sigma,s}^\dagger [U_{c,\beta}(X_M + \mathbf{q})]_{\mathbf{Q}\sigma} \tag{E33}$$

and

$$c_{Y_M+\mathbf{q},\beta,s}^\dagger = \sum_{\mathbf{Q}\sigma} \psi_{Y_M+\mathbf{q},\mathbf{Q},\sigma,s}^\dagger [U_{c,\beta}(Y_M + \mathbf{q})]_{\mathbf{Q}\sigma} . \tag{E34}$$

Their symmetry reps are

$$\begin{aligned} C_{4z} m_z c_{X_M+\mathbf{q}}^\dagger (C_{4z} m_z)^{-1} &= c_{X_M+C_{4z}\mathbf{q}}^\dagger \begin{pmatrix} -1 & 0 & 0 & 0 \\ 0 & -1 & 0 & 0 \\ 0 & 0 & -i & 0 \\ 0 & 0 & 0 & i \end{pmatrix} s_0 , \quad m_z C_{2x} c_{X_M+\mathbf{q}}^\dagger (m_z C_{2x})^{-1} = c_{X_M+\mathbf{q}}^\dagger \begin{pmatrix} 0 & -1 & 0 & 0 \\ -1 & 0 & 0 & 0 \\ 0 & 0 & 0 & i \\ 0 & 0 & -i & 0 \end{pmatrix} s_0 \\ C_{2z} c_{X_M+\mathbf{q}}^\dagger C_{2z}^{-1} &= c_{X_M-\mathbf{q}}^\dagger \begin{pmatrix} 1 & 0 & 0 & 0 \\ 0 & 1 & 0 & 0 \\ 0 & 0 & -1 & 0 \\ 0 & 0 & 0 & -1 \end{pmatrix} s_0 , \quad \mathcal{T} c_{X_M+\mathbf{q}}^\dagger \mathcal{T}^{-1} = c_{X_M-\mathbf{q}}^\dagger \begin{pmatrix} 0 & 1 & 0 & 0 \\ 1 & 0 & 0 & 0 \\ 0 & 0 & 0 & 1 \\ 0 & 0 & 1 & 0 \end{pmatrix} i s_y \\ \mathcal{C} c_{X_M+\mathbf{q}}^\dagger \mathcal{C}^{-1} &= c_{X_M+\mathbf{q}}^\dagger \begin{pmatrix} 1 & 0 & 0 & 0 \\ 0 & -1 & 0 & 0 \\ 0 & 0 & 1 & 0 \\ 0 & 0 & 0 & -1 \end{pmatrix} s_0 , \quad C_{4z} c_{X_M+\mathbf{q}}^\dagger C_{4z}^{-1} = c_{Y_M+C_{4z}\mathbf{q}}^\dagger . \end{aligned} \tag{E35}$$

With the symmetry representations, we can obtain the single-particle part of the Heavy fermion model. The resulting heavy fermion model consists of three parts: the f -mode part which we choose to have zero Hamiltonian, the c -mode part, and the $f - c$ coupling. The c -mode part reads

$$H_c = \sum_{\mathbf{p}} c_{X_M+\mathbf{p}}^\dagger h_{cc}^{X_M}(\mathbf{p}) \otimes s_0 c_{X_M+\mathbf{p}} + C_{4z} \text{ partner} , \tag{E36}$$

where $c_{X_M+\mathbf{p}}^\dagger = (c_{X_M+\mathbf{p},1}^\dagger, c_{X_M+\mathbf{p},2}^\dagger, c_{X_M+\mathbf{p},3}^\dagger, c_{X_M+\mathbf{p},4}^\dagger) \otimes (\uparrow, \downarrow)$,

$$h_{cc}^{X_M}(\mathbf{p}) = \begin{pmatrix} m\sigma_x & i v_2 [(p_x + p_y)\sigma_x + (p_x - p_y)\sigma_y] \\ h.c. & 0_{2 \times 2} \end{pmatrix} \tag{E37}$$

to the linear order of \mathbf{p} , and the C_{4z} partner term stands for the Y_M Hamiltonian:

$$h_{cc}^{Y_M}(\mathbf{p}) = h_{cc}^{X_M}(C_{4z}^{-1}\mathbf{p}) . \tag{E38}$$

The $f - c$ coupling reads

$$H_{fc} = \sum_{\mathbf{p}}^{\Lambda} f_{\mathbf{p}}^{\dagger} h_{fc}^{X_M}(\mathbf{p}) c_{X_M+\mathbf{p}} e^{-\frac{|\mathbf{p}|^2 \lambda^2}{2}} + (C_{4z} \text{ partner}) + h.c. . \quad (\text{E39})$$

where $\lambda = 0.4254a_M$ is square root of the Wannier spread of the f modes with a_M the moiré lattice constant, and

$$h_{fc}^{X_M}(\mathbf{p}) = \begin{pmatrix} i v_1 (p_x \sigma_x + p_y \sigma_y) & \gamma (\sigma_x + \sigma_y) \end{pmatrix} . \quad (\text{E40})$$

From the tight-binding parameters and the Wannier states, we compute $v_1 = -0.52/k_{\theta}$, $\gamma = 0.45$, $m = 0.51$ and $v_2 = 1.53/k_{\theta}$. The heavy fermion model matches the continuum model remarkably well (Fig. 3(d)).

3. Heavy Fermion Model: Interaction

In this part, we show the interaction of the Heavy fermion model. The microscopic Hamiltonian is the following density-density interaction

$$H_{int} = \int d^2 r \int d^2 r' V(\mathbf{r} - \mathbf{r}') : \rho(\mathbf{r}) :: \rho(\mathbf{r}') : , \quad (\text{E41})$$

where

$$\rho(\mathbf{r}) = \sum_{l, \sigma, s} \psi_{\mathbf{r}, l, \sigma, s}^{\dagger} \psi_{\mathbf{r}, l, \sigma, s} , \quad (\text{E42})$$

and $: \rho(\mathbf{r}) := \rho(\mathbf{r}) - \langle G_0 | \rho(\mathbf{r}) | G_0 \rangle$ for certain reference state $|G_0\rangle$. The idea is to project the density-density interaction to the f and c modes. In the following, we will use the general form in Eq. (E41) to do the analytical derivations, and use double-gate screened Coulomb interaction for numerical calculations:

$$V(\mathbf{r}) = \frac{1}{N\Omega} \sum_{\mathbf{p}} e^{-i\mathbf{p} \cdot \mathbf{r}} V(\mathbf{p}) , \quad (\text{E43})$$

where

$$V(\mathbf{p}) = \pi \xi^2 V_{\xi} \frac{\tanh(\xi |\mathbf{p}|/2)}{\xi |\mathbf{p}|/2} , \quad (\text{E44})$$

$\xi = 10/k_{\theta}$ is the distance between two gates, and $V_{\xi} = \frac{e^2}{4\pi\epsilon\xi} = 2$ with e the elementary charge and ϵ the dielectric constant. We will always consider the f and c modes derived from the single-particle parameters in Eq. (E27).

To do the projection, we first consider f and c modes in the real space:

$$f_{\mathbf{R}, \alpha, s}^{\dagger} = \frac{1}{\sqrt{N}} \sum_{\mathbf{k}} e^{-i\mathbf{k} \cdot \mathbf{R}} f_{\mathbf{k}, \alpha, s}^{\dagger} , \quad (\text{E45})$$

and

$$c_{\eta, \mathbf{r}, \beta}^{\dagger} = \frac{1}{\sqrt{V}} \sum_{\mathbf{q}}^{\Lambda} e^{-i(\eta + \mathbf{q}) \cdot \mathbf{r}} c_{\mathbf{k}_0 + \mathbf{q}, \beta}^{\dagger} . \quad (\text{E46})$$

Then, we can approximate $\psi_{\mathbf{r}, l, \sigma, s}^{\dagger}$ as

$$\psi_{\mathbf{r}, l, \sigma, s}^{\dagger} \approx \sum_{\alpha} \sum_{\mathbf{R}} f_{\mathbf{R}, \alpha, s}^{\dagger} e^{i\mathbf{R} \cdot \Delta K_l} w_{\alpha l \sigma}^*(\mathbf{r} - \mathbf{R}) + \sum_{\eta=X, Y} \sum_{\beta} c_{\eta, \mathbf{r}, \beta, s}^{\dagger} g_{c, \eta, \beta, l, \sigma}(\mathbf{r}) , \quad (\text{E47})$$

where

$$g_{c, \eta, \beta, l, \sigma}(\mathbf{r}) = \sum_{\mathbf{Q} \in \mathcal{Q}_l} e^{i\mathbf{Q} \cdot \mathbf{r}} [U_{c, \beta}(\eta)]_{\mathbf{Q} \sigma}^* \quad (\text{E48})$$

with $\eta = X, Y$, and the high energy modes are neglected. Therefore, the density operator can now be expanded into

$$\begin{aligned} \rho(\mathbf{r}) = & \sum_{l\sigma} \psi_{\mathbf{r},l,\sigma}^\dagger \psi_{\mathbf{r},l,\sigma} \approx \sum_{l\sigma} \sum_{\alpha_1\alpha_2} \sum_{\mathbf{R}_1\mathbf{R}_2} f_{\mathbf{R}_1,\alpha_1}^\dagger f_{\mathbf{R}_2,\alpha_2} e^{i(\mathbf{R}_1-\mathbf{R}_2)\cdot\Delta K_l} w_{\alpha_1 l\sigma}^*(\mathbf{r}-\mathbf{R}_1) w_{\alpha_2 l\sigma}(\mathbf{r}-\mathbf{R}_2) \\ & + \left(\sum_{l\sigma} \sum_{\eta_1=X,Y} \sum_{\beta_1} c_{\eta_1,\mathbf{r},\beta_1}^\dagger g_{c,\eta_1,\beta_1,l,\sigma}(\mathbf{r}) \sum_{\alpha_2\mathbf{R}_2} f_{\mathbf{R}_2\alpha_2} e^{-i\mathbf{R}_2\cdot\Delta K_l} w_{\alpha_2 l\sigma}(\mathbf{r}-\mathbf{R}_2) + h.c. \right) \\ & + \sum_{\eta_1=X,Y} \sum_{\beta_1} \sum_{\eta_2=X,Y} \sum_{\beta_2} c_{\eta_1,\mathbf{r},\beta_1}^\dagger c_{\eta_2,\mathbf{r},\beta_2} g_{c,\eta_1,\beta_1,l,\sigma}(\mathbf{r}) g_{c,\eta_2,\beta_2,l,\sigma}^*(\mathbf{r}) . \end{aligned} \quad (\text{E49})$$

With the expression of $\rho(\mathbf{r})$, we can project H_{int} in Eq. (E41) to f and c modes, and split the results into seven parts:

$$H_{int} = \int d^2d^2r' V(\mathbf{r}-\mathbf{r}') : \rho(\mathbf{r}) :: \rho(\mathbf{r}') := \sum_{i=1,\dots,7} H_{int,i} . \quad (\text{E50})$$

In the following, we will specify the form of each of $H_{int,i}$. To do so, we will use the following three functions

$$z(\mathbf{r}-\mathbf{R}_1, \mathbf{r}-\mathbf{R}_2) = \frac{1}{\sqrt{\Omega}N^2} \sum_{\mathbf{k}_1}^{\text{MBZ}} \sum_{\mathbf{p}_2}^{\mathbb{R}^2} e^{-i\mathbf{k}_1\cdot(\mathbf{r}-\mathbf{R}_1)} e^{i\mathbf{p}_2\cdot(\mathbf{r}-\mathbf{R}_2)} \frac{1}{2} \text{Tr} \left[U_f^\dagger(\mathbf{k}_1) U_f(\mathbf{p}_2) \right] , \quad (\text{E51})$$

$$\chi_{\eta_1\beta_1\alpha_2}(\mathbf{r}-\mathbf{R}) = \sum_{l\sigma} g_{c,\eta_1,\beta_1,l,\sigma}(\mathbf{r}) 0 e^{-i\mathbf{R}\cdot\Delta K_l} w_{\alpha_2 l\sigma}(\mathbf{r}-\mathbf{R}) = \frac{1}{N\sqrt{\Omega}} \sum_{\mathbf{p}}^{\mathbb{R}^2} e^{i\mathbf{p}\cdot(\mathbf{r}-\mathbf{R})} U_{c,\beta_1}^\dagger(\eta_1) U_{f,\alpha_2}(\mathbf{p}) , \quad (\text{E52})$$

and

$$y_{\eta_1\beta_1,\eta_2\beta_2}(\mathbf{r}) = \sum_{l\sigma} g_{c,\eta_1,\beta_1,l,\sigma}(\mathbf{r}) g_{c,\eta_2,\beta_2,l,\sigma}^*(\mathbf{r}) = \sum_{\mathbf{G}} e^{i\mathbf{G}\cdot\mathbf{r}} U_{c,\beta_1}^\dagger(\eta_1) U_{c,\beta_2}(\eta_2 + \mathbf{G}) \quad (\text{E53})$$

a. $H_{int,1}$

$$H_{int,1} = \int d^2r d^2r' V(\mathbf{r}-\mathbf{r}') \sum_{\mathbf{R}_1\mathbf{R}_2} : f_{\mathbf{R}_1}^\dagger f_{\mathbf{R}_2} : z(\mathbf{r}-\mathbf{R}_1, \mathbf{r}-\mathbf{R}_2) \sum_{\mathbf{R}_3\mathbf{R}_4} : f_{\mathbf{R}_3}^\dagger f_{\mathbf{R}_4} : z(\mathbf{r}'-\mathbf{R}_4, \mathbf{r}'-\mathbf{R}_4) \quad (\text{E54})$$

Owing to the effective m_z symmetry, we have

$$\begin{aligned} m_z \sum_{\mathbf{R}_1\mathbf{R}_2} f_{\mathbf{R}_1\mathbf{R}_2}^\dagger f_{\mathbf{R}_2} z(\mathbf{r}-\mathbf{R}_1, \mathbf{r}-\mathbf{R}_2) m_z^{-1} &= \sum_{\mathbf{R}_1\mathbf{R}_2} f_{\mathbf{R}_1\mathbf{R}_2}^\dagger f_{\mathbf{R}_2} z(\mathbf{r}-\mathbf{R}_1, \mathbf{r}-\mathbf{R}_2) \\ &\Rightarrow e^{i\mathbf{q}_1\cdot(\mathbf{R}_1-\mathbf{R}_2)} z(\mathbf{r}-\mathbf{R}_1, \mathbf{r}-\mathbf{R}_2) = z(\mathbf{r}-\mathbf{R}_1, \mathbf{r}-\mathbf{R}_2) \\ &\Rightarrow z(\mathbf{r}-\mathbf{R}_1, \mathbf{r}-\mathbf{R}_2) = 0 \text{ for } |\mathbf{R}_1-\mathbf{R}_2| = a_M \\ &\Rightarrow z(\mathbf{r}-\mathbf{R}_1, \mathbf{r}-\mathbf{R}_2) \approx \delta_{\mathbf{R}_1\mathbf{R}_2} n_f(\mathbf{r}-\mathbf{R}_1) , \end{aligned} \quad (\text{E55})$$

where we use the fact that the Wannier functions have a localization length (square root of the Wannier spread) about $0.43a_M$,

$$n_f(\mathbf{r}) = \frac{1}{V} \sum_{\mathbf{p}} e^{-i\mathbf{p}\cdot\mathbf{r}} \tilde{n}_f(\mathbf{p}) , \quad (\text{E56})$$

and

$$\tilde{n}_f(\mathbf{p}) = \frac{1}{2N} \sum_{\mathbf{k}}^{\text{MBZ}} \text{Tr} [U^\dagger(\mathbf{p}+\mathbf{k}) U_f(\mathbf{k})] . \quad (\text{E57})$$

As a result, we have

$$\begin{aligned} H_{int,1} &\approx \sum_{\mathbf{R}\mathbf{R}'} \int d^2r d^2r' V(\mathbf{r} - \mathbf{r}') n_f(\mathbf{r} - \mathbf{R}) n_f(\mathbf{r}' - \mathbf{R}') : \rho_f(\mathbf{R}) :: \rho_f(\mathbf{R}') : \\ &= \sum_{\mathbf{R}\mathbf{R}'} U_f(\mathbf{R} - \mathbf{R}') : \rho_f(\mathbf{R}) :: \rho_f(\mathbf{R}') : , \end{aligned} \quad (\text{E58})$$

where

$$U_f(\mathbf{R} - \mathbf{R}') = \int d^2r d^2r' V(\mathbf{r} - \mathbf{r}') n_f(\mathbf{r} - \mathbf{R}) n_f(\mathbf{r}' - \mathbf{R}') = \frac{1}{N\Omega} \sum_{\mathbf{p}} V(\mathbf{p}) |\tilde{n}_f(\mathbf{p})|^2 e^{-i\mathbf{p} \cdot (\mathbf{R} - \mathbf{R}')} . \quad (\text{E59})$$

Numerically, we have

$$U_f(\mathbf{0}) = 11.27 , \quad U_f(\mathbf{a}_{M,1}) = 2.55 , \quad (\text{E60})$$

and thus $H_{int,1}$ can further be approximated as

$$H_{int,1} \approx H_U = \sum_{\mathbf{R}} U : \rho_f(\mathbf{R}) :: \rho_f(\mathbf{R}) : \quad (\text{E61})$$

with $U = 11.27$.

b. $H_{int,2}$

$$\begin{aligned} H_{int,2} &= \int d^2r d^2r' V(\mathbf{r} - \mathbf{r}') : c_{\mathbf{r}}^\dagger y(\mathbf{r}) c_{\mathbf{r}} :: c_{\mathbf{r}'}^\dagger y(\mathbf{r}') c_{\mathbf{r}'} : \\ &= \frac{1}{\mathcal{V}} \sum_{\mathbf{G}\mathbf{G}'} \sum_{\mathbf{q}_1\mathbf{q}_2\mathbf{q}_3\mathbf{q}_4}^\Lambda \sum_{\eta_1 \dots \eta_4} \sum_{\beta_1 \dots \beta_4} : c_{\eta_1+\mathbf{q}_1, \eta_1}^\dagger c_{\eta_2+\mathbf{q}_2, \beta_2} :: c_{\eta_3+\mathbf{q}_3, \beta_3}^\dagger c_{\eta_4+\mathbf{q}_4, \beta_4} : V(\eta_3 + \mathbf{q}_3 - \eta_4 - \mathbf{q}_4 - \mathbf{G}') \\ &\quad \times U_{c, \beta_1}^\dagger(\eta_1) U_{c, \beta_2}(\eta_2 + \mathbf{G}) U_{c, \beta_3}^\dagger(\eta_3) U_{c, \beta_4}(\eta_4 + \mathbf{G}') \delta(-\eta_1 - \mathbf{q}_1 + \eta_2 + \mathbf{q}_2 + \mathbf{G} - \eta_3 - \mathbf{q}_3 + \eta_4 + \mathbf{q}_4 + \mathbf{G}') \\ &\approx \frac{1}{\mathcal{V}} \sum_{\mathbf{G}\mathbf{G}'} \sum_{\mathbf{q}_1\mathbf{q}_3}^\Lambda \sum_{\eta_1 \dots \eta_4} \sum_{\beta_1 \dots \beta_4} : c_{\eta_1+\mathbf{q}_1, \eta_1}^\dagger c_{\eta_2+\mathbf{q}_1, \beta_2} :: c_{\eta_3+\mathbf{q}_3, \beta_3}^\dagger c_{\eta_4+\mathbf{q}_3, \beta_4} : V(\eta_3 - \eta_4 - \mathbf{G}') \\ &\quad \times U_{c, \beta_1}^\dagger(\eta_1) U_{c, \beta_2}(\eta_2 + \mathbf{G}) U_{c, \beta_3}^\dagger(\eta_3) U_{c, \beta_4}(\eta_4 + \mathbf{G}') \delta(-\eta_1 + \eta_2 + \mathbf{G} - \eta_3 + \eta_4 + \mathbf{G}') \\ &= \frac{1}{N\Omega} \sum_{\mathbf{q}\mathbf{q}'}^\Lambda \sum_{\eta\eta', \beta\beta'} : c_{\eta+\mathbf{q}, \beta}^\dagger c_{\eta+\mathbf{q}, \beta} :: c_{\eta'+\mathbf{q}', \beta'}^\dagger c_{\eta'+\mathbf{q}', \beta'} : V(\mathbf{p} = 0) \\ &\quad + \frac{1}{N\Omega} \sum_{\mathbf{q}\mathbf{q}'}^\Lambda \sum_{\eta\eta'} \sum_{\beta_1\beta-2\beta_3\beta_4} : c_{\eta+\mathbf{q}, \beta_1}^\dagger c_{\eta+\mathbf{q}, \beta_2} :: c_{\eta'+\mathbf{q}', \beta_3}^\dagger c_{\eta'+\mathbf{q}', \beta_4} : V'_{\beta_1\beta_2\beta_3\beta_4}(\eta, \eta') , \end{aligned} \quad (\text{E62})$$

where

$$V'_{\beta_1\beta_2\beta_3\beta_4}(\eta, \eta') = \sum_{\mathbf{G}'} V(\mathbf{G}') U_{c, \beta_1}^\dagger(\eta) U_{c, \beta_2}(\eta + \mathbf{G}') U_{c, \beta_3}^\dagger(\eta') U_{c, \beta_4}(\eta' + \mathbf{G}') . \quad (\text{E63})$$

Numerically, we have $V(\mathbf{p} = 0) = 628.32(1/k_\theta)^2$ and $V'_{\beta_1\beta_2\beta_3\beta_4}(\eta, \eta')$ have dominating values of the same order.

c. $H_{int,3}$

$$H_{int,3} = \int d^2r d^2r' V(\mathbf{r} - \mathbf{r}') \sum_{\mathbf{R}_1\mathbf{R}_2} : f_{\mathbf{R}_1}^\dagger f_{\mathbf{R}_2} : z(\mathbf{r} - \mathbf{R}_1, \mathbf{r} - \mathbf{R}_2) : c_{\mathbf{r}'}^\dagger y(\mathbf{r}') c_{\mathbf{r}'} : + h.c. \quad (\text{E64})$$

$$\begin{aligned}
H_{int,3} &= \int d^2r d^2r' V(\mathbf{r} - \mathbf{r}') \sum_{\mathbf{R}_1 \mathbf{R}_2} : \rho_f(\mathbf{R}) : n_f(\mathbf{r} - \mathbf{R}) : c_{\mathbf{r}'}^\dagger y(\mathbf{r}') c_{\mathbf{r}'} : + h.c. \\
&= \sum_{\mathbf{R}} : \rho_f(\mathbf{R}) : \frac{1}{N\Omega} \sum_{\mathbf{q}_1 \mathbf{q}_2}^\Lambda : c_{\eta_1 + \mathbf{q}_1, \beta_1}^\dagger c_{\eta_2 + \mathbf{q}_2, \beta_2} : \sum_{\mathbf{G}} e^{i(-\eta_1 - \mathbf{q}_1 + \eta_2 + \mathbf{q}_2 + \mathbf{G}) \cdot \mathbf{R}} V(\eta_1 + \mathbf{q}_1 - \eta_2 - \mathbf{q}_2 - \mathbf{G}) \\
&\quad \times \tilde{n}_f(-\eta_1 - \mathbf{q}_1 + \eta_2 + \mathbf{q}_2 + \mathbf{G}) U_{c, \beta_1}^\dagger(\eta_1) U_{c, \beta_2}(\eta_2 + \mathbf{G}) + h.c. \\
&\approx \sum_{\mathbf{R}} : \rho_f(\mathbf{R}) : c_{\eta_1, \mathbf{R}, \beta_1}^\dagger c_{\eta_2, \mathbf{R}, \beta_2} : \sum_{\mathbf{G}} V(\eta_1 - \eta_2 - \mathbf{G}) \tilde{n}_f(-\eta_1 + \eta_2 + \mathbf{G}) U_{c, \beta_1}^\dagger(\eta_1) U_{c, \beta_2}(\eta_2 + \mathbf{G}) + h.c. \\
&= \Omega \sum_{\mathbf{R}} : \rho_f(\mathbf{R}) : c_{\mathbf{R}}^\dagger \tilde{W} c_{\mathbf{R}} : + h.c. ,
\end{aligned} \tag{E65}$$

where

$$\tilde{W}_{\eta_1 \beta_1, \eta_2 \beta_2} = \frac{1}{\Omega} \sum_{\mathbf{G}} V(\eta_1 - \eta_2 - \mathbf{G}) \tilde{n}_f(-\eta_1 + \eta_2 + \mathbf{G}) U_{c, \beta_1}^\dagger(\eta_1) U_{c, \beta_2}(\eta_2 + \mathbf{G}) . \tag{E66}$$

Numerically, we find that

$$\tilde{W}_{\eta_1 \beta_1, \eta_2 \beta_2} \approx W \delta_{\eta_1 \eta_2} \delta_{\beta_1 \beta_2} \tag{E67}$$

with $W = 32$, leading to

$$H_{int,3} \approx \Omega W \sum_{\mathbf{R}} : \rho_f(\mathbf{R}) : c_{\mathbf{R}}^\dagger c_{\mathbf{R}} : + h.c. . \tag{E68}$$

d. $H_{int,4}$

$$\begin{aligned}
H_{int,4} &= \int d^2r d^2r' V(\mathbf{r} - \mathbf{r}') \left\{ \sum_{\mathbf{R}} c_{\mathbf{r}}^\dagger \chi(\mathbf{r} - \mathbf{R}) f_{\mathbf{R}}, \sum_{\mathbf{R}'} f_{\mathbf{R}'}^\dagger \chi^\dagger(\mathbf{r}' - \mathbf{R}') c_{\mathbf{r}'} \right\} \\
&= \sum_{\mathbf{R} \mathbf{R}'} \sum_{\eta_1 \beta_1} \sum_{\alpha_2 \alpha_3} \sum_{\eta_4 \beta_4} \sum_{\mathbf{q}_1 \mathbf{q}_3} \left\{ c_{\eta_1 + \mathbf{q}_1, \beta_1}^\dagger f_{\mathbf{R}, \alpha_2}, f_{\mathbf{R}', \alpha_4}^\dagger c_{\eta_3 + \mathbf{q}_3, \beta_3} \right\} \frac{1}{N\Omega} \int d^2r d^2r' e^{-i(\eta_1 + \mathbf{q}_1) \cdot \mathbf{r}} e^{i(\eta_3 + \mathbf{q}_3) \cdot \mathbf{r}'} V(\mathbf{r} - \mathbf{r}') \\
&\quad \times \chi_{\eta_1 \beta_1, \alpha_2}(\mathbf{r} - \mathbf{R}) \chi_{\eta_3 \beta_3, \alpha_4}^*(\mathbf{r}' - \mathbf{R}')
\end{aligned} \tag{E69}$$

$$\begin{aligned}
&\frac{1}{N\Omega} \int d^2r d^2r' e^{-i(\eta_1 + \mathbf{q}_1) \cdot \mathbf{r}} e^{i(\eta_3 + \mathbf{q}_3) \cdot \mathbf{r}'} V(\mathbf{r} - \mathbf{r}') \chi_{\eta_1 \beta_1, \alpha_2}(\mathbf{r} - \mathbf{R}) \chi_{\eta_3 \beta_3, \alpha_4}^*(\mathbf{r}' - \mathbf{R}') \\
&= \frac{1}{N^2 \Omega} \sum_{\mathbf{p}} e^{-i(\mathbf{q}_1 + \eta_1 + \mathbf{p}) \cdot \mathbf{R}} e^{-i(\mathbf{q}_3 + \eta_3 + \mathbf{p}) \cdot \mathbf{R}'} V(\mathbf{p}) U_{c, \beta_1}^\dagger(\eta_1) U_{f, \alpha_2}(\mathbf{q}_1 + \eta_1 + \mathbf{p}) U_{f, \alpha_4}^\dagger(\mathbf{q}_3 + \eta_3 + \mathbf{p}) U_{c, \beta_3}(\eta_3) \\
&\approx \frac{1}{N^2 \Omega} \sum_{\mathbf{p}} e^{-i(\mathbf{q}_1 + \eta_1 + \mathbf{p}) \cdot \mathbf{R}} e^{+i(\mathbf{q}_3 + \eta_3 + \mathbf{p}) \cdot \mathbf{R}'} V(\mathbf{p}) U_{c, \beta_1}^\dagger(\eta_1) U_{f, \alpha_2}(\eta_1 + \mathbf{p}) U_{f, \alpha_4}^\dagger(\eta_3 + \mathbf{p}) U_{c, \beta_3}(\eta_3) \\
&= \frac{1}{N} e^{-i(\mathbf{q}_1 + \eta_1) \cdot \mathbf{R}} e^{i(\mathbf{q}_3 + \eta_3) \cdot \mathbf{R}'} \tilde{J}_{\eta_1 \beta_1 \alpha_2, \eta_3 \beta_3 \alpha_4}(\mathbf{R} - \mathbf{R}') ,
\end{aligned} \tag{E70}$$

where

$$\tilde{J}_{\eta_1 \beta_1 \alpha_2, \eta_3 \beta_3 \alpha_4}(\mathbf{R} - \mathbf{R}') = \frac{1}{N\Omega} \sum_{\mathbf{p}} e^{-i\mathbf{p} \cdot (\mathbf{R} - \mathbf{R}')} V(\mathbf{p}) U_{c, \beta_1}^\dagger(\eta_1) U_{f, \alpha_2}(\eta_1 + \mathbf{p}) U_{f, \alpha_4}^\dagger(\eta_3 + \mathbf{p}) U_{c, \beta_3}(\eta_3) . \tag{E71}$$

It means that

$$H_{int,4} \approx \sum_{\mathbf{R} \mathbf{R}'} \sum_{\eta_1 \beta_1} \sum_{\alpha_2} \sum_{\eta_3 \beta_3} \sum_{\alpha_4} \left\{ c_{\eta_1, \mathbf{R}, \beta_1}^\dagger f_{\mathbf{R}, \alpha_2}, f_{\mathbf{R}', \alpha_4}^\dagger c_{\eta_3, \mathbf{R}', \beta_3} \right\} \Omega \tilde{J}_{\eta_1 \beta_1 \alpha_2, \eta_3 \beta_3 \alpha_4}(\mathbf{R} - \mathbf{R}') \tag{E72}$$

Numerically, we find that $\tilde{J}_{\eta_1\beta_1\alpha_2,\eta_3\beta_3\alpha_4}(\mathbf{R}-\mathbf{R}') \approx \tilde{J}_{\eta_1\beta_1\alpha_2,\eta_3\beta_3\alpha_4}(0)\delta_{\mathbf{R},\mathbf{R}'} \approx J\delta_{\beta_1\alpha_2}\delta_{\beta_3\alpha_2}\delta_{\alpha_4\alpha_2}\delta_{\mathbf{R},\mathbf{R}'}$ with $J \approx 4.5$. As a result, we have

$$H_{int,4} \approx \Omega J \sum_{\mathbf{R}} \sum_{\eta\eta'} \sum_{\alpha} \left\{ c_{\eta,\mathbf{R},\alpha}^\dagger f_{\mathbf{R},\alpha}, f_{\mathbf{R},\alpha}^\dagger c_{\eta',\mathbf{R},\alpha} \right\}. \quad (\text{E73})$$

e. $H_{int,5}$

$$\begin{aligned} H_{int,5} &= \int d^2r d^2r' V(\mathbf{r}-\mathbf{r}') \sum_{\mathbf{R}} c_{\mathbf{r}}^\dagger \chi(\mathbf{r}-\mathbf{R}) f_{\mathbf{R}} \sum_{\mathbf{R}'} c_{\mathbf{r}'}^\dagger \chi(\mathbf{r}'-\mathbf{R}') f_{\mathbf{R}'} + h.c. \\ &= \sum_{\mathbf{q}_1, \mathbf{q}_3}^\Lambda \sum_{\eta_1\beta_1} \sum_{\alpha_2} \sum_{\eta_3\beta_3} \sum_{\alpha_4} \sum_{\mathbf{R}\mathbf{R}'} c_{\eta_1+\mathbf{q}_1, \beta_1}^\dagger f_{\mathbf{R}, \alpha_2} c_{\eta_3+\mathbf{q}_3, \beta_3}^\dagger f_{\mathbf{R}', \alpha_4} \\ &\quad \times \frac{1}{N\Omega} \int d^2r d^2r' V(\mathbf{r}-\mathbf{r}') e^{-i(\eta_1+\mathbf{q}_1)\cdot\mathbf{r}} e^{-i(\eta_3+\mathbf{q}_3)\cdot\mathbf{r}'} \chi_{\eta_1\beta_1, \alpha_2}(\mathbf{r}-\mathbf{R}) \chi_{\eta_3\beta_3, \alpha_4}(\mathbf{r}'-\mathbf{R}') + h.c., \end{aligned} \quad (\text{E74})$$

where

$$\begin{aligned} &\frac{1}{N\Omega} \int d^2r d^2r' V(\mathbf{r}-\mathbf{r}') e^{-i(\eta_1+\mathbf{q}_1)\cdot\mathbf{r}} e^{-i(\eta_3+\mathbf{q}_3)\cdot\mathbf{r}'} \chi_{\eta_1\beta_1, \alpha_2}(\mathbf{r}-\mathbf{R}) \chi_{\eta_3\beta_3, \alpha_4}(\mathbf{r}'-\mathbf{R}') \\ &= \frac{1}{N^2\Omega} \sum_{\mathbf{p}} e^{-i(\mathbf{p}+\eta_1+\mathbf{q}_1)\cdot\mathbf{R}} e^{-i(-\mathbf{p}+\eta_3+\mathbf{q}_3)\cdot\mathbf{R}'} V(\mathbf{p}) U_{c, \beta_1}^\dagger(\eta_1) U_{f, \alpha_2}(\mathbf{p}+\eta_1+\mathbf{q}_1) U_{c, \beta_3}^\dagger(\eta_3) U_{f, \alpha_4}(-\mathbf{p}+\eta_3+\mathbf{q}_3) \\ &\approx \frac{1}{N\Omega} e^{-i(\eta_1+\mathbf{q}_1)\cdot\mathbf{R}} e^{-i(\eta_3+\mathbf{q}_3)\cdot\mathbf{R}'} \Omega \tilde{J}'_{\eta_1\beta_1\alpha_2, \eta_3\beta_3\alpha_4}(\mathbf{R}-\mathbf{R}'), \end{aligned} \quad (\text{E75})$$

and

$$\tilde{J}'_{\eta_1\beta_1\alpha_2, \eta_3\beta_3\alpha_4}(\mathbf{R}-\mathbf{R}') = \frac{1}{N\Omega} \sum_{\mathbf{p}} e^{-i\mathbf{p}\cdot(\mathbf{R}-\mathbf{R}')} V(\mathbf{p}) U_{c, \beta_1}^\dagger(\eta_1) U_{f, \alpha_2}(\mathbf{p}+\eta_1) U_{c, \beta_3}^\dagger(\eta_3) U_{f, \alpha_4}(-\mathbf{p}+\eta_3). \quad (\text{E76})$$

As a result, we have

$$H_{int,5} \approx \sum_{\eta_1\beta_1} \sum_{\eta_3\beta_3} \sum_{\alpha_2\alpha_4} \sum_{\mathbf{R}\mathbf{R}'} c_{\eta_1, \mathbf{R}, \beta_1}^\dagger f_{\mathbf{R}, \alpha_2} c_{\eta_3, \mathbf{R}', \beta_3}^\dagger f_{\mathbf{R}', \alpha_4} \Omega \tilde{J}'_{\eta_1\beta_1\alpha_2, \eta_3\beta_3\alpha_4}(\mathbf{R}-\mathbf{R}') + h.c. \quad (\text{E77})$$

Owing to the TR symmetry,

$$\tilde{J}'_{\eta_1\beta_1\alpha_2, \eta_3\beta_3\alpha_4}(\mathbf{R}-\mathbf{R}') = \sum_{\beta'_3 a'_4} \begin{pmatrix} 1 & & \\ & 1 & \\ & & 1 \end{pmatrix}_{\beta'_3 a'_4} \begin{pmatrix} & 1 \\ 1 & \\ & & 1 \end{pmatrix}_{a'_4 a_4} \tilde{J}_{\eta_1\beta_1\alpha_2, \eta_3\beta_3\alpha'_4}(\mathbf{R}-\mathbf{R}'), \quad (\text{E78})$$

where $\tilde{J}_{\eta_1\beta_1\alpha_2, \eta_3\beta_3\alpha'_4}(\mathbf{R}-\mathbf{R}')$ is in Eq. (E71). Therefore, we numerically have

$$H_{int,5} \approx \Omega J \sum_{\eta\eta'} \sum_{\mathbf{R}\bar{\alpha}} c_{\eta, \mathbf{R}, \alpha}^\dagger f_{\mathbf{R}, \alpha} c_{\eta', \mathbf{R}, \bar{\alpha}}^\dagger f_{\mathbf{R}, \bar{\alpha}} + h.c. \quad (\text{E79})$$

with $J \approx 4.5$ and $\bar{\alpha} = 2, 1$ for $\alpha = 1, 2$.

$f. \quad H_{int,6}$

$$\begin{aligned}
H_{int,6} &= \int d^2r d^2r' V(\mathbf{r} - \mathbf{r}') \left\{ \sum_{\mathbf{R}_1 \mathbf{R}_2} : f_{\mathbf{R}_1}^\dagger f_{\mathbf{R}_2} : z(\mathbf{r} - \mathbf{R}_1, \mathbf{r} - \mathbf{R}_2) , \sum_{\mathbf{R}'} : c_{\mathbf{r}'}^\dagger \chi(\mathbf{r}' - \mathbf{R}') f_{\mathbf{R}'} : \right\} + h.c. \\
&\approx \int d^2r d^2r' V(\mathbf{r} - \mathbf{r}') \sum_{\mathbf{R} \mathbf{R}'} \left\{ : \rho_f(\mathbf{R}) : n_f(\mathbf{r} - \mathbf{R}) , : c_{\mathbf{r}'}^\dagger \chi(\mathbf{r}' - \mathbf{R}') f_{\mathbf{R}'} : \right\} + h.c. \\
&= \sum_{\mathbf{R} \mathbf{R}'} \sum_{\eta' \beta' \alpha'} \sum_{\mathbf{q}'}^\Omega \left\{ : \rho_f(\mathbf{R}) : , : c_{\eta' + \mathbf{q}', \beta'}^\dagger f_{\mathbf{R}', \alpha'} : \right\} \\
&\quad \times \frac{1}{\sqrt{N\Omega}} \int d^2r d^2r' V(\mathbf{r} - \mathbf{r}') e^{-i(\eta' + \mathbf{q}') \cdot \mathbf{r}'} n_f(\mathbf{r} - \mathbf{R}) \chi_{\eta' \beta', \alpha'} \chi(\mathbf{r}' - \mathbf{R}') + h.c. ,
\end{aligned} \tag{E80}$$

where

$$\begin{aligned}
&\frac{1}{\sqrt{N\Omega}} \int d^2r d^2r' V(\mathbf{r} - \mathbf{r}') e^{-i(\eta' + \mathbf{q}') \cdot \mathbf{r}'} n_f(\mathbf{r} - \mathbf{R}) \chi_{\eta' \beta', \alpha'} \chi(\mathbf{r}' - \mathbf{R}') \\
&= \frac{1}{\sqrt{N}} e^{-i(\eta' + \mathbf{q}') \cdot \mathbf{R}'} \frac{1}{\mathcal{N}\Omega} \sum_{\mathbf{p}} e^{-i\mathbf{p} \cdot (\mathbf{R} - \mathbf{R}')} V(\mathbf{p}) \tilde{n}(-\mathbf{p}) U_{c, \beta'}^\dagger(\eta') U_{f, \alpha'}(-\mathbf{p} + \eta') \\
&= \frac{1}{\sqrt{N}} e^{-i(\eta' + \mathbf{q}') \cdot \mathbf{R}'} \tilde{K}'_{\eta' \beta' \alpha'}(\mathbf{R} - \mathbf{R}') ,
\end{aligned} \tag{E81}$$

and

$$\tilde{K}'_{\eta' \beta' \alpha'}(\mathbf{R} - \mathbf{R}') = \frac{1}{\mathcal{N}\Omega} \sum_{\mathbf{p}} e^{-i\mathbf{p} \cdot (\mathbf{R} - \mathbf{R}')} V(\mathbf{p}) \tilde{n}(\mathbf{p}) U_{c, \beta'}^\dagger(\eta') U_{f, \alpha'}(\mathbf{p} + \eta') . \tag{E82}$$

Thus, we obtain

$$H_{int,6} \approx \sum_{\mathbf{R} \mathbf{R}'} \sum_{\eta' \beta' \alpha'} \left\{ : \rho_f(\mathbf{R}) : , : c_{\eta', \mathbf{R}', \beta'}^\dagger f_{\mathbf{R}', \alpha'} : \right\} \sqrt{\Omega} \tilde{K}'_{\eta' \beta' \alpha'}(\mathbf{R} - \mathbf{R}') + h.c. . \tag{E83}$$

$\tilde{K}'_{\eta' \beta' \alpha'}(\mathbf{R} - \mathbf{R}') \approx \tilde{K}'_{\eta' \beta' \alpha'}(0) \delta_{\mathbf{R}, \mathbf{R}'}$, which has dominating values around 0.001 and thus is negligible.

$g. \quad H_{int,7}$

$$\begin{aligned}
H_{int,7} &= \int d^2r d^2r' V(\mathbf{r} - \mathbf{r}') \left\{ \sum_{\mathbf{R}} c_{\mathbf{r}}^\dagger \chi(\mathbf{r} - \mathbf{R}) f_{\mathbf{R}} , : c_{\mathbf{r}'}^\dagger y(\mathbf{r}') c_{\mathbf{r}'} : \right\} + h.c. \\
&= \frac{1}{\Omega \sqrt{N^3}} \sum_{\mathbf{q} \mathbf{q}_1' \mathbf{q}_2'}^\Lambda \sum_{\eta \beta \alpha} \sum_{\eta_1' \beta_1' \eta_2' \beta_2'} \left\{ \sum_{\mathbf{R}} c_{\eta + \mathbf{q}, \beta}^\dagger f_{\mathbf{R}, \alpha} , : c_{\eta_1' + \mathbf{q}_1', \beta_1'}^\dagger c_{\eta_2' + \mathbf{q}_2', \beta_2'} : \right\} \sum_{\mathbf{G}'} e^{-i(\eta_1' + \mathbf{q}_1' - \eta_2' - \mathbf{q}_2' - \mathbf{G}' - \eta - \mathbf{q}) \cdot \mathbf{R}} \\
&\quad \times V(\eta_1' + \mathbf{q}_1' - \eta_2' - \mathbf{q}_2' - \mathbf{G}') U_{c, \beta}^\dagger(\eta) U_{f, \alpha}(\eta + \mathbf{q} + \eta_1' + \mathbf{q}_1' - \eta_2' - \mathbf{q}_2' - \mathbf{G}') U_{c, \beta_1'}^\dagger(\eta_1') U_{c, \beta_2'}(\eta_2' + \mathbf{G}') + h.c. \\
&\approx \Omega^{3/2} \sum_{\eta \beta \alpha} \sum_{\eta_1' \beta_1' \eta_2' \beta_2'} \left\{ \sum_{\mathbf{R}} c_{\eta, \mathbf{R}, \beta}^\dagger f_{\mathbf{R}, \alpha} , : c_{\eta_1', \mathbf{R}, \beta_1'}^\dagger c_{\eta_2', \mathbf{R}, \beta_2'} : \right\} \tilde{K}_{\eta \beta \alpha, \eta_1' \beta_1' \eta_2' \beta_2'} ,
\end{aligned} \tag{E84}$$

where

$$\tilde{K}_{\eta \beta \alpha, \eta_1' \beta_1' \eta_2' \beta_2'} = \frac{1}{\Omega} \sum_{\mathbf{G}'} V(\eta_1' - \eta_2' - \mathbf{G}') U_{c, \beta}^\dagger(\eta) U_{f, \alpha}(\eta + \eta_1' - \eta_2' - \mathbf{G}') U_{c, \beta_1'}^\dagger(\eta_1') U_{c, \beta_2'}(\eta_2' + \mathbf{G}') . \tag{E85}$$

We find that

$$\begin{aligned}\tilde{K}_{\eta\beta\alpha,\eta'_1\beta'_1\eta'_2\beta'_2} &= \delta_{\eta'_1\eta}\delta_{\eta'_2\bar{\eta}}\tilde{K}_{\eta\beta\alpha,\eta\beta'_1\bar{\eta}\beta'_2} + \delta_{\eta'_1\bar{\eta}}\delta_{\eta'_2\eta}\tilde{K}_{\eta\beta\alpha,\bar{\eta}\beta'_1\eta\beta'_2} \\ \tilde{K}_{\eta\beta\alpha,\eta\beta'_1\bar{\eta}\beta'_2} &= \tilde{K}_{\bar{\eta}\beta\alpha,\bar{\eta}\beta'_1\eta\beta'_2} \\ \tilde{K}_{K\beta\alpha,K\beta'_1K'\beta'_2} &= -\tilde{K}_{K'\beta\alpha,K'\beta'_1K\beta'_2}^*,\end{aligned}\quad (\text{E86})$$

and we numerically find

$$\tilde{K}_{K\beta\alpha,K\beta'_1K'\beta'_2} = \delta_{\beta\alpha}\delta_{\beta'_1\alpha}\delta_{\beta'_2,\alpha+2}[\text{Re}(K) + (-1)^{a-1}i\text{Im}(K)] + \delta_{\beta\alpha}\delta_{\beta'_1,5-\alpha}\delta_{\beta'_2,3-\alpha}[-\text{Re}(K) + (-1)^{a-1}i\text{Im}(K)] , \quad (\text{E87})$$

where

$$K \approx -2.7 + 2.7i . \quad (\text{E88})$$

h. Summary of The Interaction

In sum, the total interaction reads

$$H_{int} \approx H_U + H_V + H_W + H_J + H_K , \quad (\text{E89})$$

where

$$H_U = \sum_{\mathbf{R}} U : \rho_f(\mathbf{R}) :: \rho_f(\mathbf{R}) : \quad (\text{E90})$$

with $U = 11.27$,

$$\begin{aligned}H_V &= \frac{1}{N\Omega} \sum_{\mathbf{q}\mathbf{q}'}^{\Lambda} \sum_{\eta\eta',\beta\beta'} : c_{\eta+\mathbf{q},\beta}^{\dagger} c_{\eta+\mathbf{q},\beta} :: c_{\eta'+\mathbf{q}',\beta'}^{\dagger} c_{\eta'+\mathbf{q}',\beta'} : V(\mathbf{p}=0) \\ &+ \frac{1}{N\Omega} \sum_{\mathbf{q}\mathbf{q}'}^{\Lambda} \sum_{\eta\eta'} \sum_{\beta_1\beta-2\beta_3\beta_4} : c_{\eta+\mathbf{q},\beta_1}^{\dagger} c_{\eta+\mathbf{q},\beta_2} :: c_{\eta'+\mathbf{q}',\beta_3}^{\dagger} c_{\eta'+\mathbf{q}',\beta_4} : V'_{\beta_1\beta_2\beta_3\beta_4}(\eta,\eta') ,\end{aligned}\quad (\text{E91})$$

$$H_W = \Omega W \sum_{\mathbf{R}} : \rho_f(\mathbf{R}) :: c_{\mathbf{R}}^{\dagger} c_{\mathbf{R}} : + h.c. \quad (\text{E92})$$

with $W = 32$,

$$H_J = \Omega J \sum_{\mathbf{R}} \sum_{\eta\eta'} \sum_{\alpha} \left[\left\{ c_{\eta,\mathbf{R},\alpha}^{\dagger} f_{\mathbf{R},\alpha}, f_{\mathbf{R},\alpha}^{\dagger} c_{\eta',\mathbf{R},\alpha} \right\} + (c_{\eta,\mathbf{R},\alpha}^{\dagger} f_{\mathbf{R},\alpha} c_{\eta',\mathbf{R},\bar{\alpha}}^{\dagger} f_{\mathbf{R},\bar{\alpha}} + h.c.) \right] \quad (\text{E93})$$

with $J = 4.5$ and $\bar{\alpha} = 2, 1$ for $\alpha = 1, 2$, and

$$H_K = \Omega^{3/2} \sum_{\eta\beta\alpha} \sum_{\eta'_1\beta'_1\eta'_2\beta'_2} \left\{ \sum_{\mathbf{R}} c_{\eta,\mathbf{R},\beta}^{\dagger} f_{\mathbf{R},\alpha}, : c_{\eta'_1,\mathbf{R},\beta'_1}^{\dagger} c_{\eta'_2,\mathbf{R},\beta'_2} : \right\} \tilde{K}_{\eta\beta\alpha,\eta'_1\beta'_1\eta'_2\beta'_2} \quad (\text{E94})$$

with the expression of $\tilde{K}_{\eta\beta\alpha,\eta'_1\beta'_1\eta'_2\beta'_2}$ in Eq. (E86).

4. Alternative Convention

There is an alternative convention where where m_z and C_{2x} do not have momentum shifts as Eq.(E32). It is achieved by doubling the unit cell, and we will discuss it in this subsection for completeness. Define

$$\psi_{\pm,\mathbf{r}}^{\dagger} = \frac{1}{\sqrt{2}} \left(\psi_{t,\mathbf{r}}^{\dagger} \pm \psi_{b,\mathbf{r}}^{\dagger} \right) . \quad (\text{E95})$$

Then, the Hamiltonian reads

$$H = \sum_{\alpha=\pm} H_{\alpha} , \quad (\text{E96})$$

with

$$H_{\alpha} = \int d^2r \psi_{\alpha,\mathbf{r}}^{\dagger} [-t\partial_x\partial_y\tau_x - t'(\partial_x^2 - \partial_y^2)\tau_y + \alpha W(\mathbf{r})] \psi_{\alpha,\mathbf{r}} , \quad (\text{E97})$$

and the symmetry operations read

$$\begin{aligned} C_{4z}\psi_{\alpha,\mathbf{r}}^{\dagger}C_{4z}^{-1} &= \psi_{\alpha,C_{4z}\mathbf{r}}^{\dagger}(-i\tau_z) \\ C_{2x}\psi_{\alpha,\mathbf{r}}^{\dagger}C_{2x}^{-1} &= \psi_{\alpha,C_{2x}\mathbf{r}}^{\dagger}(\alpha\tau_y) \\ \mathcal{T}\psi_{\alpha,\mathbf{r}}^{\dagger}\mathcal{T}^{-1} &= \psi_{\alpha,\mathbf{r}}^{\dagger}(i\tau_x) \\ T_{\mathbf{R}'_M}\psi_{\alpha,\mathbf{r}}^{\dagger}T_{\mathbf{R}'_M}^{-1} &= e^{-i\mathbf{M}_-\cdot\mathbf{R}'_M}\psi_{\mathbf{r}+\mathbf{R}'_M,\alpha}^{\dagger} \\ T_{\mathbf{a}_{M,1}}\psi_{\alpha,\mathbf{r}}^{\dagger}T_{\mathbf{a}_{M,1}}^{-1} &= -e^{-i\mathbf{M}_-\cdot\mathbf{a}_{M,1}}\psi_{-\alpha,\mathbf{r}+\mathbf{a}_{M,1}}^{\dagger} \\ m_z\psi_{\alpha,\mathbf{r}}^{\dagger}m_z^{-1} &= \psi_{\alpha,\mathbf{r}}^{\dagger}\alpha \end{aligned} \quad (\text{E98})$$

where $\mathbf{R}'_M = \begin{pmatrix} \mathbf{a}'_{M,1} & \mathbf{a}'_{M,2} \end{pmatrix} \mathbb{Z}^2$ with $\mathbf{a}'_{M,1} = \mathbf{a}_{M,1} + \mathbf{a}_{M,2}$ and $\mathbf{a}'_{M,2} = -\mathbf{a}_{M,1} + \mathbf{a}_{M,2}$. The new $\mathbf{a}'_{M,1}$ and $\mathbf{a}'_{M,2}$ show that the unit cell is doubled.

By defining

$$\begin{aligned} \mathbf{b}'_{M,1} &= \mathbf{q}_1 \\ \mathbf{b}'_{M,2} &= \mathbf{q}_2 \\ \mathbf{G}'_M &= \begin{pmatrix} \mathbf{b}'_{M,1} & \mathbf{b}'_{M,2} \end{pmatrix} \mathbb{Z}^2 , \end{aligned} \quad (\text{E99})$$

we have

$$\begin{aligned} C_{4z}\psi_{\alpha,\mathbf{k}-\mathbf{G}'_M}^{\dagger}C_{4z}^{-1} &= \psi_{\alpha,C_{4z}\mathbf{k}-C_{4z}\mathbf{G}'_M}^{\dagger}(-i\tau_z) \\ C_{2x}\psi_{\alpha,\mathbf{k}-\mathbf{G}'_M}^{\dagger}C_{2x}^{-1} &= \psi_{\alpha,C_{2x}\mathbf{k}-C_{2x}\mathbf{G}'_M}^{\dagger}(\alpha\tau_y) \\ \mathcal{T}\psi_{\alpha,\mathbf{k}-\mathbf{G}'_M}^{\dagger}\mathcal{T}^{-1} &= \psi_{\alpha,-\mathbf{k}+\mathbf{G}'_M}^{\dagger}(i\tau_x) \\ m_z\psi_{\alpha,\mathbf{k}-\mathbf{G}'_M}^{\dagger}m_z^{-1} &= \alpha\psi_{\alpha,\mathbf{k}-\mathbf{G}'_M}^{\dagger} . \end{aligned} \quad (\text{E100})$$

This convention shows that the twisted Checkerboard model can be treated as two copies of Ref. [21].

Appendix F: Lieb Lattice and Analytical Wannier States from the Instanton Action

The Lieb lattice is built on the $1b = (1/2, 1/2)$ and $2c = (1/2, 0), (0, 1/2)$ positions. The real space model with nearest neighbor hoppings is

$$H = t \sum_{\mathbf{R}} \left(c_{\mathbf{R},b}^{\dagger} (c_{\mathbf{R},c_1}^{\dagger} + c_{\mathbf{R}+\hat{x},c_1}^{\dagger} + c_{\mathbf{R},c_2}^{\dagger} + c_{\mathbf{R}+\hat{y},c_2}^{\dagger}) \right) + h.c. . \quad (\text{F1})$$

It forms an S -matrix model in the order basis b, c_1, c_2 with

$$h(\mathbf{k}) = 2t \begin{pmatrix} \cos k_y/2 & \cos k_x/2 \\ \cos k_y/2 & \\ \cos k_x/2 & \end{pmatrix} \quad (\text{F2})$$

which has chiral symmetry $S = \text{diag}(1, -1, -1)$, $C_{4z} = 1 \oplus \sigma_1$, and $\mathcal{T} = K$. This Hamiltonian is very simple, and its spectrum can be obtained analytically:

$$E_n = 0, \pm t \sqrt{4 + 2(\cos k_x + \cos k_y)} \quad (\text{F3})$$

with eigenvectors

$$\begin{aligned} U_0(\mathbf{k}) &= (0, -\cos \frac{k_x}{2}, \cos \frac{k_y}{2})^T / \sqrt{\cos^2 \frac{k_x}{2} + \cos^2 \frac{k_y}{2}} \\ U_{\pm 1}(\mathbf{k}) &= (\pm \frac{1}{\sqrt{2}}, \frac{\cos k_y/2}{\sqrt{2 + \cos k_x + \cos k_y}}, \frac{\cos k_x/2}{\sqrt{2 + \cos k_x + \cos k_y}})^T. \end{aligned} \quad (\text{F4})$$

Symmetries play a crucial role in identifying the heavy fermion wavefunction. We will use the language of topological quantum chemistry [72] (see Ref. [285] for a pedagogical review with an emphasis on group theory, or [286] for a brief introduction to the formalism in tight-binding models). The momentum space representations of the atomic basis in the space group $G = p41'$ (number 75 in the BNS notation) are written

$$\begin{aligned} L' : \quad & A_{1b} \uparrow G = \Gamma_1 + X_2 + M_2 \\ L : \quad & A_{2c} \uparrow G = \Gamma_1 \oplus \Gamma_2 + X_1 \oplus X_2 + M_3 M_4 \end{aligned} \quad (\text{F5})$$

where L is the larger sublattice consisting of s orbitals at the $2c = (1/2, 0), (0, 1/2)$ position, and L' is the smaller sublattice consisting of an s orbital at the $1b = (1/2, 1/2)$ position. These real space orbitals induce the momentum space irreps Eq. (F5) where Γ, X, M denote the high-symmetry momenta with little group $41', 2$, and $41'$ respectively. Their character tables are

$$\begin{array}{c|ccc} & 1 & C_4 & C_2 & C_4^3 \\ \hline \Gamma_1, M_1 & 1 & 1 & 1 & 1 \\ \Gamma_2, M_2 & 1 & -1 & 1 & -1 \\ \Gamma_3 \Gamma_4, M_3 M_4 & 2 & 0 & -2 & 0 \end{array}, \quad \begin{array}{c|cc} & 1 & C_2 \\ \hline X_1 & 1 & 1 \\ X_2 & 1 & -1 \end{array}. \quad (\text{F6})$$

As discussed in the Main Text, the Γ and X irreps uniquely restrict any possible Wannier state to transform in a single irrep. For completeness, we enumerate all atomic limits in $p41'$. They are

$$\begin{aligned} A_{1a} &= \Gamma_1 + X_1 + M_1, & B_{1a} &= \Gamma_2 + X_1 + M_2, & {}^1E^2 E_{1a} &= \Gamma_3 \Gamma_4 + X_2 + M_3 M_4 \\ A_{1b} &= \Gamma_1 + X_2 + M_2, & B_{1b} &= \Gamma_2 + X_2 + M_1, & {}^1E^2 E_{1b} &= \Gamma_3 \Gamma_4 + X_1 + M_3 M_4 \\ A_{2c} &= \Gamma_1 \oplus \Gamma_2 + X_1 \oplus X_2 + M_3 M_4, & B_{2c} &= \Gamma_3 \Gamma_4 + X_1 \oplus X_2 + M_1 M_2. \end{aligned} \quad (\text{F7})$$

Since the Wannier state must carry the Γ_2, X_1 irreps of the flat band, only the B_{1a} irrep is possible as one can see above. Thus our ansatz for the HF wannier state is the following

$$U_f(\mathbf{k}) = U_0(\mathbf{k}) \cos \theta(\mathbf{k}) + \begin{pmatrix} 1 \\ 0 \\ 0 \end{pmatrix} \sin \theta(\mathbf{k}) = U(\mathbf{k}) \begin{pmatrix} -\frac{1}{\sqrt{2}} \sin \theta \\ \cos \theta \\ \frac{1}{\sqrt{2}} \sin \theta \end{pmatrix} \quad (\text{F8})$$

where $U(\mathbf{k})$ is the 3×3 eigenvector matrix whose columns are $U_{-1}(\mathbf{k}), U_0(\mathbf{k}), U_{+1}(\mathbf{k})$. Since the f -mode wavefunction $U_f(\mathbf{k})$ of the Wannier state must occupy the M_2 irrep at M and then transition into the flat band, we expect $\theta \rightarrow \pi/2$ at $\mathbf{k} = M$ with decay to $\theta = 0$ away from M . The functional form of $\theta(\mathbf{k})$ can now be determined.

We now compute the Wannier spread of $U_f(\mathbf{k})$. Since $U_f(\mathbf{k})$ is $C_2\mathcal{T}$ -symmetric and $D[C_2\mathcal{T}] = K$, we can choose $U_f(\mathbf{k})$ to be real so its Berry connection vanishes, and thus the Wannier spread is the single integral

$$\frac{1}{2} \langle r^2 \rangle = \int \frac{d^2 k}{(2\pi)^2} \frac{1}{2} \partial_i U_f^\dagger \partial_i U_f = \int \frac{d^2 k}{(2\pi)^2} \left(\frac{1}{2} (\nabla \theta)^2 + \frac{1}{2} g(\mathbf{k}) \cos^2 \theta \right), \quad g(\mathbf{k}) = (\partial U_0)^2 = \frac{1 - \cos k_x \cos k_y}{2(2 + \cos k_x + \cos k_y)^2} \geq 0. \quad (\text{F9})$$

Here $g(\mathbf{k})$ is the Fubini-Study quantum metric. In general, $g(\mathbf{k})$ is given by the equivalent expressions

$$g(\mathbf{k}) = \frac{1}{2} \text{Tr} \partial_i P(\mathbf{k}) \partial_i P(\mathbf{k}) = \partial_i U^\dagger \partial_i U + U^\dagger \partial_i U U^\dagger \partial_i U \quad (\text{F10})$$

where $P = U U^\dagger$, and here we have used $U^\dagger \partial_i U = 0$ since U is real.

The key observation is that minimization of $\langle r^2 \rangle$ (the maximal localization condition of the Wannier function) can be phrased as an Euler-Lagrange problem. To make the problem analytically tractable, we focus near $\mathbf{k} = M$

where $\theta \sim \pi/2$ and $g(M + \mathbf{k}) \sim \frac{1}{|\mathbf{k}|^2}$. We fix a cutoff Λ (the Wannier disentanglement window) and impose Dirichlet boundary conditions $\theta(\mathbf{k} + M) = 0$ for $|\mathbf{k}| = \Lambda$. The rotational symmetry emerges naturally in the low energy limit around M . Thus we have

$$\frac{1}{2} \langle r^2 \rangle = S + \int_{\mathbf{k}: |\mathbf{k}-M| \geq \Lambda} \frac{d^2 k}{(2\pi)^2} \frac{1}{2} g(\mathbf{k}) \quad (\text{F11})$$

where S is the action

$$S = \int_{\Lambda} \frac{d^2 k}{(2\pi)^2} \left(\frac{1}{2} (\nabla \theta)^2 + \frac{1}{2|\mathbf{k}|^2} \cos^2 \theta \right). \quad (\text{F12})$$

Note that $(\nabla \theta)^2 = (\partial_{|\mathbf{k}|} \theta)^2 + \frac{1}{|\mathbf{k}|^2} (\partial_{\phi} \theta)^2$ in polar coordinates, so the minimum is achieved when $\partial_{\phi} \theta = 0$ (the s -wave circular harmonic). Thus we can assume $\theta(\mathbf{k}) = \theta(|\mathbf{k}|)$. Since the Lagrangian is scale-invariant, we are motivated to change variables to $|\mathbf{k}| = e^t$ so that $|\mathbf{k}| = 0$ maps to $t = -\infty$. We find

$$\begin{aligned} S &= \int \frac{e^{2t} dt}{(2\pi)^2} \left(\frac{1}{2} (e^{-t} \dot{\theta})^2 + \frac{1}{2e^{2t}} \cos^2 \theta \right) \\ &= \int \frac{dt}{(2\pi)^2} \left(\frac{1}{2} \dot{\theta}^2 + \frac{1}{2} \cos^2 \theta \right) \end{aligned} \quad (\text{F13})$$

which is just the Lagrangian of a particle in the periodic potential $-\frac{1}{2} \cos^2 \theta$. At time $t = -\infty$, we must have $\cos \theta = 0$, which is at the top of the potential. We can now use known techniques from the theory of instantons to reduce the second order Euler-Lagrange equations to a first order differential equation which is immediately integrable. First we observe

$$\begin{aligned} S &= \frac{1}{2} \int \frac{dt}{(2\pi)^2} \left(\dot{\theta}^2 + \cos^2 \theta \right) = \frac{1}{2} \int \frac{dt}{(2\pi)^2} \left(\dot{\theta} \pm \cos \theta \right)^2 \mp \int \frac{dt}{(2\pi)^2} \dot{\theta} \cos \theta \\ &= \frac{1}{2} \int \frac{dt}{(2\pi)^2} \left(\dot{\theta} \pm \cos \theta \right)^2 \mp \int \frac{d\theta}{(2\pi)^2} \cos \theta. \end{aligned} \quad (\text{F14})$$

The θ integral we can perform since we know θ interpolates from $\pi/2$ at M to 0 on the boundary. Thus we have

$$\begin{aligned} S &= \frac{1}{2} \int \frac{dt}{(2\pi)^2} \left(\dot{\theta} + \cos \theta \right)^2 - \int_{\pi/2}^0 \frac{d\theta}{(2\pi)^2} \cos \theta \\ &= \frac{1}{2} \int \frac{dt}{(2\pi)^2} \left(\dot{\theta} + \cos \theta \right)^2 + \frac{1}{(2\pi)^2} \end{aligned} \quad (\text{F15})$$

which shows the action is lower-bounded. This lower bound can be reached by taking

$$\dot{\theta} = -\cos \theta \quad (\text{F16})$$

which can be directly integrated to find

$$\theta(t) = -2 \arctan \left(\tanh \frac{t - t_0}{2} \right) \quad (\text{F17})$$

where t_0 is the only undetermined constant. Note that this instanton solution obeys

$$\begin{aligned} \lim_{t \rightarrow -\infty} \theta(t) &= -2 \arctan(-1) = \frac{\pi}{2} \\ \lim_{t \rightarrow t_0} \theta(t) &= -2 \arctan 0 = 0 \end{aligned} \quad (\text{F18})$$

so for any value of the cutoff $\Lambda = e^{t_0}$, we can produce a function that strictly minimizes the action. In terms of the original variables, we find

$$\theta = -2 \arctan \frac{|k|/\Lambda - 1}{|k|/\Lambda + 1}, \quad \cos \theta = \frac{2|k|/\Lambda}{(|k|/\Lambda)^2 + 1} \quad (\text{F19})$$

where $M + \mathbf{k} = |k|(\cos \phi, \sin \phi)$.

Note that $\cos \theta \sim |k|$ is not smooth in \mathbf{k} . However, the flat band wavefunction is also not smooth, and obeys $U_0(M + \mathbf{k}) \rightarrow (0, \cos \theta, -\sin \phi)$. Thus we see that

$$U_f(\mathbf{k}) = U_0(\mathbf{k}) \cos \theta(\mathbf{k}) + \begin{pmatrix} 1 \\ 0 \\ 0 \end{pmatrix} \sin \theta(\mathbf{k}) \quad (\text{F20})$$

which approaches $(1, |k| \cos \phi, |k| \sin \phi)$ with $M + \mathbf{k} = |k|(\cos \phi, \sin \phi)$ as $|k| \rightarrow 0$. We see that the wavefunction is smoothed at M through the instanton profile, and hence can give a localized Wannier function.

1. Conduction electrons and Hamiltonian

We will now determine the conduction electron wavefunctions by requiring smoothness and orthogonality with the HF fermion wavefunction $U_f(\mathbf{k})$. Recall from Eq. (F8) that $U_f(\mathbf{k}) = U(\mathbf{k})\Omega_f(\theta(\mathbf{k}))$ where $\Omega_f(\theta) = (-\frac{1}{\sqrt{2}} \sin \theta, \cos \theta, \frac{1}{\sqrt{2}} \sin \theta)$ is the transformation from the band basis (ordered 1, 0, -1) to the f -mode wavefunction. $\Omega_f(\theta)$ is one column of the full unitary matrix transforming the band basis to the c - f basis. The two vectors $\Omega_1 = (1, 0, 1)^T/\sqrt{2}$, $\Omega_2 = (\cos \theta, -\sqrt{2} \sin \theta, -\cos \theta)^T/\sqrt{2}$ form a complete orthonormal basis with Ω_f . We then choose the time-reversal symmetric gauge $\Omega_{\pm} = e^{\pm i\phi}(\pm i\Omega_1 + \Omega_2)$ to form the following unitary matrix $\Omega(\theta(\mathbf{k})) = (\Omega_+, \Omega_-, \Omega_f)$

$$\Omega(\mathbf{k}) = \begin{pmatrix} \frac{e^{i\phi}}{2}(1 - i \cos \theta) & \frac{e^{-i\phi}}{2}(1 + i \cos \theta) & -\sin \theta/\sqrt{2} \\ -\frac{ie^{i\phi}}{\sqrt{2}} \sin \theta & \frac{ie^{-i\phi}}{\sqrt{2}} \sin \theta & \cos \theta \\ \frac{e^{i\phi}}{2}(1 + i \cos \theta) & \frac{e^{-i\phi}}{2}(1 - i \cos \theta) & \sin \theta/\sqrt{2} \end{pmatrix}, \quad \mathbf{k} = M + |k|(\cos \phi, \sin \phi), \quad \theta = \theta(|k|) = -2 \arctan \frac{|k|/\Lambda - 1}{|k|/\Lambda + 1} \quad (\text{F21})$$

defines a smooth, symmetry-preserving transformation into $\gamma_{\mathbf{k},c+}^\dagger, \gamma_{\mathbf{k},c-}^\dagger, \gamma_{\mathbf{k},f}^\dagger$, the two conduction electrons and the Wannier state respectively. One can verify that the conduction electron wavefunctions are smooth using the explicit form of the band eigenvectors,

$$U(\mathbf{k}) = \begin{pmatrix} -1/\sqrt{2} & 0 & 1/\sqrt{2} \\ \frac{\cos k_y/2}{\sqrt{2+\cos k_x+\cos k_y}} & -\frac{\sqrt{2} \cos k_x/2}{\sqrt{2+\cos k_x+\cos k_y}} & \frac{\cos k_y/2}{\sqrt{2+\cos k_x+\cos k_y}} \\ \frac{\cos k_x/2}{\sqrt{2+\cos k_x+\cos k_y}} & \frac{\sqrt{2} \cos k_y/2}{\sqrt{2+\cos k_x+\cos k_y}} & \frac{\cos k_x/2}{\sqrt{2+\cos k_x+\cos k_y}} \end{pmatrix} \rightarrow \begin{pmatrix} -\frac{1}{\sqrt{2}} & 0 & \frac{1}{\sqrt{2}} \\ -\frac{\sin \phi}{\sqrt{2}} & \cos \phi & -\frac{\sin \phi}{\sqrt{2}} \\ -\frac{\cos \phi}{\sqrt{2}} & -\sin \phi & -\frac{\cos \phi}{\sqrt{2}} \end{pmatrix} \quad (\text{F22})$$

approaching the singular point at M . Note that individually, Ω and U are discontinuous at M . However, their product is smooth:

$$U(\mathbf{k})\Omega(\mathbf{k}) = \begin{pmatrix} \frac{i\sqrt{2}k}{\Lambda} & -\frac{i\sqrt{2}\bar{k}}{\Lambda} & 1 \\ -\frac{i}{\sqrt{2}} & \frac{i}{\sqrt{2}} & \frac{2k_x}{\Lambda} \\ -\frac{1}{\sqrt{2}} & -\frac{1}{\sqrt{2}} & -\frac{2k_y}{\Lambda} \end{pmatrix} + O(k^2), \quad k_x + ik_y = k, \quad k_x - ik_y = \bar{k}. \quad (\text{F23})$$

Thus we see explicitly that the HF states

$$\gamma_{\mathbf{k},\mu}^\dagger = \sum_{\alpha} c_{\mathbf{k},\alpha}^\dagger [U(\mathbf{k})\Omega(\mathbf{k})]_{\alpha\mu} \quad (\text{F24})$$

have smooth wavefunctions everywhere on the BZ for any value of the cutoff Λ . It is now a simple matter to write down the single-particle Hamiltonian in the HF basis. Defining $E(\mathbf{k}) = \text{diag}(E_+(\mathbf{k}), 0, E_-(\mathbf{k}))$, we have

$$H_0 = \sum_{\alpha\beta} c_{\mathbf{k},\alpha}^\dagger h_{\alpha\beta}(\mathbf{k}) c_{\mathbf{k},\beta} = \sum_{\mu\nu} \gamma_{\mathbf{k},\mu}^\dagger [\Omega^\dagger(\mathbf{k})E(\mathbf{k})\Omega(\mathbf{k})]_{\mu\nu} \gamma_{\mathbf{k},\nu} = \sum_{\mu\nu} \gamma_{\mathbf{k},\mu}^\dagger h_{\mu\nu}^{HF}(\mathbf{k}) \gamma_{\mathbf{k},\nu} \quad (\text{F25})$$

$$h^{HF}(\mathbf{k}) = \Omega^\dagger(\mathbf{k})E(\mathbf{k})\Omega(\mathbf{k}) = t \begin{pmatrix} i2\bar{k}^2/\Lambda & -\bar{k}/\sqrt{2} \\ -i2k^2/\Lambda & -k/\sqrt{2} \\ -k/\sqrt{2} & -\bar{k}/\sqrt{2} \end{pmatrix} + \dots$$

so we identify the conduction electron Hamiltonian as a 2π Berry phase topological semi-metal with a quadratic band touching, the heavy electron block being completely flat, and the linear coupling between them giving the Dirac band structure $0, \pm t|k|$. Note that Eq. (F23) shows there is a spinless representation of time-reversal,

$$\mathcal{T}\gamma_{\mathbf{k},c\pm}^\dagger\mathcal{T}^{-1}=\gamma_{-\mathbf{k},c\mp}^\dagger, \quad (\text{F26})$$

as is appropriate for spinor wavefunctions with 2π Berry phase.

2. Anderson Model

Choosing the Hubbard interaction, we have

$$H_{int} = U \sum_{\mathbf{R}\alpha} n_{\mathbf{R},\alpha,\uparrow} n_{\mathbf{R},\alpha,\downarrow} = U \sum_{\mathbf{q}\alpha} \rho_{\mathbf{q},\alpha,\uparrow} \rho_{-\mathbf{q},\alpha,\downarrow} \quad (\text{F27})$$

where the density operator is

$$\rho_{\mathbf{q},\alpha,\sigma} = \frac{1}{\sqrt{N}} \sum_{\mathbf{k}\mu\nu} M_{\mu\nu}^\alpha(\mathbf{k}, \mathbf{q}) \gamma_{\mathbf{k}+\mathbf{q},\mu,\sigma}^\dagger \gamma_{\mathbf{k},\nu,\sigma}, \quad M_{\mu\nu}^\alpha(\mathbf{k}, \mathbf{q}) = U_{\alpha\mu}^*(\mathbf{k} + \mathbf{q}) U_{\alpha\nu}(\mathbf{k}) \quad (\text{F28})$$

and N is the number of unit cells. Here μ, ν denotes the f, c basis.

We compute a series of terms by separating out the various flavour interactions. First we have the $ffff$ term:

$$\begin{aligned} H_U &= \frac{U}{N} \sum_{\mathbf{q}\mathbf{k}\mathbf{k}'\mu\nu\mu'\nu'\alpha} M_{ff}^\alpha(\mathbf{k}, \mathbf{q}) f_{\mathbf{k}+\mathbf{q},\uparrow}^\dagger f_{\mathbf{k},\uparrow} M_{ff}^\alpha(\mathbf{k}', -\mathbf{q}) f_{\mathbf{k}'-\mathbf{q},\uparrow}^\dagger f_{\mathbf{k}',\downarrow} \\ &= \sum_{\mathbf{R}_1\mathbf{R}'_1\mathbf{R}_2\mathbf{R}'_2} U_{\mathbf{R}_1,\mathbf{R}'_1,\mathbf{R}_2,\mathbf{R}'_2} f_{\mathbf{R}_1,\uparrow}^\dagger f_{\mathbf{R}'_1,\uparrow} f_{\mathbf{R}_2,\downarrow}^\dagger f_{\mathbf{R}'_2,\downarrow} \\ U_{\mathbf{R}_1,\mathbf{R}'_1,\mathbf{R}_2,\mathbf{R}'_2} &= \frac{U}{N^3} \sum_{\mathbf{q}\mathbf{k}\mathbf{k}',\alpha} M_{ff}^\alpha(\mathbf{k}, \mathbf{q}) M_{ff}^\alpha(\mathbf{k}', -\mathbf{q}) e^{-i(\mathbf{k}+\mathbf{q})\cdot\mathbf{R}_1 + i\mathbf{k}\cdot\mathbf{R}'_1 - i(\mathbf{k}'-\mathbf{q})\cdot\mathbf{R}_2 + i\mathbf{k}'\cdot\mathbf{R}'_2} \end{aligned} \quad (\text{F29})$$

where the real-space interaction $U_{\mathbf{R}_1,\mathbf{R}_2,\mathbf{R}_3,\mathbf{R}_4}$ is large when $|\mathbf{R}_i - \mathbf{R}_j| \leq 1$ due to the lobe-like structure of the Wannier state with large onsite and next-nearest neighbor overlap as shown in the Main Text.

To gain a more intuitive understanding of the f -mode density-density terms, we analyze them directly in real space in the approximation

$$f_{\mathbf{R},\sigma}^\dagger \approx \frac{1}{2} \sum_{\boldsymbol{\delta}} (-1)^{2\boldsymbol{\delta}\cdot\hat{\mathbf{y}}} c_{\mathbf{R}+\boldsymbol{\delta},\sigma}^\dagger, \quad \boldsymbol{\delta} \in \{\pm\frac{1}{2}\hat{x}, \pm\frac{1}{2}\hat{y}\}. \quad (\text{F30})$$

This approximation is motivated by the large amplitudes of the f -mode on the bonds of its plaquette, and much smaller amplitudes (by a factor of 10) otherwise. Fourier transforming to momentum space, Eq. (F30) is equivalent to the approximation

$$U_{f,\alpha}(\mathbf{k}) \approx (0, -\cos\frac{k_x}{2}, \cos\frac{k_y}{2})_\alpha. \quad (\text{F31})$$

We then obtain an expression for the density operator (throughout, $\bar{\mathcal{O}}^f$ denotes the projection of \mathcal{O} onto the f mode

basis)

$$\begin{aligned}
\bar{n}_{\mathbf{R},\alpha,\sigma}^f &\approx \frac{1}{N} \sum_{\mathbf{k}\mathbf{k}'} e^{-i(\mathbf{k}-\mathbf{k}')\cdot(\mathbf{R}+\mathbf{r}_\alpha)} \bar{c}_{\mathbf{k},\alpha,\sigma}^{\dagger f} \bar{c}_{\mathbf{k}',\alpha,\sigma}^f \\
&= \frac{1}{N} \sum_{\mathbf{k}\mathbf{k}'} e^{-i(\mathbf{k}-\mathbf{k}')\cdot(\mathbf{R}+\mathbf{r}_\alpha)} f_{\mathbf{k},\sigma}^\dagger U_{f,\alpha}^\dagger(\mathbf{k}) U_{f,\alpha}(\mathbf{k}') f_{\mathbf{k}',\sigma} \\
&= \frac{1}{N^2} \sum_{\mathbf{L},\mathbf{L}'} \sum_{\mathbf{k}\mathbf{k}'} e^{-i(\mathbf{k}-\mathbf{k}')\cdot(\mathbf{R}+\mathbf{r}_\alpha) + i\mathbf{k}\cdot\mathbf{L} - i\mathbf{k}'\cdot\mathbf{L}'} f_{\mathbf{L},\sigma}^\dagger U_{f,\alpha}^\dagger(\mathbf{k}) U_{f,\alpha}(\mathbf{k}') f_{\mathbf{L}',\sigma} \\
&= \sum_{\mathbf{L},\mathbf{L}'} f_{\mathbf{L},\sigma}^\dagger f_{\mathbf{L}',\sigma} \left(\frac{1}{N^2} \sum_{\mathbf{k}\mathbf{k}'} e^{-i(\mathbf{k}-\mathbf{k}')\cdot(\mathbf{R}+\mathbf{r}_\alpha) + i\mathbf{k}\cdot\mathbf{L} - i\mathbf{k}'\cdot\mathbf{L}'} U_{f,\alpha}^\dagger(\mathbf{k}) U_{f,\alpha}(\mathbf{k}') \right) \\
&= \sum_{\mathbf{L},\mathbf{L}'} f_{\mathbf{L},\sigma}^\dagger f_{\mathbf{L}',\sigma} \left(\frac{1}{N} \sum_{\mathbf{k}} e^{-i\mathbf{k}\cdot(\mathbf{R}-\mathbf{L}+\mathbf{r}_\alpha)} U_{f,\alpha}^\dagger(\mathbf{k}) \right) \left(\frac{1}{N} \sum_{\mathbf{k}'} e^{i\mathbf{k}'\cdot(\mathbf{R}-\mathbf{L}'+\mathbf{r}_\alpha)} U_{f,\alpha}(\mathbf{k}') \right) \\
&= \sum_{\mathbf{L},\mathbf{L}'} f_{\mathbf{L},\sigma}^\dagger f_{\mathbf{L}',\sigma} \frac{1}{4} (\delta_{\mathbf{R}-\mathbf{L},\mathbf{0}} + \delta_{\mathbf{R}-\mathbf{L},-2\mathbf{r}_\alpha}) (\delta_{\mathbf{R}-\mathbf{L}',\mathbf{0}} + \delta_{\mathbf{R}-\mathbf{L}',-2\mathbf{r}_\alpha}), \quad \alpha = 2, 3 \\
\bar{n}_{\mathbf{R},\alpha,\sigma}^f &\approx \frac{1}{4} (f_{\mathbf{R},\sigma}^\dagger + f_{\mathbf{R}+2\mathbf{r}_\alpha,\sigma}^\dagger) (f_{\mathbf{R},\sigma} + f_{\mathbf{R}+2\mathbf{r}_\alpha,\sigma})
\end{aligned} \tag{F32}$$

and $\bar{n}_{\mathbf{R},1,\sigma}^f \approx 0$, since the f -modes have small weight on the L ($\alpha = 1$) sublattice. To write this in a simple way, we define the bond-centered operators

$$f_{\langle\mathbf{R}\mathbf{R}'\rangle,\sigma}^\dagger = \frac{f_{\mathbf{R},\sigma}^\dagger + f_{\mathbf{R}',\sigma}^\dagger}{\sqrt{2}}, \quad n_{\langle\mathbf{R}\mathbf{R}'\rangle,\sigma} = f_{\mathbf{R}\mathbf{R}',\sigma}^\dagger f_{\mathbf{R}\mathbf{R}',\sigma}. \tag{F33}$$

We now obtain

$$H_U = U \sum_{\mathbf{R}\alpha} \bar{n}_{\mathbf{R},\alpha,\uparrow}^f \bar{n}_{\mathbf{R},\alpha,\downarrow}^f \approx \frac{U}{4} \sum_{\langle\mathbf{R}\mathbf{R}'\rangle} n_{\langle\mathbf{R}\mathbf{R}'\rangle,\uparrow} n_{\langle\mathbf{R}\mathbf{R}'\rangle,\downarrow} \tag{F34}$$

We now consider the other interactions terms. Since each band operator is broken into f and c terms and the interaction contains 4 band operators, there are in total 16 terms. We will give explicit expressions for the dominant terms in the TBG Anderson-‘+’ model, which are the W and J terms to be explained below.

The W term is a density-density interaction between the c modes and f modes. It can be written

$$H_W = U \sum_{\mathbf{R}\alpha} (\bar{n}_{\mathbf{R},\alpha,\uparrow}^f \bar{n}_{\mathbf{R},\alpha,\downarrow}^c + \bar{n}_{\mathbf{R},\alpha,\downarrow}^f \bar{n}_{\mathbf{R},\alpha,\uparrow}^c) \tag{F35}$$

where $\bar{n}_{\mathbf{R},\alpha,\sigma}^c$ is the projection of the density onto the c -electrons:

$$\bar{n}_{\mathbf{R},\alpha,\sigma}^c = \frac{1}{N} \sum_{\mathbf{k}\mathbf{k}',\mu\nu=c\pm} e^{-i(\mathbf{k}-\mathbf{k}')\cdot(\mathbf{R}+\mathbf{r}_\alpha)} \gamma_{\mathbf{k},\mu,\sigma}^\dagger U_{\mu,\alpha}^\dagger(\mathbf{k}) U_{\nu,\alpha}(\mathbf{k}') \gamma_{\mathbf{k}',\nu,\sigma}. \tag{F36}$$

A convenient approximation is to now drop the \mathbf{k} dependence in the c -electron wavefunction, replacing $U_{\mu,\alpha}(\mathbf{k}) \rightarrow U_{\mu,\alpha}(M)$ since away from the M point, the c -electrons are high-energy and errors in their wavefunctions will be irrelevant. We find that

$$e^{-i(\mathbf{k}-\mathbf{k}')\cdot\mathbf{r}_\alpha} U_{\mu,\alpha}^\dagger(\mathbf{k}) U_{\nu,\alpha}(\mathbf{k}') \rightarrow \frac{1}{2} (-1)^{\delta_{\alpha,2}(1-\delta_{\mu\nu})}, \quad (\alpha = 2, 3) \tag{F37}$$

and thus the W term can be written

$$H_W = \frac{U}{4N} \sum_{\mathbf{R}\alpha,\mathbf{k}\mathbf{k},\mu\nu} n_{\langle\mathbf{R},\mathbf{R}+2\mathbf{r}_\alpha\rangle,\uparrow} e^{-i(\mathbf{k}-\mathbf{k}')\cdot\mathbf{R}} \gamma_{\mathbf{k},\mu,\downarrow}^\dagger (-1)^{\delta_{\alpha,2}(1-\delta_{\mu\nu})} \gamma_{\mathbf{k}',\nu,\downarrow} + (\uparrow \leftrightarrow \downarrow). \tag{F38}$$

The last term we will consider is the J term, which is an fc -exchange term taking the form

$$\begin{aligned}
 H_J &= \frac{U}{N} \sum_{\mathbf{q}\alpha} \sum_{\mathbf{k}\mu\nu,\mathbf{k}'} M_{f\nu}^{\alpha}(\mathbf{k},\mathbf{q}) M_{\mu f}^{\alpha}(\mathbf{k}',-\mathbf{q}) f_{\mathbf{k}+\mathbf{q},\uparrow}^{\dagger} \gamma_{\mathbf{k},\nu,\uparrow} \gamma_{\mathbf{k}'-\mathbf{q},\mu',\downarrow}^{\dagger} f_{\mathbf{k}',\downarrow} + h.c. \\
 &= \frac{U}{N} \sum_{\mathbf{q}\alpha} \sum_{\mathbf{k}\mu\nu,\mathbf{k}'} M_{f\nu}^{\alpha}(\mathbf{k}-\mathbf{q},\mathbf{q}) M_{\mu f}^{\alpha}(\mathbf{k}',-\mathbf{q}) f_{\mathbf{k},\uparrow}^{\dagger} \gamma_{\mathbf{k}-\mathbf{q},\nu,\uparrow} \gamma_{\mathbf{k}'-\mathbf{q},\mu',\downarrow}^{\dagger} f_{\mathbf{k}',\downarrow} + h.c. \\
 &\sim \frac{U}{N} \sum_{\mathbf{q}} \sum_{\mathbf{k}\mu\nu,\mathbf{k}'} \left(\sum_{\alpha} U_{\alpha f}^{*}(\mathbf{k}) U_{\alpha\nu}(M) U_{\alpha\mu}^{*}(M) U_{\alpha f}(\mathbf{k}') \right) f_{\mathbf{k},\uparrow}^{\dagger} \gamma_{\mathbf{k}-\mathbf{q},\nu,\uparrow} \gamma_{\mathbf{k}'-\mathbf{q},\mu',\downarrow}^{\dagger} f_{\mathbf{k}',\downarrow} + h.c.
 \end{aligned} \tag{F39}$$

where we have again replaced the conduction mode wavefunctions with their value at the band crossing point.

-
- [1] J. G. Checkelsky, B. A. Bernevig, P. Coleman, Q. Si, and S. Paschen, [arXiv e-prints](#), [arXiv:2312.10659](#) (2023), [arXiv:2312.10659 \[cond-mat.str-el\]](#).
 - [2] L. Balents, C. R. Dean, D. K. Efetov, and A. F. Young, [Nature Physics](#) **16**, 725 (2020).
 - [3] N. Regnault, Y. Xu, M.-R. Li, D.-S. Ma, M. Jovanovic, A. Yazdani, S. S. P. Parkin, C. Felser, L. M. Schoop, N. P. Ong, R. J. Cava, L. Elcoro, Z.-D. Song, and B. A. Bernevig, [Nature \(London\)](#) **603**, 824 (2022), [arXiv:2106.05287 \[cond-mat.str-el\]](#).
 - [4] E. H. Lieb, [Phys. Rev. Lett.](#) **62**, 1201 (1989).
 - [5] D. Călugăru, A. Chew, L. Elcoro, Y. Xu, N. Regnault, Z.-D. Song, and B. A. Bernevig, [Nature Physics](#) **18**, 185 (2022).
 - [6] C. S. Chiu, D.-S. Ma, Z.-D. Song, B. A. Bernevig, and A. A. Houck, [Phys. Rev. Research](#) **2**, 043414 (2020).
 - [7] J.-W. Rhim and B.-J. Yang, [Phys. Rev. B](#) **99**, 045107 (2019).
 - [8] Y. Hwang, J.-W. Rhim, and B.-J. Yang, [Phys. Rev. B](#) **104**, 085144 (2021).
 - [9] J.-X. Yin, B. Lian, and M. Z. Hasan, [Nature](#) **612**, 647 (2022).
 - [10] M. Kang, S. Fang, L. Ye, H. C. Po, J. Denlinger, C. Jozwiak, A. Bostwick, E. Rotenberg, E. Kaxiras, J. G. Checkelsky, *et al.*, [Nature communications](#) **11**, 4004 (2020).
 - [11] Z. Li, J. Zhuang, L. Wang, H. Feng, Q. Gao, X. Xu, W. Hao, X. Wang, C. Zhang, K. Wu, *et al.*, [Science advances](#) **4**, eaau4511 (2018).
 - [12] M. Kang, L. Ye, S. Fang, J.-S. You, A. Levitan, M. Han, J. I. Facio, C. Jozwiak, A. Bostwick, E. Rotenberg, *et al.*, [Nature materials](#) **19**, 163 (2020).
 - [13] J. Huang, C. Setty, L. Deng, J.-Y. You, H. Liu, S. Shao, J. S. Oh, Y. Guo, Y. Zhang, Z. Yue, J.-X. Yin, M. Hashimoto, D. Lu, S. Gorovikov, P. Dai, J. D. Denlinger, M. Zahid Hasan, Y.-P. Feng, R. J. Birgeneau, Y. Shi, C.-W. Chu, G. Chang, Q. Si, and M. Yi, [arXiv e-prints](#), [arXiv:2304.09066](#) (2023), [arXiv:2304.09066 \[cond-mat.str-el\]](#).
 - [14] J. P. Wakefield, M. Kang, P. M. Neves, D. Oh, S. Fang, R. McTigue, S. Frank Zhao, T. N. Lamichhane, A. Chen, S. Lee, *et al.*, [Nature](#) **623**, 301 (2023).
 - [15] R. Bistritzer and A. H. MacDonald, [Proceedings of the National Academy of Sciences](#) **108**, 12233 (2011).
 - [16] F. Wu, T. Lovorn, E. Tutuc, I. Martin, and A. H. MacDonald, [Phys. Rev. Lett.](#) **122**, 086402 (2019).
 - [17] G. Tarnopolsky, A. J. Kruchkov, and A. Vishwanath, [Phys. Rev. Lett.](#) **122**, 106405 (2019).
 - [18] V. Crépel, A. Dunbrack, D. Guerci, J. Bonini, and J. Cano, [Phys. Rev. B](#) **108**, 075126 (2023).
 - [19] P. J. Ledwith, E. Khalaf, Z. Zhu, S. Carr, E. Kaxiras, and A. Vishwanath, Tb or not tb? contrasting properties of twisted bilayer graphene and the alternating twist n -layer structures ($n = 3, 4, 5, \dots$) (2021), [arXiv:2111.11060 \[cond-mat.str-el\]](#).
 - [20] J. Wang, Y. Zheng, A. J. Millis, and J. Cano, [Phys. Rev. Res.](#) **3**, 023155 (2021).
 - [21] S. Sarkar, X. Wan, S.-Z. Lin, and K. Sun, Symmetry-based classification of exact flat bands in single and bilayer moiré systems (2023), [arXiv:2310.02218 \[cond-mat.mes-hall\]](#).
 - [22] J. Kang and O. Vafek, [Phys. Rev. Lett.](#) **122**, 246401 (2019).
 - [23] B. Lian, Z.-D. Song, N. Regnault, D. K. Efetov, A. Yazdani, and B. A. Bernevig, [Phys. Rev. B](#) **103**, 205414 (2021).
 - [24] B. A. Bernevig, B. Lian, A. Cowsik, F. Xie, N. Regnault, and Z.-D. Song, [Phys. Rev. B](#) **103**, 205415 (2021).
 - [25] N. Bultinck, E. Khalaf, S. Liu, S. Chatterjee, A. Vishwanath, and M. P. Zaletel, [Phys. Rev. X](#) **10**, 031034 (2020).
 - [26] J. Kang, T. Oh, J. Lee, and B.-J. Yang, [arXiv e-prints](#), [arXiv:2402.07171](#) (2024), [arXiv:2402.07171 \[cond-mat.str-el\]](#).
 - [27] M. Tovmasyan, S. Peotta, P. Törmä, and S. D. Huber, [Phys. Rev. B](#) **94**, 245149 (2016).
 - [28] X. Zhang, K. Sun, H. Li, G. Pan, and Z. Y. Meng, [Phys. Rev. B](#) **106**, 184517 (2022).
 - [29] J. Herzog-Arbeitman, A. Chew, K.-E. Huhtinen, P. Törmä, and B. A. Bernevig, [arXiv e-prints](#), [arXiv:2209.00007](#) (2022), [arXiv:2209.00007 \[cond-mat.str-el\]](#).
 - [30] K. Sun and H. Deng, [arXiv e-prints](#), [arXiv:2308.15963](#) (2023), [arXiv:2308.15963 \[cond-mat.str-el\]](#).
 - [31] Z. Han, J. Herzog-Arbeitman, B. A. Bernevig, and S. A. Kivelson, [arXiv e-prints](#), [arXiv:2401.04163](#) (2024), [arXiv:2401.04163 \[cond-mat.str-el\]](#).
 - [32] E. Khalaf, A. J. Kruchkov, G. Tarnopolsky, and A. Vishwanath, [Phys. Rev. B](#) **100**, 085109 (2019).
 - [33] Z.-D. Song and B. A. Bernevig, [Phys. Rev. Lett.](#) **129**, 047601 (2022).
 - [34] H. Shi and X. Dai, [arXiv:2209.09515](#) (2022).

- [35] D. Călugăru, M. Borovkov, L. L. H. Lau, P. Coleman, Z.-D. Song, and B. A. Bernevig, *Low Temp. Phys.* **49**, 640 (2023).
- [36] K. Singh, A. Chew, J. Herzog-Arbeitman, B. A. Bernevig, and O. Vafek, *arXiv e-prints*, [arXiv:2305.08171](#) (2023), [arXiv:2305.08171 \[cond-mat.str-el\]](#).
- [37] L. L. H. Lau and P. Coleman, *arXiv e-prints*, [arXiv:2303.02670](#) (2023), [arXiv:2303.02670 \[cond-mat.str-el\]](#).
- [38] M. Koshino, N. F. Q. Yuan, T. Koretsune, M. Ochi, K. Kuroki, and L. Fu, *Phys. Rev. X* **8**, 031087 (2018).
- [39] N. N. T. Nam and M. Koshino, *Phys. Rev. B* **96**, 075311 (2017).
- [40] Z. Bi, N. F. Q. Yuan, and L. Fu, *Phys. Rev. B* **100**, 035448 (2019).
- [41] O. Vafek and J. Kang, *Phys. Rev. B* **107**, 075123 (2023).
- [42] J. Kang and O. Vafek, *Phys. Rev. B* **107**, 075408 (2023), [arXiv:2208.05953 \[cond-mat.str-el\]](#).
- [43] T. Cea, P. A. Pantaleón, and F. Guinea, *Phys. Rev. B* **102**, 155136 (2020).
- [44] H. Hu, B. A. Bernevig, and A. M. Tsvelik, to appear.
- [45] H. Hu, G. Rai, L. Crippa, J. Herzog-Arbeitman, D. Călugăru, T. Wehling, G. Sangiovanni, R. Valentí, A. M. Tsvelik, and B. A. Bernevig, *Phys. Rev. Lett.* **131**, 166501 (2023).
- [46] Y.-Z. Chou and S. D. Sarma, *arXiv:2211.15682* (2022).
- [47] Y.-Z. Chou and S. D. Sarma, *Physical Review B* **108**, 125106 (2023).
- [48] A. Datta, M. J. Calderón, A. Camjayi, and E. Bascones, *Nature Communications* **14**, 5036 (2023), [arXiv:2301.13024 \[cond-mat.str-el\]](#).
- [49] G.-D. Zhou, Y.-J. Wang, N. Tong, and Z.-D. Song, *Phys. Rev. B* **109**, 045419 (2024).
- [50] G. Rai, L. Crippa, D. Călugăru, H. Hu, L. de' Medici, A. Georges, B. A. Bernevig, R. Valentí, G. Sangiovanni, and T. Wehling, *Dynamical correlations and order in magic-angle twisted bilayer graphene* (2023), [arxiv:2309.08529 \[cond-mat, physics.quant-ph\]](#).
- [51] D. Călugăru, H. Hu, R. Luque Merino, N. Regnault, D. K. Efetov, and B. A. Bernevig, *arXiv e-prints*, [arXiv:2402.14057](#) (2024), [arXiv:2402.14057 \[cond-mat.str-el\]](#).
- [52] Y.-J. Wang, G.-D. Zhou, S.-Y. Peng, B. Lian, and Z.-D. Song, *arXiv e-prints*, [arXiv:2402.00869](#) (2024), [arXiv:2402.00869 \[cond-mat.supr-con\]](#).
- [53] D. Calugaru, B. A. Bernevig, and H. Hu, In preparation.
- [54] J. Yu, M. Xie, B. A. Bernevig, and S. Das Sarma, *Phys. Rev. B* **108**, 035129 (2023), [arXiv:2301.04171 \[cond-mat.mes-hall\]](#).
- [55] M.-R. Li, A.-L. He, and H. Yao, *Phys. Rev. Res.* **4**, 043151 (2022).
- [56] Y. Cao, V. Fatemi, A. Demir, S. Fang, S. L. Tomarken, J. Y. Luo, J. D. Sanchez-Yamagishi, K. Watanabe, T. Taniguchi, E. Kaxiras, *et al.*, *Nature* **556**, 80 (2018).
- [57] Y. Cao, V. Fatemi, S. Fang, K. Watanabe, T. Taniguchi, E. Kaxiras, and P. Jarillo-Herrero, *Nature* **556**, 43 (2018).
- [58] Z. Song, Z. Wang, W. Shi, G. Li, C. Fang, and B. A. Bernevig, *Phys. Rev. Lett.* **123**, 036401 (2019).
- [59] H. C. Po, L. Zou, T. Senthil, and A. Vishwanath, *Phys. Rev. B* **99**, 195455 (2019).
- [60] Z.-D. Song, B. Lian, N. Regnault, and B. A. Bernevig, *Phys. Rev. B* **103**, 205412 (2021).
- [61] G. Tarnopolsky, A. J. Kruchkov, and A. Vishwanath, *Phys. Rev. Lett.* **122**, 106405 (2019).
- [62] C.-X. Liu, Y. Chen, A. Yazdani, and B. A. Bernevig, *Electron-k-phonon interaction in twisted bilayer graphene* (2023), [arXiv:2303.15551 \[cond-mat.supr-con\]](#).
- [63] B. A. Bernevig, T. L. Hughes, and S.-C. Zhang, *Science* **314**, 1757 (2006), <https://www.science.org/doi/pdf/10.1126/science.1133734>.
- [64] Y. Liu, K. Yang, and C. Liu, to appear.
- [65] Z.-D. Song, B. Lian, N. Regnault, and B. A. Bernevig, *Physical Review B* **103**, 10.1103/physrevb.103.205412 (2021).
- [66] C.-K. Chiu, J. C. Y. Teo, A. P. Schnyder, and S. Ryu, *Rev. Mod. Phys.* **88**, 035005 (2016).
- [67] M.-R. Li, A.-L. He, and H. Yao, *Phys. Rev. Res.* **4**, 043151 (2022).
- [68] M. I. Aroyo, A. Kirov, C. Capillas, J. Perez-Mato, and H. Wondratschek, *Acta Crystallographica Section A* **62**, 115 (2006).
- [69] N. Marzari, A. A. Mostofi, J. R. Yates, I. Souza, and D. Vanderbilt, *Rev. Mod. Phys.* **84**, 1419 (2012).
- [70] E. B. Bogomolny, *Sov. J. Nucl. Phys.* **24**, 449 (1976).
- [71] D. Tong, *arXiv e-prints*, [hep-th/0509216](#) (2005), [arXiv:hep-th/0509216 \[hep-th\]](#).
- [72] B. Bradlyn, L. Elcoro, J. Cano, M. Vergniory, Z. Wang, C. Felser, M. Aroyo, and B. A. Bernevig, *Nature* **547**, 298 (2017).
- [73] K.-E. Huhtinen, J. Herzog-Arbeitman, A. Chew, B. A. Bernevig, and P. Törmä, *Phys. Rev. B* **106**, 014518 (2022).
- [74] P. Törmä, L. Liang, and S. Peotta, *Phys. Rev. B* **98**, 220511 (2018).
- [75] M. Iskin, *Phys. Rev. B* **107**, 224505 (2023), [arXiv:2304.03613 \[cond-mat.supr-con\]](#).
- [76] J.-X. Hu, S. A. Chen, and K. T. Law, *arXiv e-prints*, [arXiv:2308.05686](#) (2023), [arXiv:2308.05686 \[cond-mat.supr-con\]](#).
- [77] S. A. Chen and K. T. Law, *Phys. Rev. Lett.* **132**, 026002 (2024).
- [78] S. A. Chen and K. T. Law, *Phys. Rev. Lett.* **132**, 026002 (2024), [arXiv:2303.15504 \[cond-mat.supr-con\]](#).
- [79] A. Julku, S. Peotta, T. I. Vanhala, D.-H. Kim, and P. Törmä, *Phys. Rev. Lett.* **117**, 045303 (2016).
- [80] K.-E. Huhtinen and P. Törmä, *Phys. Rev. B* **103**, L220502 (2021).
- [81] Z. Han and S. A. Kivelson, *Phys. Rev. Lett.* **130**, 186404 (2023), [arXiv:2210.16321 \[cond-mat.str-el\]](#).
- [82] D. Monaco, G. Panati, A. Pisante, and S. Teufel, *Communications in Mathematical Physics* **359**, 61 (2018), [arXiv:1612.09552 \[math-ph\]](#).
- [83] J. Zang, J. Wang, A. Georges, J. Cano, and A. J. Millis, *arXiv e-prints*, [arXiv:2210.11573](#) (2022), [arXiv:2210.11573 \[cond-mat.mes-hall\]](#).
- [84] O. Vafek and J. Kang, *Phys. Rev. B* **104**, 075143 (2021).
- [85] A. Mielke, *Journal of Physics A: Mathematical and General* **24**, L73 (1991).

- [86] Y. Jiang, H. Hu, D. Călugăru, C. Felser, S. Blanco-Canosa, H. Weng, Y. Xu, and B. A. Bernevig, [arXiv e-prints](#) , [arXiv:2311.09290](#) (2023), [arXiv:2311.09290 \[cond-mat.str-el\]](#).
- [87] R. Resta, [The European Physical Journal B](#) **79**, 121 (2011).
- [88] R. Roy, [arXiv e-prints](#) , [arXiv:1208.2055](#) (2012), [arXiv:1208.2055 \[cond-mat.str-el\]](#).
- [89] B. Mera and J. Mitscherling, [Phys. Rev. B](#) **106**, 165133 (2022).
- [90] A. Ghosh, S. Chakraborty, R. Dutta, A. Agarwala, K. Watanabe, T. Taniguchi, S. Banerjee, N. Trivedi, S. Mukerjee, and A. Das, [Evidence of enhanced thermopower from emergent local moments in flatbands of magic-angle twisted bilayer graphene](#) (2024), [arxiv:2403.08686 \[cond-mat\]](#).
- [91] R. L. Merino, D. Calugaru, H. Hu, J. Diez-Merida, A. Diez-Carlón, T. Taniguchi, K. Watanabe, P. Seifert, B. A. Bernevig, and D. K. Efetov, [Evidence of heavy fermion physics in the thermoelectric transport of magic angle twisted bilayer graphene](#) (2024), [arxiv:2402.11749 \[cond-mat\]](#).
- [92] J. Díez-Mérida, A. Díez-Carlón, S. Y. Yang, Y.-M. Xie, X.-J. Gao, J. Senior, K. Watanabe, T. Taniguchi, X. Lu, A. P. Higginbotham, K. T. Law, and D. K. Efetov, [Nat. Commun.](#) **14**, 2396 (2023).
- [93] H. Tian, X. Gao, Y. Zhang, S. Che, T. Xu, P. Cheung, K. Watanabe, T. Taniguchi, M. Randeria, F. Zhang, C. N. Lau, and M. W. Bockrath, [Nature](#) **614**, 440 (2023).
- [94] G. Di Battista, P. Seifert, K. Watanabe, T. Taniguchi, K. C. Fong, A. Principi, and D. K. Efetov, [Nano Lett.](#) **22**, 6465 (2022).
- [95] B. Lian, [Nature](#) **592**, 191 (2021).
- [96] J. Yu, B. A. Foutty, Y. H. Kwan, M. E. Barber, K. Watanabe, T. Taniguchi, Z.-X. Shen, S. A. Parameswaran, and B. E. Feldman, [Nat. Commun.](#) **14**, 6679 (2023), [arxiv:2206.11304 \[cond-mat\]](#).
- [97] S. Hubmann, P. Soul, G. Di Battista, M. Hild, K. Watanabe, T. Taniguchi, D. K. Efetov, and S. D. Ganichev, [Phys. Rev. Mater.](#) **6**, 024003 (2022).
- [98] S. Grover, M. Bocarsly, A. Uri, P. Stepanov, G. Di Battista, I. Roy, J. Xiao, A. Y. Meltzer, Y. Myasoedov, K. Pareek, K. Watanabe, T. Taniguchi, B. Yan, A. Stern, E. Berg, D. K. Efetov, and E. Zeldov, [Nat. Phys.](#) **18**, 885 (2022).
- [99] A. Jaoui, I. Das, G. Di Battista, J. Díez-Mérida, X. Lu, K. Watanabe, T. Taniguchi, H. Ishizuka, L. Levitov, and D. K. Efetov, [Nat. Phys.](#) **18**, 633 (2022).
- [100] A. K. Paul, A. Ghosh, S. Chakraborty, U. Roy, R. Dutta, K. Watanabe, T. Taniguchi, A. Panda, A. Agarwala, S. Mukerjee, S. Banerjee, and A. Das, [Nat. Phys.](#) **18**, 691 (2022).
- [101] B. Ghawri, P. S. Mahapatra, M. Garg, S. Mandal, S. Bhowmik, A. Jayaraman, R. Soni, K. Watanabe, T. Taniguchi, H. R. Krishnamurthy, M. Jain, S. Banerjee, U. Chandni, and A. Ghosh, [Nat. Commun.](#) **13**, 1522 (2022).
- [102] S. Wu, Z. Zhang, K. Watanabe, T. Taniguchi, and E. Y. Andrei, [Nat. Mater.](#) **20**, 488 (2021).
- [103] I. Das, X. Lu, J. Herzog-Arbeitman, Z.-D. Song, K. Watanabe, T. Taniguchi, B. A. Bernevig, and D. K. Efetov, [Nat. Phys.](#) **17**, 710 (2021).
- [104] J. M. Park, Y. Cao, K. Watanabe, T. Taniguchi, and P. Jarillo-Herrero, [Nature](#) **592**, 43 (2021).
- [105] X. Lu, B. Lian, G. Chaudhary, B. A. Piot, G. Romagnoli, K. Watanabe, T. Taniguchi, M. Poggio, A. H. MacDonald, B. A. Bernevig, and D. K. Efetov, [PNAS](#) **118**, e2100006118 (2021).
- [106] Y. Saito, F. Yang, J. Ge, X. Liu, T. Taniguchi, K. Watanabe, J. I. A. Li, E. Berg, and A. F. Young, [Nature](#) **592**, 220 (2021).
- [107] Y. Cao, D. Rodan-Legrain, J. M. Park, N. F. Q. Yuan, K. Watanabe, T. Taniguchi, R. M. Fernandes, L. Fu, and P. Jarillo-Herrero, [Science](#) **372**, 264 (2021).
- [108] G. Chen, A. L. Sharpe, E. J. Fox, Y.-H. Zhang, S. Wang, L. Jiang, B. Lyu, H. Li, K. Watanabe, T. Taniguchi, Z. Shi, T. Senthil, D. Goldhaber-Gordon, Y. Zhang, and F. Wang, [Nature](#) **579**, 56 (2020).
- [109] Y. Saito, J. Ge, L. Rademaker, K. Watanabe, T. Taniguchi, D. A. Abanin, and A. F. Young, [Nat. Phys.](#) **17**, 478 (2021).
- [110] H. Polshyn, M. Yankowitz, S. Chen, Y. Zhang, K. Watanabe, T. Taniguchi, C. R. Dean, and A. F. Young, [Nat. Phys.](#) **15**, 1011 (2019).
- [111] Y. Cao, D. Chowdhury, D. Rodan-Legrain, O. Rubies-Bigorda, K. Watanabe, T. Taniguchi, T. Senthil, and P. Jarillo-Herrero, [Phys. Rev. Lett.](#) **124**, 076801 (2020).
- [112] M. Serlin, C. L. Tschirhart, H. Polshyn, Y. Zhang, J. Zhu, K. Watanabe, T. Taniguchi, L. Balents, and A. F. Young, [Science](#) **367**, 900 (2020).
- [113] P. Stepanov, I. Das, X. Lu, A. Fahimniya, K. Watanabe, T. Taniguchi, F. H. L. Koppens, J. Lischner, L. Levitov, and D. K. Efetov, [Nature](#) **583**, 375–378 (2020).
- [114] Y. Saito, J. Ge, K. Watanabe, T. Taniguchi, and A. F. Young, [Nat. Phys.](#) **16**, 926 (2020).
- [115] M. Yankowitz, S. Chen, H. Polshyn, Y. Zhang, K. Watanabe, T. Taniguchi, D. Graf, A. F. Young, and C. R. Dean, [Science](#) **363**, 1059 (2019).
- [116] X. Lu, P. Stepanov, W. Yang, M. Xie, M. A. Aamir, I. Das, C. Urgell, K. Watanabe, T. Taniguchi, G. Zhang, A. Bachtold, A. H. MacDonald, and D. K. Efetov, [Nature](#) **574**, 653 (2019).
- [117] Y. Cao, V. Fatemi, A. Demir, S. L. Tomarken, J. Y. Luo, J. D. Sanchez-Yamagishi, K. Watanabe, T. Taniguchi, E. Kaxiras, R. C. Ashoori, and P. Jarillo-Herrero, [Nature](#) **556**, 80 (2018).
- [118] X.-F. Zhou, Y.-W. Liu, C.-Y. Hao, C. Yan, Q. Zheng, Y.-N. Ren, Y.-X. Zhao, K. Watanabe, T. Taniguchi, and L. He, [Phys. Rev. B](#) **107**, 125410 (2023).
- [119] T. Benschop, T. A. de Jong, P. Stepanov, X. Lu, V. Stalman, S. J. van der Molen, D. K. Efetov, and M. P. Allan, [Phys. Rev. Res.](#) **3**, 013153 (2021).
- [120] D. Călugăru, N. Regnault, M. Oh, K. P. Nuckolls, D. Wong, R. L. Lee, A. Yazdani, O. Vafek, and B. A. Bernevig, [Phys. Rev. Lett.](#) **129**, 117602 (2022).

- [121] K. P. Nuckolls, R. L. Lee, M. Oh, D. Wong, T. Soejima, J. P. Hong, D. Călugăru, J. Herzog-Arbeitman, B. A. Bernevig, K. Watanabe, T. Taniguchi, N. Regnault, M. P. Zaletel, and A. Yazdani, *Nature* **620**, 525 (2023).
- [122] N. C. H. Hesp, I. Torre, D. Rodan-Legrain, P. Novelli, Y. Cao, S. Carr, S. Fang, P. Stepanov, D. Barcons-Ruiz, H. Herzig Sheinfux, K. Watanabe, T. Taniguchi, D. K. Efetov, E. Kaxiras, P. Jarillo-Herrero, M. Polini, and F. H. L. Koppens, *Nat. Phys.* **17**, 1162 (2021).
- [123] S. Lisi, X. Lu, T. Benschop, T. A. de Jong, P. Stepanov, J. R. Duran, F. Margot, I. Cucchi, E. Cappelli, A. Hunter, A. Tamai, V. Kandyba, A. Giampietri, A. Barinov, J. Jobst, V. Stalman, M. Leeuwenhoek, K. Watanabe, T. Taniguchi, L. Rademaker, S. J. van der Molen, M. P. Allan, D. K. Efetov, and F. Baumberger, *Nat. Phys.* **17**, 189 (2021).
- [124] Y. Choi, H. Kim, Y. Peng, A. Thomson, C. Lewandowski, R. Polski, Y. Zhang, H. S. Arora, K. Watanabe, T. Taniguchi, J. Alicea, and S. Nadj-Perge, *Nature* **589**, 536 (2021).
- [125] C. L. Tschirhart, M. Serlin, H. Polshyn, A. Shragai, Z. Xia, J. Zhu, Y. Zhang, K. Watanabe, T. Taniguchi, M. E. Huber, and A. F. Young, *Science* **372**, 1323 (2021).
- [126] Y. Choi, H. Kim, Y. Peng, A. Thomson, C. Lewandowski, R. Polski, Y. Zhang, H. S. Arora, K. Watanabe, T. Taniguchi, J. Alicea, and S. Nadj-Perge, arXiv:2008.11746 [cond-mat] (2020), [arxiv:2008.11746 \[cond-mat\]](#).
- [127] D. Wong, K. P. Nuckolls, M. Oh, B. Lian, Y. Xie, S. Jeon, K. Watanabe, T. Taniguchi, B. A. Bernevig, and A. Yazdani, *Nature* **582**, 198 (2020).
- [128] Y. Jiang, X. Lai, K. Watanabe, T. Taniguchi, K. Haule, J. Mao, and E. Y. Andrei, *Nature* **573**, 91 (2019).
- [129] A. Kerelsky, L. J. McGilly, D. M. Kennes, L. Xian, M. Yankowitz, S. Chen, K. Watanabe, T. Taniguchi, J. Hone, C. Dean, A. Rubio, and A. N. Pasupathy, *Nature* **572**, 95 (2019).
- [130] Y. Choi, J. Kemmer, Y. Peng, A. Thomson, H. Arora, R. Polski, Y. Zhang, H. Ren, J. Alicea, G. Refael, F. von Oppen, K. Watanabe, T. Taniguchi, and S. Nadj-Perge, *Nat. Phys.* **15**, 1174 (2019).
- [131] K. P. Nuckolls, M. Oh, D. Wong, B. Lian, K. Watanabe, T. Taniguchi, B. A. Bernevig, and A. Yazdani, *Nature* **588**, 610 (2020).
- [132] Y. Xie, B. Lian, B. Jäck, X. Liu, C.-L. Chiu, K. Watanabe, T. Taniguchi, B. A. Bernevig, and A. Yazdani, *Nature* **572**, 101 (2019).
- [133] O. Vafek and J. Kang, *Phys. Rev. B* **107**, 075123 (2023).
- [134] M. J. Calderón and E. Bascones, *Phys. Rev. B* **102**, 155149 (2020).
- [135] S. Fang, S. Carr, Z. Zhu, D. Massatt, and E. Kaxiras, *Angle-Dependent $Ab initio$ Low-Energy Hamiltonians for a Relaxed Twisted Bilayer Graphene Heterostructure* (2019), [arxiv:1908.00058 \[cond-mat\]](#).
- [136] S. Carr, S. Fang, Z. Zhu, and E. Kaxiras, *Phys. Rev. Res.* **1**, 013001 (2019).
- [137] J. Kang and O. Vafek, *Phys. Rev. B* **107**, 075408 (2023).
- [138] S. Carr, S. Fang, H. C. Po, A. Vishwanath, and E. Kaxiras, *Phys. Rev. Res.* **1**, 033072 (2019).
- [139] N. N. T. Nam and M. Koshino, *Phys. Rev. B* **96**, 075311 (2017).
- [140] Y. H. Kwan, S. A. Parameswaran, and S. L. Sondhi, *Phys. Rev. B* **101**, 205116 (2020).
- [141] P. J. Ledwith, E. Khalaf, Z. Zhu, S. Carr, E. Kaxiras, and A. Vishwanath, *TB or not TB? Contrasting properties of twisted bilayer graphene and the alternating twist n -layer structures ($n = 3, 4, 5, \dots$)* (2021), [arxiv:2111.11060 \[cond-mat\]](#).
- [142] L. Rademaker, D. A. Abanin, and P. Mellado, *Phys. Rev. B* **100**, 205114 (2019).
- [143] Y. Sheffer and A. Stern, *Phys. Rev. B* **104**, L121405 (2021).
- [144] A. Davydov, K. Choo, M. H. Fischer, and T. Neupert, *Phys. Rev. B* **105**, 165153 (2022).
- [145] J. Cao, M. Wang, S.-F. Qian, C.-C. Liu, and Y. Yao, *Phys. Rev. B* **104**, L081403 (2021).
- [146] K. Hejazi, X. Chen, and L. Balents, *Phys. Rev. Research* **3**, 013242 (2021).
- [147] J. Wang, Y. Zheng, A. J. Millis, and J. Cano, *Phys. Rev. Research* **3**, 023155 (2021).
- [148] Y. Ren, Q. Gao, A. H. MacDonald, and Q. Niu, *Phys. Rev. Lett.* **126**, 016404 (2021).
- [149] B. A. Bernevig, Z.-D. Song, N. Regnault, and B. Lian, *Phys. Rev. B* **103**, 205411 (2021).
- [150] S. Carr, S. Fang, and E. Kaxiras, *Nat. Rev. Mater.* **5**, 748 (2020).
- [151] J. H. Wilson, Y. Fu, S. Das Sarma, and J. H. Pixley, *Phys. Rev. Research* **2**, 023325 (2020).
- [152] Y. Huang, P. Hosur, and H. K. Pal, *Phys. Rev. B* **102**, 155429 (2020).
- [153] J. Liu, Z. Ma, J. Gao, and X. Dai, *Phys. Rev. X* **9**, 031021 (2019).
- [154] M. Koshino, N. F. Q. Yuan, T. Koretsune, M. Ochi, K. Kuroki, and L. Fu, *Phys. Rev. X* **8**, 031087 (2018).
- [155] J. Kang and O. Vafek, *Phys. Rev. X* **8**, 031088 (2018).
- [156] D. K. Efimkin and A. H. MacDonald, *Phys. Rev. B* **98**, 035404 (2018).
- [157] Y. Fu, E. J. König, J. H. Wilson, Y.-Z. Chou, and J. H. Pixley, *npj Quantum Mater.* **5**, 1 (2020).
- [158] S. K. Jain, V. Juričić, and G. T. Barkema, *2D Mater.* **4**, 015018 (2016).
- [159] S. Dai, Y. Xiang, and D. J. Srolovitz, *Nano Lett.* **16**, 5923 (2016).
- [160] M. M. van Wijk, A. Schuring, M. I. Katsnelson, and A. Fasolino, *2D Mater.* **2**, 034010 (2015).
- [161] K. Uchida, S. Furuya, J.-I. Iwata, and A. Oshiyama, *Phys. Rev. B* **90**, 155451 (2014).
- [162] L. Zou, H. C. Po, A. Vishwanath, and T. Senthil, *Phys. Rev. B* **98**, 085435 (2018).
- [163] E. Suárez Morell, J. D. Correa, P. Vargas, M. Pacheco, and Z. Barticevic, *Phys. Rev. B* **82**, 121407 (2010).
- [164] J. M. B. Lopes dos Santos, N. M. R. Peres, and A. H. Castro Neto, *Phys. Rev. Lett.* **99**, 256802 (2007).
- [165] R. Bistritzer and A. H. MacDonald, *PNAS* **108**, 12233 (2011).
- [166] G. Tarnopolsky, A. J. Kruchkov, and A. Vishwanath, *Phys. Rev. Lett.* **122**, 106405 (2019).
- [167] S. M. Davis and S. D. Sarma, *The kinetic theory of ultra-subsonic fermion systems and applications to flat band magic angle twisted bilayer graphene* (2023), [arXiv:2305.09120 \[cond-mat.mes-hall\]](#).
- [168] S. M. Davis, Y.-Z. Chou, F. Wu, and S. Das Sarma, *Phys. Rev. B* **107**, 045426 (2023).

- [169] S. M. Davis, F. Wu, and S. Das Sarma, *Phys. Rev. B* **107**, 235155 (2023).
- [170] H. Ochoa and R. M. Fernandes, *Phys. Rev. B* **108**, 075168 (2023).
- [171] D. Călugăru, H. Hu, R. L. Merino, N. Regnault, D. K. Efetov, and B. A. Bernevig, The Thermoelectric Effect and Its Natural Heavy Fermion Explanation in Twisted Bilayer and Trilayer Graphene (2024), [arxiv:2402.14057 \[cond-mat\]](#).
- [172] J. P. Hong, T. Soejima, and M. P. Zaletel, *Phys. Rev. Lett.* **129**, 147001 (2022).
- [173] X. Wang, J. Finney, A. L. Sharpe, L. K. Rodenbach, C. L. Hsueh, K. Watanabe, T. Taniguchi, M. A. Kastner, O. Vafek, and D. Goldhaber-Gordon, *PNAS* **120**, e2307151120 (2023).
- [174] P. Moon and M. Koshino, *Phys. Rev. B* **87**, 205404 (2013).
- [175] J. Liu and X. Dai, *npj Comput. Mater.* **6**, 1 (2020).
- [176] A. Kruchkov, *Phys. Rev. B* **107**, L241102 (2023).
- [177] A. García-Ruiz, J. J. P. Thompson, M. Mucha-Kruczyński, and V. I. Fal'ko, *Phys. Rev. Lett.* **125**, 197401 (2020).
- [178] B. Padhi, A. Tiwari, T. Neupert, and S. Ryu, *Phys. Rev. Research* **2**, 033458 (2020).
- [179] K. Hejazi, C. Liu, and L. Balents, *Phys. Rev. B* **100**, 035115 (2019).
- [180] B. Lian, F. Xie, and B. A. Bernevig, *Phys. Rev. B* **102**, 041402 (2020).
- [181] K. Hejazi, C. Liu, H. Shapourian, X. Chen, and L. Balents, *Phys. Rev. B* **99**, 035111 (2019).
- [182] J. Ahn, S. Park, and B.-J. Yang, *Phys. Rev. X* **9**, 021013 (2019).
- [183] F. Xie, Z. Song, B. Lian, and B. A. Bernevig, *Phys. Rev. Lett.* **124**, 167002 (2020).
- [184] Z. Song, Z. Wang, W. Shi, G. Li, C. Fang, and B. A. Bernevig, *Phys. Rev. Lett.* **123**, 036401 (2019).
- [185] E. Khalaf, N. Bultinck, A. Vishwanath, and M. P. Zaletel, *Soft modes in magic angle twisted bilayer graphene* (2020), [arxiv:2009.14827 \[cond-mat\]](#).
- [186] Y. H. Kwan, G. Wagner, N. Bultinck, S. H. Simon, and S. A. Parameswaran, *Phys. Rev. X* **12**, 031020 (2022).
- [187] J. Kang, B. A. Bernevig, and O. Vafek, *Phys. Rev. Lett.* **127**, 266402 (2021).
- [188] A. Kumar, M. Xie, and A. H. MacDonald, *Phys. Rev. B* **104**, 035119 (2021).
- [189] F. Xie, A. Cowsik, Z.-D. Song, B. Lian, B. A. Bernevig, and N. Regnault, *Phys. Rev. B* **103**, 205416 (2021).
- [190] F. Wu and S. Das Sarma, *Phys. Rev. Lett.* **124**, 046403 (2020).
- [191] O. Vafek and J. Kang, *Phys. Rev. Lett.* **125**, 257602 (2020).
- [192] I. Maccari, J. Carlström, and E. Babaev, *Phys. Rev. B* **107**, 064501 (2023).
- [193] A. Thomson and J. Alicea, *Phys. Rev. B* **103**, 125138 (2021).
- [194] E. Brillaux, D. Carpentier, A. A. Fedorenko, and L. Savary, *Phys. Rev. Res.* **4**, 033168 (2022).
- [195] Y. H. Kwan, G. Wagner, N. Bultinck, S. H. Simon, E. Berg, and S. A. Parameswaran, *Electron-phonon coupling and competing Kekulé orders in twisted bilayer graphene* (2023), [arxiv:2303.13602 \[cond-mat\]](#).
- [196] Y. H. Kwan, G. Wagner, N. Chakraborty, S. H. Simon, and S. A. Parameswaran, *Phys. Rev. B* **104**, 115404 (2021).
- [197] F. Xie, J. Kang, B. A. Bernevig, O. Vafek, and N. Regnault, *Phys. Rev. B* **107**, 075156 (2023).
- [198] M. Angeli, E. Tosatti, and M. Fabrizio, *Phys. Rev. X* **9**, 041010 (2019).
- [199] Y. H. Kwan, Y. Hu, S. H. Simon, and S. A. Parameswaran, *Phys. Rev. Lett.* **126**, 137601 (2021).
- [200] A. Blason and M. Fabrizio, *Phys. Rev. B* **106**, 235112 (2022).
- [201] L. Rademaker and P. Mellado, *Phys. Rev. B* **98**, 235158 (2018).
- [202] P. Cha, A. A. Patel, and E.-A. Kim, *Phys. Rev. Lett.* **127**, 266601 (2021).
- [203] Z.-D. Song and B. A. Bernevig, *Phys. Rev. Lett.* **129**, 047601 (2022).
- [204] B. Padhi, C. Setty, and P. W. Phillips, *Nano Lett.* **18**, 6175 (2018).
- [205] O. Vafek and J. Kang, *Phys. Rev. B* **104**, 075143 (2021).
- [206] X. Zhang, G. Pan, Y. Zhang, J. Kang, and Z. Y. Meng, *Chinese Phys. Lett.* **38**, 077305 (2021).
- [207] J. S. Hofmann, E. Khalaf, A. Vishwanath, E. Berg, and J. Y. Lee, *Phys. Rev. X* **12**, 011061 (2022).
- [208] G. Wagner, Y. H. Kwan, N. Bultinck, S. H. Simon, and S. A. Parameswaran, *Phys. Rev. Lett.* **128**, 156401 (2022).
- [209] Y. H. Kwan, G. Wagner, T. Soejima, M. P. Zaletel, S. H. Simon, S. A. Parameswaran, and N. Bultinck, *Phys. Rev. X* **11**, 041063 (2021).
- [210] M. Xie and A. H. MacDonald, *Phys. Rev. Lett.* **127**, 196401 (2021).
- [211] P. Potasz, M. Xie, and A. H. MacDonald, *Phys. Rev. Lett.* **127**, 147203 (2021).
- [212] D. V. Chichinadze, L. Classen, and A. V. Chubukov, *Phys. Rev. B* **102**, 125120 (2020).
- [213] D. E. Parker, T. Soejima, J. Hauschild, M. P. Zaletel, and N. Bultinck, *Phys. Rev. Lett.* **127**, 027601 (2021).
- [214] B.-B. Chen, Y. D. Liao, Z. Chen, O. Vafek, J. Kang, W. Li, and Z. Y. Meng, *Nat. Commun.* **12**, 5480 (2021).
- [215] S. Chatterjee, N. Bultinck, and M. P. Zaletel, *Phys. Rev. B* **101**, 165141 (2020).
- [216] Y. Da Liao, J. Kang, C. N. Breið, X. Y. Xu, H.-Q. Wu, B. M. Andersen, R. M. Fernandes, and Z. Y. Meng, *Phys. Rev. X* **11**, 011014 (2021).
- [217] C. Repellin, Z. Dong, Y.-H. Zhang, and T. Senthil, *Phys. Rev. Lett.* **124**, 187601 (2020).
- [218] T. Huang, L. Zhang, and T. Ma, *Sci. Bull.* **64**, 310 (2019).
- [219] P. Eugenio and C. Dag, *SciPost Physics Core* **3**, 015 (2020).
- [220] D. M. Kennes, J. Lischner, and C. Karrasch, *Phys. Rev. B* **98**, 241407 (2018).
- [221] L. Classen, C. Honerkamp, and M. M. Scherer, *Phys. Rev. B* **99**, 195120 (2019).
- [222] Y. Da Liao, Z. Y. Meng, and X. Y. Xu, *Phys. Rev. Lett.* **123**, 157601 (2019).
- [223] S. Liu, E. Khalaf, J. Y. Lee, and A. Vishwanath, *Phys. Rev. Research* **3**, 013033 (2021).
- [224] Y. Zhang, K. Jiang, Z. Wang, and F. Zhang, *Phys. Rev. B* **102**, 035136 (2020).
- [225] T. Cea and F. Guinea, *Phys. Rev. B* **102**, 045107 (2020).
- [226] M. Xie and A. H. MacDonald, *Phys. Rev. Lett.* **124**, 097601 (2020).

- [227] M. Christos, S. Sachdev, and M. S. Scheurer, *PNAS* **117**, 29543 (2020).
- [228] T. Soejima, D. E. Parker, N. Bultinck, J. Hauschild, and M. P. Zaletel, *Phys. Rev. B* **102**, 205111 (2020).
- [229] J. Kang and O. Vafeek, *Phys. Rev. B* **102**, 035161 (2020).
- [230] N. F. Q. Yuan and L. Fu, *Phys. Rev. B* **98**, 045103 (2018).
- [231] J. F. Dodaro, S. A. Kivelson, Y. Schattner, X. Q. Sun, and C. Wang, *Phys. Rev. B* **98**, 075154 (2018).
- [232] A. Thomson, S. Chatterjee, S. Sachdev, and M. S. Scheurer, *Phys. Rev. B* **98**, 075109 (2018).
- [233] X.-C. Wu, C.-M. Jian, and C. Xu, *Phys. Rev. B* **99**, 161405 (2019).
- [234] N. Bultinck, S. Chatterjee, and M. P. Zaletel, *Phys. Rev. Lett.* **124**, 166601 (2020).
- [235] J. W. F. Venderbos and R. M. Fernandes, *Phys. Rev. B* **98**, 245103 (2018).
- [236] X. Y. Xu, K. T. Law, and P. A. Lee, *Phys. Rev. B* **98**, 121406 (2018).
- [237] M. Ochi, M. Koshino, and K. Kuroki, *Phys. Rev. B* **98**, 081102 (2018).
- [238] J. Liu, J. Liu, and X. Dai, *Phys. Rev. B* **99**, 155415 (2019).
- [239] N. Bultinck, E. Khalaf, S. Liu, S. Chatterjee, A. Vishwanath, and M. P. Zaletel, *Phys. Rev. X* **10**, 031034 (2020).
- [240] K. Seo, V. N. Kotov, and B. Uchoa, *Phys. Rev. Lett.* **122**, 246402 (2019).
- [241] H. C. Po, L. Zou, A. Vishwanath, and T. Senthil, *Phys. Rev. X* **8**, 031089 (2018).
- [242] M. Christos, S. Sachdev, and M. S. Scheurer, *Nat Commun* **14**, 7134 (2023).
- [243] J. Yu, Y.-A. Chen, and S. Das Sarma, *Phys. Rev. B* **105**, 104515 (2022).
- [244] Y. W. Choi and H. J. Choi, *Phys. Rev. Lett.* **127**, 167001 (2021).
- [245] Y.-Z. Chou, F. Wu, J. D. Sau, and S. Das Sarma, *Phys. Rev. Lett.* **127**, 217001 (2021).
- [246] X. Hu, T. Hyart, D. I. Pikulin, and E. Rossi, *Phys. Rev. Lett.* **123**, 237002 (2019).
- [247] G. Wagner, Y. H. Kwan, N. Bultinck, S. H. Simon, and S. A. Parameswaran, *Superconductivity from repulsive interactions in Bernal-stacked bilayer graphene* (2023), [arxiv:2302.00682 \[cond-mat\]](#).
- [248] G. Wagner, Y. H. Kwan, N. Bultinck, S. H. Simon, and S. A. Parameswaran, *Coulomb-driven band unflattening suppresses k -phonon pairing in moiré graphene* (2023), [arxiv:2308.10938 \[cond-mat\]](#).
- [249] S. Chatterjee, M. Ippoliti, and M. P. Zaletel, *Phys. Rev. B* **106**, 035421 (2022).
- [250] R. M. Fernandes and L. Fu, *Phys. Rev. Lett.* **127**, 047001 (2021).
- [251] D. V. Chichinadze, L. Classen, and A. V. Chubukov, *Phys. Rev. B* **101**, 224513 (2020).
- [252] C. Lewandowski, D. Chowdhury, and J. Ruhman, *Phys. Rev. B* **103**, 235401 (2021).
- [253] E. Khalaf, S. Chatterjee, N. Bultinck, M. P. Zaletel, and A. Vishwanath, *Sci. Adv.* **7**, eabf5299 (2021).
- [254] Y. Wang, J. Kang, and R. M. Fernandes, *Phys. Rev. B* **103**, 024506 (2021).
- [255] B. Roy and V. Juričić, *Phys. Rev. B* **99**, 121407 (2019).
- [256] F. Wu, E. Hwang, and S. Das Sarma, *Phys. Rev. B* **99**, 165112 (2019).
- [257] H. Guo, X. Zhu, S. Feng, and R. T. Scalettar, *Phys. Rev. B* **97**, 235453 (2018).
- [258] E. J. König, P. Coleman, and A. M. Tsvelik, *Phys. Rev. B* **102**, 104514 (2020).
- [259] A. Julku, T. J. Peltonen, L. Liang, T. T. Heikkilä, and P. Törmä, *Phys. Rev. B* **101**, 060505 (2020).
- [260] J. González and T. Stauber, *Phys. Rev. Lett.* **122**, 026801 (2019).
- [261] Y.-Z. You and A. Vishwanath, *npj Quantum Mater.* **4**, 1 (2019).
- [262] F. Guinea and N. R. Walet, *PNAS* **115**, 13174 (2018).
- [263] B. Lian, Z. Wang, and B. A. Bernevig, *Phys. Rev. Lett.* **122**, 257002 (2019).
- [264] T. J. Peltonen, R. Ojajärvi, and T. T. Heikkilä, *Phys. Rev. B* **98**, 220504 (2018).
- [265] C.-C. Liu, L.-D. Zhang, W.-Q. Chen, and F. Yang, *Phys. Rev. Lett.* **121**, 217001 (2018).
- [266] F. Wu, A. H. MacDonald, and I. Martin, *Phys. Rev. Lett.* **121**, 257001 (2018).
- [267] H. Isobe, N. F. Q. Yuan, and L. Fu, *Phys. Rev. X* **8**, 041041 (2018).
- [268] C. Xu and L. Balents, *Phys. Rev. Lett.* **121**, 087001 (2018).
- [269] B. A. Bernevig, Z.-D. Song, N. Regnault, and B. Lian, *Phys. Rev. B* **103**, 205413 (2021).
- [270] F. Xie, A. Cowsik, Z.-D. Song, B. Lian, B. A. Bernevig, and N. Regnault, *Phys. Rev. B* **103**, 205416 (2021).
- [271] D. Călugăru, F. Xie, Z.-D. Song, B. Lian, N. Regnault, and B. A. Bernevig, *Phys. Rev. B* **103**, 195411 (2021).
- [272] F. Xie, N. Regnault, D. Călugăru, B. A. Bernevig, and B. Lian, *Phys. Rev. B* **104**, 115167 (2021).
- [273] L. L. H. Lau and P. Coleman, *Topological Mixed Valence Model for Twisted Bilayer Graphene* (2023), [arxiv:2303.02670 \[cond-mat\]](#).
- [274] Y.-Z. Chou and S. Das Sarma, *Phys. Rev. Lett.* **131**, 026501 (2023).
- [275] H. Hu, B. A. Bernevig, and A. M. Tsvelik, *Phys. Rev. Lett.* **131**, 026502 (2023).
- [276] J. Yu, M. Xie, B. A. Bernevig, and S. Das Sarma, *Phys. Rev. B* **108**, 035129 (2023).
- [277] Y. Li, B. M. Fregoso, and M. Dzero, *Topological Mixed Valence Model in Magic-Angle Twisted Bilayer Graphene* (2023), [arxiv:2309.03416 \[cond-mat\]](#).
- [278] Y.-J. Wang, G.-D. Zhou, S.-Y. Peng, B. Lian, and Z.-D. Song, *Molecular Pairing in Twisted Bilayer Graphene Superconductivity* (2024), [arxiv:2402.00869 \[cond-mat\]](#).
- [279] J. Ahn, S. Park, and B.-J. Yang, *Phys. Rev. X* **9**, 021013 (2019).
- [280] H. C. Po, H. Watanabe, and A. Vishwanath, *Phys. Rev. Lett.* **121**, 126402 (2018).
- [281] B. Kang, K. Shiozaki, and G. Y. Cho, *Phys. Rev. B* **100**, 245134 (2019).
- [282] J. Kang and O. Vafeek, *Phys. Rev. X* **8**, 031088 (2018).
- [283] C. Brouder, G. Panati, M. Calandra, C. Mourougane, and N. Marzari, *Phys. Rev. Lett.* **98**, 046402 (2007).
- [284] Y. Li and F. D. M. Haldane, *Phys. Rev. Lett.* **120**, 067003 (2018).
- [285] J. Cano and B. Bradlyn, *Annual Review of Condensed Matter Physics* **12**, 225 (2021), [arXiv:2006.04890 \[cond-mat.mes-](#)

[hall](#)].

- [286] J. Herzog-Arbeitman, V. Peri, F. Schindler, S. D. Huber, and B. A. Bernevig, [Phys. Rev. Lett.](#) **128**, 087002 (2022).